

AN EXPERIMENTAL CLASSIFICATION OF ENERGIES NECESSARY TO CRIMP SEAL  
COPPER AND STAINLESS STEEL TUBING

by  
Tyler James Krob

A thesis submitted in partial fulfillment  
of the requirements for the degree

of  
Master of Science  
in  
Mechanical Engineering

MONTANA STATE UNIVERSITY  
Bozeman, Montana

August 2011

©COPYRIGHT

by

Tyler James Krob

2011

All Rights Reserved

APPROVAL

of a thesis submitted by

Tyler James Krob

This thesis has been read by each member of the thesis committee and has been found to be satisfactory regarding content, English usage, format, citation, bibliographic style, and consistency, and is ready for submission to The Graduate School.

David Miller, Ph.D.

Approved for the Department of Mechanical Engineering

Christopher H.M. Jenkins, Ph.D., P.E.

Approved for The Graduate School

Dr. Carl A. Fox

STATEMENT OF PERMISSION TO USE

In presenting this thesis in partial fulfillment of the requirements for a master's degree at Montana State University, I agree that the Library shall make it available to borrowers under rules of the Library.

If I have indicated my intention to copyright this thesis by including a copyright notice page, copying is allowable only for scholarly purposes, consistent with "fair use" as prescribed in the U.S. Copyright Law. Requests for permission for extended quotation from or reproduction of this thesis in whole or in parts may be granted only by copyright holder.

Tyler James Krob

August 2011

## ACKNOWLEDGEMENTS

First, I would like to thank the Los Alamos National Laboratory in conjunction with National Nuclear Security Administration for providing much needed funding, a fantastic challenge to enrich my life, and an opportunity for everyone to advance in the technological age that we live in. I would like to thank the professors that made a difference in my education, especially my committee members Dr. David Miller, Dr. Ahsan Mian, Dr. John Davis as well as several other professors and instructors who provided assistance and essential guidance during my years at MSU. Thanks to all the office staff, Terry, Kathy, Beverly, and Michelle for much needed assistance and guidance. A thank you goes to all my undergraduate and graduate colleagues for making my college experience fun, bearable and worthwhile. Finally, a special thanks to my dearest family for their unconditional support and belief in me.

## TABLE OF CONTENTS

1. INTRODUCTION.....	1
Problem Statement.....	1
Progression of Study.....	1
2. BACKGROUND.....	3
Commercially Available Crimping Devices .....	3
Powder Actuated Tool Description .....	6
Hermetic Seal.....	7
Literature Review .....	8
Strain Hardening.....	8
Power Law .....	10
Residual Stresses .....	10
Spring Back.....	11
3. EXPERIMENTATION.....	14
Testing Setup.....	14
Instron Machine .....	14
3-Point Adaptation into Crimping Setup .....	15
Die Set Creation .....	16
Tube Mounting Conditions .....	18
Vacuum Pump and Components.....	20
LabVIEW Program and Data Acquisition System.....	23
Calibration.....	23
Vacuum Setup and Allowable Leak Rate Declaration .....	23
Mechanized Testing.....	25
Material Selection and Specimen Designation.....	25
Initial Zeroing/Alignment.....	30
Run Times per Segment (load, cease and hold, release, leak down).....	31
Repeatability .....	33
Sectioning/Polishing.....	34
Cutting with Buehler Saw.....	34
Polishing within Epoxy Cylinders.....	35
Building New Die Set.....	37
4. ANALYTICAL CALCULATIONS USING DEFORMATION LAWS.....	39
Beam Buckling Theory .....	39
5. ANALYSIS AND TESTING RESULTS .....	46
Leak Rates of Tested Specimens.....	46
Maximum Loads and Displacements Seen During Test Runs .....	52
Work-Energy Required to Seal a Tube.....	56

## TABLE OF CONTENTS - CONTINUED

Sectioning/Polishing Results.....	62
Die Shape Optimization Result .....	65
6. OPTIMIZATION CONCLUSIONS.....	72
Least Leak Rate Basis.....	72
Least Load Application Basis .....	72
Least Work Energy Basis and Energy Per Unit Area .....	72
Cross Section of Dies.....	73
Asymmetry in Test Setup.....	78
7. FUTURE WORK .....	80
REFERENCES .....	82
APPENDIX A: Comparative Vacuum And Load Versus Time Plots Of All Test Runs .....	84

## LIST OF TABLES

Table	Page
1. Table of available cross sections of copper and 304 stainless steel between 0.125" and 0.25" .....	26
2. Table displaying specimen designation for all copper testing samples .....	27
3. Table displaying specimen designation for all stainless steel testing samples .....	29
4. Table of copper buckling law load calculations for varying end conditions .....	43
5. Table of stainless steel buckling law load calculations for varying end conditions .....	44
6. Table showing leak rates of stainless steel crimped samples with load on and load off for 3 die sets .....	49
7. Table showing leak rates of copper crimped samples with load on and load off for 3 die sets .....	50
8. Tabulated work energy for all test runs of copper material .....	57
9. Tabulated work energy for all test runs of stainless steel material .....	58
10. Table of all average loads and displacements .....	69
11. Decision matrix to classify optimal die .....	78

## LIST OF FIGURES

Figure	Page
1. Image of hand operated crimping pliers [1] .....	3
2. Image of hose pinch-off pliers [2] .....	4
3. Image of the “Tube Terminator” [3] .....	5
4. Image of a tube crimped by the “Tube Terminator” [3].....	5
5. Figure of sponsor’s tool head for powder driven crimper .....	7
6. Graph of power law stress/strain curves for some materials [10].....	10
7. Graph of characteristic springback on stress/strain curve .....	12
8. Image of Instron 5882 load frame materials testing apparatus.....	14
9. Image of 3point bending fixture .....	16
10. Image of die sets from outside agency .....	16
11. Image of hammer and anvil pairs which mimic the shape of known dies.....	18
12. Image of crimped sample in Instron after a test run.....	18
13. Image showing purpose of aluminum deflection inhibitors .....	19
14. Image of completed test setup with vacuum line.....	20
15. Image of <i>DuoSeal</i> vacuum pump used in testing.....	21
16. Image of Vaccoon Products’ Ultraminiature vacuum sensor [14].....	21
17. Image of power supply and DAQ .....	22
18. Image showing vacuum line testing setup.....	23
19. Plot of corrected vacuum vs. Time after proper scaling.....	24
20. Image of home screen for LabView monitoring program.....	32
21. Image of holding fixture clamped onto tube and Buehler Isomet 1000 saw .....	34
22. Image of longitudinal slit produced by sectioning blade.....	35

## LIST OF FIGURES - CONTINUED

Figure	Page
23. Image of Buehler polishing apparatus.....	36
24. Image of crimped samples mounted in epoxy and polished.....	37
25. Image of attempted optimized die shape hammer and anvil .....	38
26. Image of an axially loaded column [16].....	39
27. Chart showing $K$ values for varying end conditions [17].....	41
28. Figure of load placement on a curved beam with pinned end conditions .....	42
29. Figure of curved beam section cut for analysis .....	43
30. Graph of S-125-049 vacuum vs. time for flat die runs.....	47
31. Graph of S-125-049 vacuum vs. time for shear die runs.....	47
32. Graph of S-125-049 vacuum vs. time for wedge die runs.....	48
33. Chart depicting leak rates of stainless steel crimped samples for 3 die sets with force on.....	50
34. Chart depicting leak rates of stainless steel crimped samples for 3 die sets with force off .....	51
35. Chart depicting leak rates of copper crimped samples for 3 die sets with force on.....	51
36. Chart depicting leak rates of copper crimped samples for 3 die sets with force off .....	52
37. Image of resulting crimped sample shape after testing for 3 die sets.....	53
38. Chart of maximum loads required to reach sealing point for copper material.....	54
39. Chart of maximum displacement required to reach sealing point for copper material .....	55
40. Example plot of load vs. Displacement up to sealing point .....	56
41. Chart of copper work energy for each cross section and each die set.....	59

## LIST OF FIGURES - CONTINUED

Figure	Page
42. Chart of stainless steel work energy for each cross section and each die set .....	59
43. Chart of work energy compared to cross-sectional area for copper .....	60
44. Chart of work energy compared to cross sectional area for stainless steel .....	62
45. Image of polished flat crimped sample .....	63
46. Image of polished shear crimped sample .....	63
47. Image of polished wedge crimped sample .....	64
48. Schematic of the MY attempted optimized die shape .....	66
49. Chart depicting leak rates of copper material with force on with the addition of the MY die .....	67
50. Chart depicting leak rates of copper material with force off with the addition of the MY die .....	67
51. Chart of maximum load required to reach sealing point for copper material with addition of the MY die .....	68
52. Chart of maximum displacement required to reach sealing point for copper material with addition of my die .....	68
53. Chart of copper work energy for each cross section with the addition of the MY die.....	70
54. Image of the polished my die set crimped sample (a).....	71
55. Image of the polished my die set crimped sample (b).....	71
56. Image displaying the flat die's recovery force direction .....	74
57. Image showing friction forces resulting from a change in length of the flat crimped tube .....	74
58. Image displaying the shear die's recovery force direction .....	75

LIST OF FIGURES - CONTINUED

Figure	Page
59. Image showing friction forces resulting from a change in length of the shear crimped tube .....	76
60. Image displaying the wedge die's recovery force direction .....	77
61. Image showing friction forces resulting from a change in length of the wedge crimped tube .....	77

## ABSTRACT

Crimping by means of deformation is a process commonly performed which restricts the flow of a substance through a tube. This process is unique by requiring large amounts of deformation between the inner tube walls which must lock and seal together allowing no flow to occur. This research studies how much energy is required to seal tubes constructed of copper or stainless steel between 0.125" and 0.25" encompassing all wall thicknesses available. Each cross section of tubing was cut, tightened into the end of a compression fitting, and plumbed through an integral vacuum sensor via plastic tubing running back to an oil-filled vacuum pump. This setup was mounted into a crimping fixture with interchangeable die sets within an Instron 5882 load frame and compressed at a quasi-static rate while monitoring load, displacement and vacuum level through a LabVIEW data acquisition program. All testing was analyzed to identify which die set produced the most efficient seal and required the least amount of input energy. Several sets of crimped samples were laid on their sides, mounted within epoxy and ground down to expose the sealing interface of the inside walls. From all acquired information, a new die set was constructed in an optimizing attempt to minimize both the leak rate and the energy required in creating the seal. The shape and contours of the optimized die set were the parameters changed from the 3 original sets. Final results showed that a shear shaped die set required the least amount of energy to establish a seal. The flat die created the best seal having the lowest resulting leak rate. The optimized die set created did not minimize the energy, but did produce a comparable leak rate to the flat set. This research develops a strict testing regimen to be followed when crimping a tube using a quasi-static deformation technique.

## INTRODUCTION

### Problem Statement

The problem to be solved within this research was titled “A Technical Study to Gain Technical Content and a Hardware Deliverable”. This problem targeted the process of sealing a tube closed via compressive deformation so that the flow of any substance within no longer occurs. The mechanical deformation technique known as crimping involves displacing the inside walls of a tube toward each other in hopes that they lock together preventing the flow of the substance inside. Closing the tube so that no flow is possible was the main problem focused on with this work.

The shape of the crimped area plays a large role in how the inner walls interact with one another when sealed. Combining the pressing load with a properly shaped die set lends itself to more effectively keeping the tube sealed and leak-free. For this work, analysis of this die shape was studied and optimized to impart enough locking stress to seal the inner walls together. Comparing resulting leak rates of three already constructed die sets offers information into which shapes create the best seal. Minimizing the amount of energy required to complete the seal was the second factor in determining which type of shape is best suited for a crimping application. Examination of 2 different materials, copper and 304 series stainless steel were examined in all available wall thicknesses within 0.125” and 0.25” outside diameters.

### Progression of Study

Only quasi-static methods were employed to study this crimping process. Within this quasi-static testing method, the study collected data relating to forces exerted during testing of the various tubing samples, displacements imparted to the tubes, and the consequential leak rate from

the resulting crimp. Analyzing the crimp shape via a sectioning method revealed how the internal walls of the tube locked together which leads to a seal. Seeing the internal wall unification shed light on which aspects of each die work best to seal the tubes. By comparing the seal shaping with the maximum load/work energies/leak from the crimp, the question of which die shape seals best is answered. From this information, a new die was built in an attempt to create the best sealing shape with a lower input energy – thus adequately answering the main question of the problem statement.

## BACKGROUND

### Commercially Available Crimping Devices

The crimping process is an essential operation in a wide variety of scenarios. A common use for a crimping tool is during the wiring of an electrical system. Many times, the end of wire is stripped of its casing, a terminal placed over the bare wire area, and a tool shown in Figure 1 positioned around the two to link the connector to the wire. This device relies on the deformable and conductive material existing in the terminal to bend and crimp onto the wire. Operation of this electrical crimper is done by hand and utilizes a principle identical to a common pair of pliers to transfer the gripping force of a human hand into crimping the connection. This crimped connection must ensure that conductivity is present and that a sufficient crimp is in place to hold the terminal securely affixed to wire.

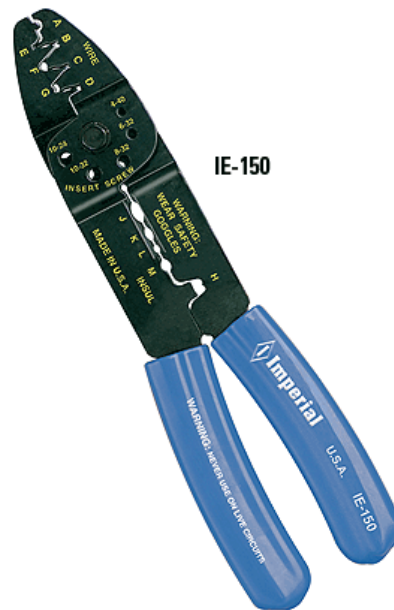


Figure 1: Image of hand operated crimping pliers [1]

A different type of crimping tool shown in Figure 2 produces a non-permanent pinched section used most often to clamp off tubing. This tool is commonly used for maintenance purposes when a fluid flow needs to be stopped allowing a hose to be removed from its end connection.



Figure 2: Image of hose pinch-off pliers [2]

A state of the art tool that is slightly more similar to this research is the “Tube Terminator” produced by *SonoBond Ultrasonic* visible in Figure 3. This tool is a portable crimper and sealer suited for use on copper and aluminum materials. It can seal tubes that are charged with gases or liquids, and exerts a clamping force up to 540lbf on 80PSI of compressor pressure. Once clamped, the unit induces the patented Wedge-Reed low amplitude vibration which, when coupled with the high clamping force, ensures a dependable weld and sealed tube. A key difference between this unit and the others is the vibration induced welding. Most hand tools only utilize a clamping force between the points of contact to accomplish the crimp. Figure 4 shows a typical example of a crimped tube after use of the “Tube Terminator”.

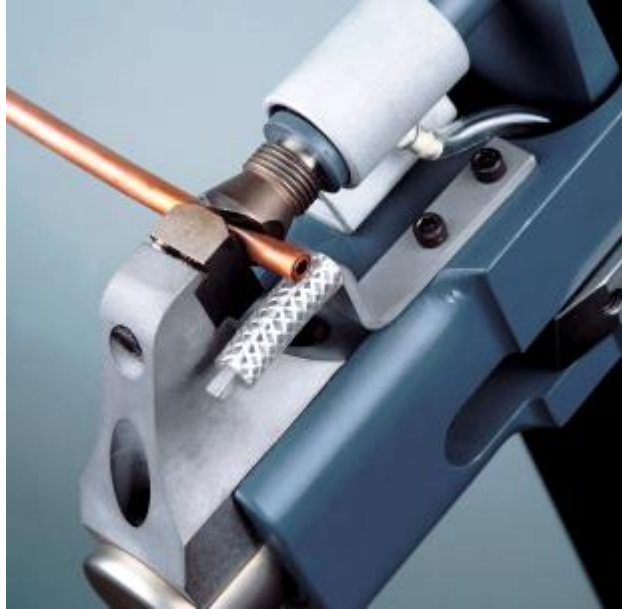


Figure 3: Image of the “Tube Terminator” [3]



Figure 4: Image of a tube crimped by the “Tube Terminator” [3]

### Powder Actuated Tool Description

Commonly used powder-actuated tools are often used to join materials to a hard base material like concrete. Sometimes called a “Ramset” or “Hilti” gun, these devices are powered by a chemical propellant known as cordite that is exploded within a casing releasing energy similar to a firearm. By using principles similar to the Ramset gun as a guide, a crimping tool capturing the exploding force exerted by the chemical powder focusing the energy on a sliding hammer is a feasible modification to enable crimping. This principle of a sliding mechanism fired by a powder charge classifies the tool as a low velocity piston operation. The head of a tool illustrating this modification is shown in Figure 5 . The left end of the figure illustrates the end where the hammer will impact the anvil after firing. This tool hinges open to extract the spent shell casing so another powder charge can be inserted. Various commercially available powers of these charges exist depending on the application and which substrate material the fastener is being driven into. These charges are: Grey firing at 315fps, Brown firing at 385fps, Green firing at 490fps, Yellow firing at 575fps, Red firing at 675fps, and Purple firing at 755fps. The velocities given are maximum speeds that the charge will fire a 0.125” diameter, 3” long hardened steel nail. [4]

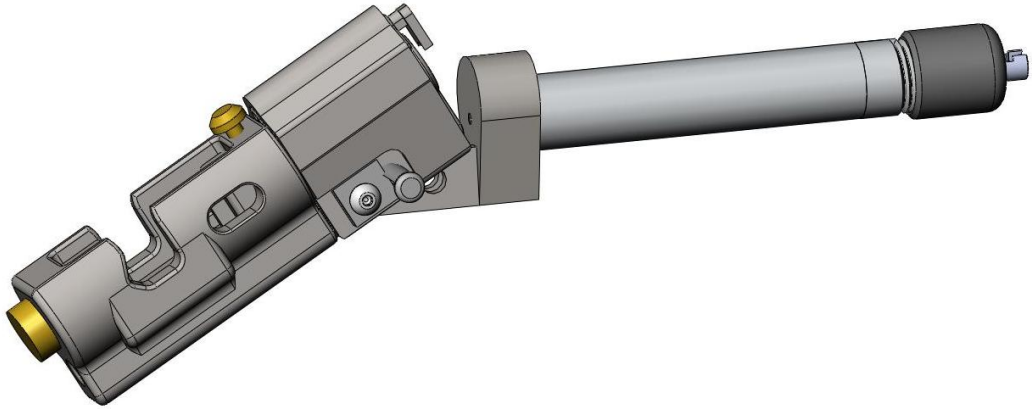


Figure 5: Figure of sponsor's tool head for powder driven crimper

### Hermetic Seal

A hermetic seal is the property of being airtight. A result of being airtight, a hermetically sealed container becomes impervious to liquids or gases. Most common uses of airtight containers exist in packaging of foods, pharmaceuticals, and chemicals. In other consumer goods, lighting fixtures for indoor or outdoor use are an example of products sealed to an airtight degree to function properly while providing safety. Hermetic seals are also used to eliminate deterioration of valuable documents or artwork. The Constitution of the United States has been placed in a sealed case charged with argon for preservation purposes. [5]

In the end, all things leak. Even the most technically advanced structure such as the International Space Station (ISS) can lose air pressure from inside its cabins. In 2004 while 2 people were aboard the ISS, it began losing pressure at a rate of  $9.113 \times 10^{-7}$  inHg/sec [6]. While this value is a very small rate, after 1 week the astronauts in the station will feel the effect of a pressure drop totaling .55inHg. A goal set by the sponsor of this research desired that the tubes sealed after using their tool remain sealed as hermetically possible. If any gases leak beyond the

interface of the crimped area, the goal of sealing was not achieved and the tool setup/input energies must be altered to achieve this parameter.

### Literature Review

Experimentation or research directly focusing on optimizing the shape of a die to crimp seal a tube does not exist in published form. Other works have been done on the tube forming processes like drawing where the tube is pulled through a narrowing chamber to reduce its overall diameter, or tube hydroforming where dies are used to bend the outside while the inside is pressurized with a hydraulic fluid to prohibit pinching.

The cold drawing of tubes has been studied to determine the degree to which a curvilinear matrix is able to deform a tube. Parameters like normal anisotropy and overall strengthening of the material under bulk deformation while cold adds to the difficulty when attempting to calculate the resulting diameters after drawing. Found within the literature is the limit of pressing being the loss of stability of a thin-walled tube occurring under high pressures or radial forces. A model has been created utilizing the momentless theory of a rigid-plastic shell with quadratic plasticity. From this model, the thickness change, meridional stress, contact pressure, and fluidity stress is obtained. [7] While numerically valid to the case of drawing a tube through a reducing chamber, this work does not offer assistive information into the crimping aspect of tube deformation. Instead, the results found within the articles focus on reactive loads, points of inflection, and curving angles within the die chamber.

### Strain Hardening

Strain hardening or work hardening is the strengthening of materials through plastic deformation. Plastic deformation begins to occur in a material when a large enough load is

introduced pushing the material higher than its yield stress. This strengthening is a direct result from dislocation motion in the lattice structure of a metallic structure. Lattice structures attempt to maintain their orderly, non-defected internal pattern prior to work hardening. When a material begins to work harden, the structure is imparted with new dislocations, and the addition of these new defects increase the resistance of movement of the lattice, thus resulting in overall strengthening. The number of new dislocations formed is the quantified amount of work hardening. After new dislocations have formed with the material, the lattice now being more resistive to motion has fundamentally decreased the ductility of the material and increased the yield strength. Ductility refers to the degree to which a material can undergo plastic deformation without fracture. At the point which dislocations saturate the lattice enough to prohibit additional movement, fracture occurs. [8]

In the case of crimping the inside of a tube closed, a large amount of deformation is required to achieve a seal between the inner walls. During the process of crimping, the tube begins to displace more and more as the tool presses the inside closed. This deformation creates dislocations which resist movement inside the lattice structure. Thus the initial stages of pressing require lower forces, while as deformation increases the load required to continuing deforming also must increase to counter the dislocation resistance. A widely used mathematical description of this hardening feature is the power law relation shown as

$$\sigma = K * \varepsilon^n \quad (1)$$

where  $K$  is a strength index,  $\varepsilon$  the plastic strain, and  $n$  the strain hardening exponent all combined to equal the stress  $\sigma$ . [9]

### Power Law

Calculation of material stresses on some deformed bodies is best done with a power law approximation. Depending on material construction and atomic structure, the power law can account for the strain hardening within the material when dislocations begin to pile up and restrict movement. This method allows the stress to be solved explicitly and returns a smooth curve. [10] Characteristic curves of stress versus strain using the power law for some materials are shown in Figure 6.

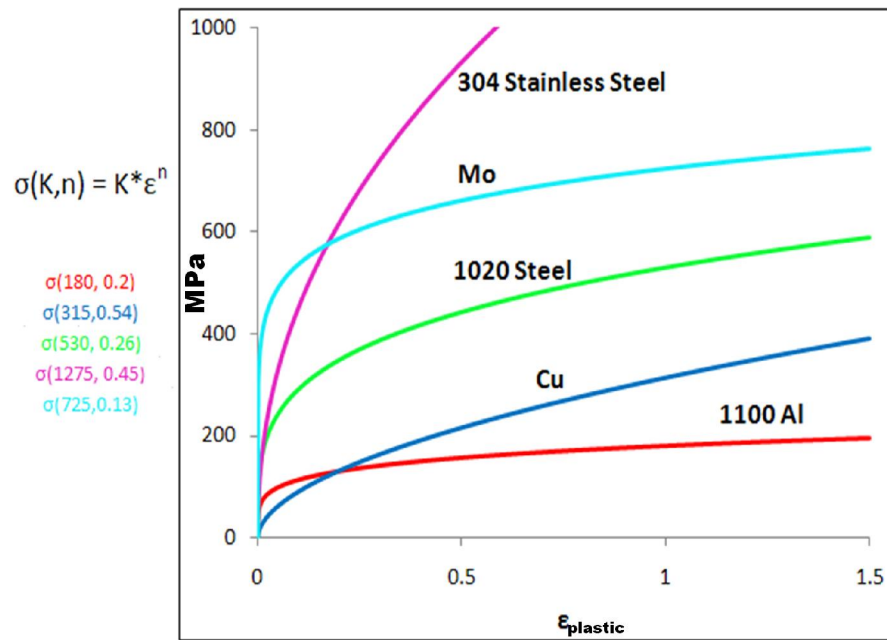


Figure 6: Graph of power law stress/strain curves for some materials [10]

### Residual Stresses

Residual stresses are internal stresses that continue to exist after releasing an external load or a temperature difference. Often times these stresses are a direct result from initial manufacturing process such as rolling, welding, machining or heat treatment. In excessive

amounts, the buildup of residual stress can fail a material or result in visual deformation. In some cases, however, essential designs rely on residuals to function like pre-stressed concrete or tempered glass. An essential attachment method known as press-fits relies on residual stresses between interface of the separate parts to hold the assembly together. A secondary finishing process called shot-peening introduces residual stresses intentionally to increase the surface strength of the material. [11]

### Spring Back

Directly linked to the residual stress concept is another phenomenon known as springback. Items that are subjected to large deformations resulting in cold working suffer from a springback characteristic. When the deforming force is released from the material, the piece springs back slightly in an attempt to return to its original shape. A common occurrence of this phenomenon is the metal tube bending process. After a tube has been bent to a desired shape and the bending force released, the tube straightens out slightly. To compensate for this, the tradesmen operating the bender over-run the desired bend by a known scalable amount. The amount that the material springs back follows the Young's Modulus for that material from final load to zero load as depicted in Figure 7 labeled as the elastic recovery. [8]

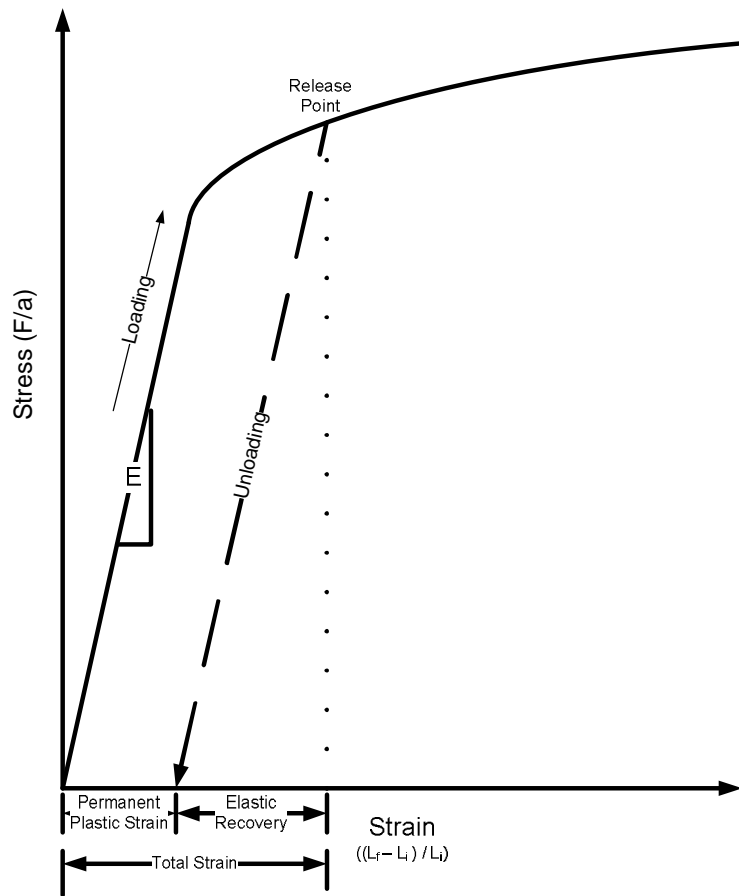


Figure 7: Graph of characteristic springback on stress/strain curve

This phenomenon has undesirable consequences when attempting to seal a tube closed. Upon release of the crimping device whether it is a pliers-type tool or impact driven tool, the crimped tube will attempt to spring back open. If the tube walls are able to separate after releasing, the seal will be lost and will no longer be airtight.

In order to completely understand how a tube is sealed off by means of compressive deformation, the concepts of strain hardening, residual stresses, springback, and hermetic sealing must be combined and related through testing. The effect of springback will enter the study as a consequential leak rate as the inner walls of the tube attempt to return to their original pre-crimped state. Strain hardening during the crimping will exist because of the high strain levels

that each tube will undergo to become sealed. Determining how the die shape affects the resulting leak rate is identifiable. This research links these concepts together via experimental analysis and develops a strict testing regimen to be followed when crimping a tube using a quasi-static deformation technique.

## EXPERIMENTATION

### Testing Setup

#### Instron Machine Overview

All testing for this research was conducted at Montana State University. The testing frame used was the Instron 5882-P7891 load frame shown in Figure 8 having a capacity of 100kN. This machine utilizes lead screws rotated by high torque DC servo motors positioned on a moveable head to exert either a tensile or compressive force on a specimen loaded in the frame. Atop this moveable head is a drop-through load cell to monitor the amount of force imparted onto the specimen. [12]



Figure 8: Image of Instron 5882 load frame materials testing apparatus

### 3-Point Adaptation into Crimping Setup

For a compressive load direction, a complete 3-point bend fixture was created to facilitate completion of this research. Initially, this fixture was solely intended for 3-point bending tests, but was adapted to encompass the crimp loading setup by fabricating additional parts. The fixture consists of an upper plate welded to a shaft that mounts in the moveable head via the same attachment used in tensile testing. Through this plate, 2 mounting holes which allow for a wedge shape to be attached producing the third point of contact required during 3-point tests. The lower section of this fixture incorporates a flat base welded to a shaft which pins through the Instron mounting hole. An array of holes is drilled in the lower base plate every 1 inch apart to allow variable spacing of 3-point tests. Two rectangular towers with dowel pins fitted into the bottom surfaces slip into the array of holes on the base. The material used on the plates and the shafts are 4000 series steel while the towers are composed of standard carbon steel. When machining all parts of this fixture, special care was taken to hold tolerances to within .0005" of the specified dimension and all welding performed slowly to not induce warping. The addition of 1/8" radius free-rotating dowels resting within grooves atop each tower make this fixture conform to ASTM testing spec A855. This whole setup is displayed in Figure 9.

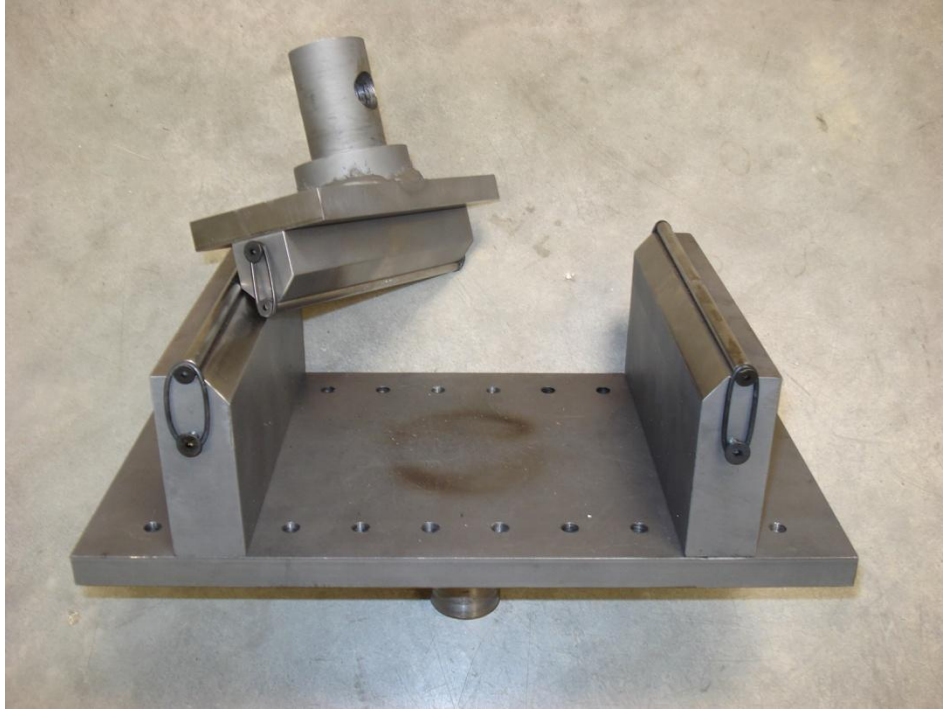


Figure 9: Image of 3point bending fixture

### Die Set Creation

Using a picture provided in Figure 10, additional parts were machined to convert the 3-point fixture into a single point crimping setup by creating an upper portion of a die - the hammer, and a lower portion - the anvil.



Figure 10: Image of die sets from outside agency

Each of these parts, whether hammer or anvil, is constructed of 4000 series alloy steel in a cross section of approximately 0.6" square and 6" in length. In each hammer's top surface, a 5/16 x 18 tapped hole has been formed for securing the hammer to the upper plate. Drilled in the bottom surface of each anvil is a blind 0.25" hole which locates the anvil directly under the head of the machine using stand-off pins. The anvil for the flat die has a top surface width of 0.5" with slightly rounded fillet dropping down to a lower shelf at its edges. The hammer for the flat set incorporates tapered lateral surfaces at 5° angles from vertical to reduce the section width from 0.6" to 0.5" which then lines up with the top surface of the flat anvil. The anvil for the shear set has a channel cut down the middle of its long side at a depth of 0.125". This channel is .1875" wide which was cut using a ball-nosed end mill. The hammer corresponding to the shear die was created by removing material at the outboard corners of the lower surface leaving a protruding spar of material 0.125" in width and depth. This section of the hammer results in a clearance within the channel on the anvil of 0.05625" on each side. The hammer for the wedge set also has two tapered lateral sides similar to the flat hammer. These tapered sides are at 45° angles from vertical and come to a pointed V shape at a right angle to one another. This V lines up directly over the channel which was cut in the anvil used for the shear die. A figure of the die sets is seen below in Figure 11. These dies were also created while holding the .0005" tolerance to provide an accurate testing frame. When affixing these dies to the 3-point fixture, these parts become aligned with each other.



Figure 11: Image of hammer and anvil pairs which mimic the shape of sponsor's dies

Once securely tightened, pinned to the Instron, and the sample aligned under the head of the upper plate, the machine compresses a tube into a shape like the one below in Figure 12.

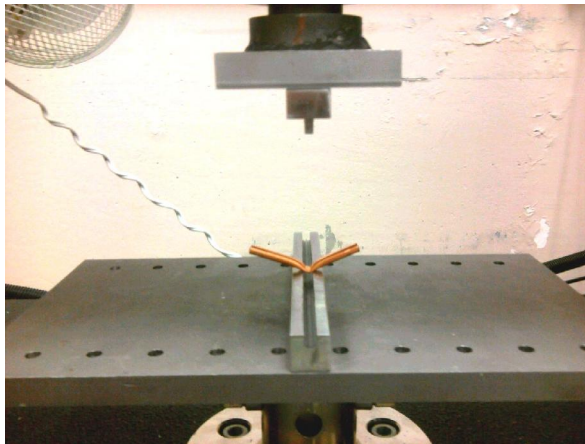


Figure 12: Image of crimped sample in Instron after a test run

### Tube Mounting Conditions

A noticeable problem occurring in Figure 12 is the large upward deflection of the ends of the tube. To more closely simulate the boundary conditions of a tube in service such as a tube

running along a wall which cannot move its ends being placed in a crimping device; it was desired to restrict this upward end motion during testing. A C-shape protrudes inward toward the head of the machine and over the top surface of the tube sample to prevent any upward movement. Figure 13 shows how all of these parts come together.

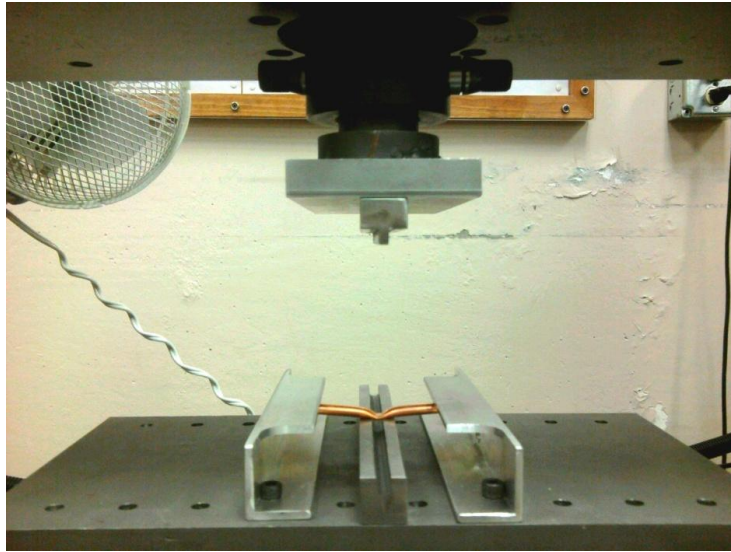


Figure 13: Image showing purpose of aluminum deflection inhibitors

The addition of a vacuum line to each sample required an access hole on one of these aluminum pieces. This vacuum line enables the monitoring of any leakage from the crimp during the test run. Figure 14 shows the completed testing setup.

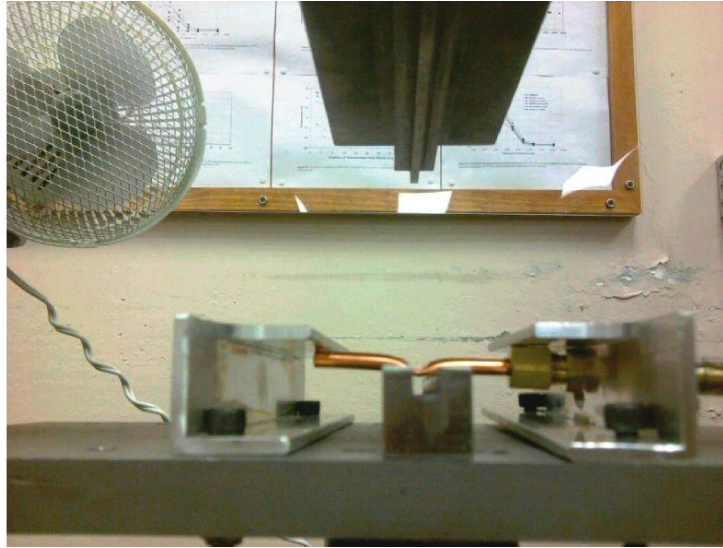


Figure 14: Image of completed test setup with vacuum line

#### Vacuum Pump and Components

After constructing all components for the crimping fixture and ensuring its smooth operation during testing, it was decided that exploring the leak rates of a crimped sample was required. In order to create a pressure difference in the crimped tube, either a vacuum or a compressor was needed. A *DuoSeal* vacuum pump model number 1400 was located and deemed capable of producing a negative pressure difference to be monitored in the system. This vacuum pump is oil filled, powered by a 1/2HP motor on standard 110V AC, and is shown in Figure 15. This pump has an ultimate pressure of .0001 Torr (29.916 inHg gage) [13]



Figure 15: Image of *DuoSeal* vacuum pump used in testing

An electronic vacuum sensor was now required to monitor the vacuum level of the system during the test. Procured from *Vacoon Vacuum Products*, a VTMV-QD ultra-miniature vacuum sensor with an output of 1-5V and a range of 0-30 inHg proportional to vacuum level fit the needs of this project by encompassing all capable ranges of testing equipment. This sensor is displayed in Figure 16.



Figure 16: Image of *Vacoon Products'* Ultraminiature vacuum sensor [14]

In order to operate this sensor, a power supply from a standard computer with integrated  $\pm 12V$  DC circuitry was used and presented in Figure 17.



Figure 17: Image of power supply and DAQ

To create a leak-free seal around the round tubing specimen, a compression fitting with a compression sleeve was slipped over the tube and tightened leaving the opposite end open to the atmosphere. A series of brass barb fittings and  $\frac{1}{4}$ " vinyl tube link the pump, sensor chamber, and sample together. All threaded ends of the fittings were wrapped in Teflon tape before assembling, and all barb connections secured with hose clamps. The setup of this is shown in Figure 18 below.

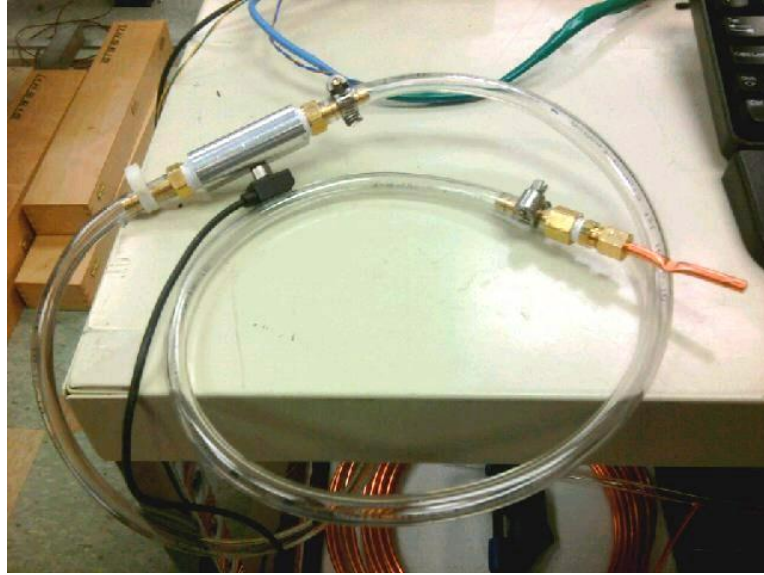


Figure 18: Image showing vacuum line testing setup

#### LabVIEW Program and Data Acquisition System

Monitoring of each test was accomplished using the *National Instruments* NI USB 6221 Data Acquisition System (DAQ) and the LabVIEW software program. This program was set up to capture the load from the Instron, the displacement of the Instron head, and the vacuum level of the system. These values plotted against time or each other enable calculation of leak rate and other necessary experimental results. The output voltage of the power supply going into the vacuum sensor was also monitored within the DAQ to ensure that consistent power was being fed into the system.

#### Calibration

#### Vacuum Setup and Allowable Leak Rate Declaration

After completing the setup of all required testing equipment, viewing and calibration of the leak rate of the system was now possible. All materials have cracks, crevices or even

microscopic holes, therefore perfect vacuum is difficult to obtain because everything leaks. Maintaining a vacuum at a constant level is also difficult when any connection between a tube and fitting is involved. Therefore, a leak rate inherent to the system was necessary to establish. This leak rate would be the known rate that the system itself loses vacuum through any connections, purging of air back through the oil in the pump, or other possible locations of any vacuum loss. By conducting isolation tests monitoring the vacuum of only the vacuum pump, tubing, and connections, this known permissible leak rate was detected. After running the vacuum pump for 40 seconds which ensured that the vacuum pump had reached its maximum capability, the pump was shut off and allowed to run out for 800 seconds. This method was repeated 7 times to obtain a statistically correct average for the allowable leak rate. After accounting for the possible points of vacuum loss, the final allowable leak rate of the testing system was found to be .0026 inHg/sec. Examine Figure 19 for an example plot of this characteristic leak. When compared to the leak seen in the ISS described in the background chapter, this inherent leaking rate is 2800x greater than the space station.

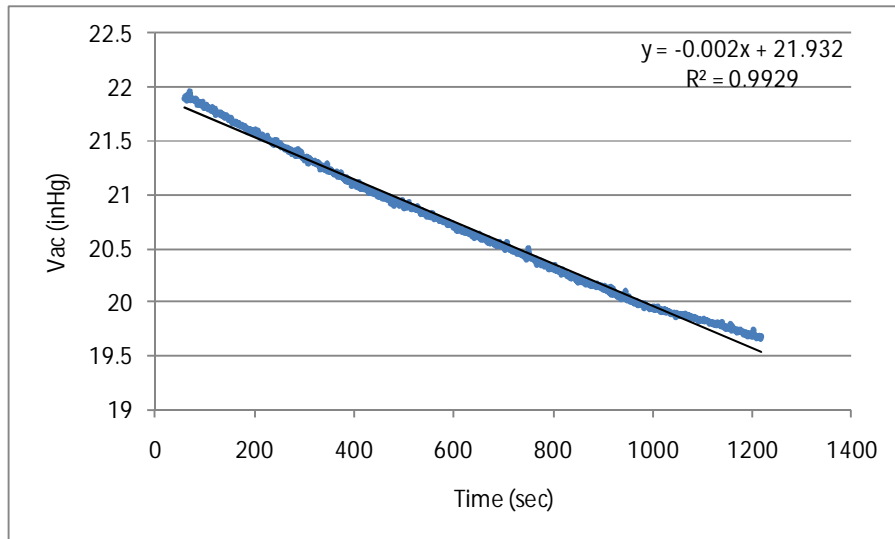


Figure 19: Plot of corrected vacuum vs. Time after proper scaling

Another outside factor that altered the vacuum obtainable by the vacuum pump was the atmospheric pressure within the room and tubing with the system at rest. A higher initial daily barometric pressure would result in a lower possible vacuum value than on a day with a lower barometric pressure. After collecting samples of air that can be averaged together, this average was used to offset the vacuum sensor to a zero value corresponding to atmospheric pressure on that day. This provides a consistent offset to the vacuum sensor therefore allowing the pump to achieve the same level of vacuum each day that tests were run.

### Mechanized Testing

#### Material Selection and Specimen Designation

The scope regarding selection of material for this work was constrained to stainless steel and copper per desire of the research sponsor. Within each of these materials there exist several grades of each, such as type 304 and type 316 in the stainless steel, and variations built to ASTM B75, B251, or B280 classification in the copper. In the stainless steel, type 304 seamless was selected as the material to be tested. The copper material used for testing was ASTM B75. The cross-section within each material class was selected to be 0.125", 0.1875", and 0.250" corresponding to the available sizes of compression ferrules. The wall thicknesses of the sections encompassed all available thicknesses within the outside diameter limits procurable from the McMaster-Carr supplier. Selecting the various diameters and thicknesses resulted in 19 possibilities available for testing within this work. A complete table of the stainless steel and copper cross sections is displayed in Table 1.

Table 1: Table of available cross sections of copper and 304 stainless steel between 0.125” and 0.25”

MATERIAL	OUTSIDE DIAMETER (in)	WALL THICKNESS (in)
COPPER	0.12500	0.014
		0.03
		0.032
	0.1875	0.03
		0.032
	0.25	0.03
		0.032
		0.049
		0.065
STAINLESS STEEL	0.12500	0.02
		0.028
		0.035
		0.049
	0.1875	0.03
		0.032
	0.25	0.01
		0.02
		.02X
		0.028

In order to keep track of each sample run and enable a cross-reference to check each run with its resulting crimped specimen, a labeling identification system was implemented. Table 2 and Table 3 show a complete series of the test specimens. The only alternate form within this designation code is seen in the stainless steel material with a diameter of 0.250” and a wall thickness of 0.020”. A modified version of this cross section was available in an aircraft grade, extra-hard type. This material is denoted with an X in the first position of the code.

Table 2: Table displaying specimen designation for all copper testing samples

MATERIAL	OUTSIDE DIAMETER	WALL THICKNESS	DIE SET	SPECIMEN ID
COPPER	0.12500	0.014	WEDGE	C-125-014-W-1
				C-125-014-W-2
				C-125-014-W-3
			SHEAR	C-125-014-S-1
				C-125-014-S-2
				C-125-014-S-3
			FLAT	C-125-014-F-1
				C-125-014-F-2
				C-125-014-F-3
		0.03	WEDGE	C-125-030-W-1
				C-125-030-W-2
				C-125-030-W-3
			SHEAR	C-125-030-S-1
				C-125-030-S-2
				C-125-030-S-3
			FLAT	C-125-030-F-1
				C-125-030-F-2
				C-125-030-F-3
		0.032	WEDGE	C-125-032-W-1
				C-125-032-W-2
				C-125-032-W-3
SHEAR	C-125-032-S-1			
	C-125-032-S-2			
	C-125-032-S-3			
FLAT	C-125-032-F-1			
	C-125-032-F-2			
	C-125-032-F-3			
COPPER	0.1875	0.03	WEDGE	C-187-030-W-1
				C-187-030-W-2
				C-187-030-W-3
			SHEAR	C-187-030-S-1
				C-187-030-S-2
				C-187-030-S-3
			FLAT	C-187-030-F-1
				C-187-030-F-2
				C-187-030-F-3
		0.032	WEDGE	C-187-032-W-1
				C-187-032-W-2
				C-187-032-W-3
			SHEAR	C-187-032-S-1
				C-187-032-S-2
				C-187-032-S-3
			FLAT	C-187-032-F-1
				C-187-032-F-2
				C-187-032-F-3

Table 2: Continued

COPPER	0.25	0.03	WEDGE	C-250-030-W-1
				C-250-030-W-2
				C-250-030-W-3
			SHEAR	C-250-030-S-1
				C-250-030-S-2
				C-250-030-S-3
			FLAT	C-250-030-F-1
				C-250-030-F-2
				C-250-030-F-3
		0.032	WEDGE	C-250-032-W-1
				C-250-032-W-2
				C-250-032-W-3
			SHEAR	C-250-032-S-1
				C-250-032-S-2
				C-250-032-S-3
			FLAT	C-250-032-F-1
				C-250-032-F-2
				C-250-032-F-3
		0.049	WEDGE	C-250-049-W-1
				C-250-049-W-2
				C-250-049-W-3
			SHEAR	C-250-049-S-1
				C-250-049-S-2
				C-250-049-S-3
			FLAT	C-250-049-F-1
				C-250-049-F-2
				C-250-049-F-3
0.065	WEDGE	C-250-065-W-1		
		C-250-065-W-2		
		C-250-065-W-3		
	SHEAR	C-250-065-S-1		
		C-250-065-S-2		
		C-250-065-S-3		
	FLAT	C-250-065-F-1		
		C-250-065-F-2		
		C-250-065-F-3		

Table 3: Table displaying specimen designation for all stainless steel testing samples

STAINLESS STEEL	0.12500	0.02	WEDGE	S-125-020-W-1
				S-125-020-W-2
				S-125-020-W-3
			SHEAR	S-125-020-S-1
				S-125-020-S-2
				S-125-020-S-3
		FLAT	S-125-020-F-1	
			S-125-020-F-2	
			S-125-020-F-3	
		0.028	WEDGE	S-125-028-W-1
				S-125-028-W-2
				S-125-028-W-3
	SHEAR		S-125-028-S-1	
			S-125-028-S-2	
			S-125-028-S-3	
	FLAT	S-125-028-F-1		
		S-125-028-F-2		
		S-125-028-F-3		
	0.035	WEDGE	S-125-035-W-1	
			S-125-035-W-2	
			S-125-035-W-3	
		SHEAR	S-125-035-S-1	
			S-125-035-S-2	
			S-125-035-S-3	
FLAT	S-125-035-F-1			
	S-125-035-F-2			
	S-125-035-F-3			
0.049	WEDGE	S-125-049-W-1		
		S-125-049-W-2		
		S-125-049-W-3		
	SHEAR	S-125-049-S-1		
		S-125-049-S-2		
		S-125-049-S-3		
FLAT	S-125-049-F-1			
	S-125-049-F-2			
	S-125-049-F-3			
STAINLESS STEEL	0.18750	0.02	WEDGE	S-187-020-W-1
				S-187-020-W-2
				S-187-020-W-3
			SHEAR	S-187-020-S-1
				S-187-020-S-2
				S-187-020-S-3
	FLAT	S-187-020-F-1		
		S-187-020-F-2		
		S-187-020-F-3		
	0.028	WEDGE	S-187-028-W-1	
			S-187-028-W-2	
			S-187-028-W-3	
SHEAR		S-187-028-S-1		
		S-187-028-S-2		
		S-187-028-S-3		
FLAT	S-187-028-F-1			
	S-187-028-F-2			
	S-187-028-F-3			

Table 3: Continued

STAINLESS STEEL	0.25	0.01	WEDGE	S-250-010-W-1
				S-250-010-W-2
				S-250-010-W-3
			SHEAR	S-250-010-S-1
				S-250-010-S-2
				S-250-010-S-3
			FLAT	S-250-010-F-1
				S-250-010-F-2
				S-250-010-F-3
		0.02	WEDGE	S-250-020-W-1
				S-250-020-W-2
				S-250-020-W-3
			SHEAR	S-250-020-S-1
				S-250-020-S-2
				S-250-020-S-3
			FLAT	S-250-020-F-1
				S-250-020-F-2
				S-250-020-F-3
		0.02	WEDGE	X-250-020-W-1
				X-250-020-W-2
				X-250-020-W-3
			SHEAR	X-250-020-S-1
				X-250-020-S-2
				X-250-020-S-3
			FLAT	X-250-020-F-1
				X-250-020-F-2
				X-250-020-F-3
0.028	WEDGE	S-250-028-W-1		
		S-250-028-W-2		
		S-250-028-W-3		
	SHEAR	S-250-028-S-1		
		S-250-028-S-2		
		S-250-028-S-3		
	FLAT	S-250-028-F-1		
		S-250-028-F-2		
		S-250-028-F-3		

### Initial Zeroing/Alignment

The actual testing performed on each sample needed to be as precise as possible to obtain statistically correct data. In total, 90 stainless steel and 81 copper specimens were tested with varying diameters and wall thicknesses. To collect precise data during each test run, it was

essential that these 171 test runs be set up the same relative to each other to prevent human error from entering the collected test data.

The first aspect of creating consistency in the testing was the length of each test sample. Samples were cut to a length of 3.5” utilizing a tubing cutter which employs a sharp disc to cut through the tube. A pliers-style cutting device would be sufficient to cut the material to the necessary length, but the cutting action deforms the ends thus disallowing placement of a compression fitting and ferrule over the tube. The next area that required consistency was the alignment of the tube under the head of the Instron. On the right hand side where the tube enters the fixture through the vacuum access hole in the aluminum deflection inhibitor, this hole provided a rough alignment point locating the tube in a position near the center of the head. Visually, a line created with a marker on each aluminum support provided an additional locating method. Finally, a square head combination square measuring from the front edge of the base plate to the sample ensured a pinpoint location and alignment of the sample in the machine. Now with the specimen loaded in the machine, the head of the Instron was lowered to touch the surface of the tube. Then using the fine adjustment function, the head was then fed downward onto the sample until any free play or motion in the system was eliminated. At this location, the gage length was zeroed and the load balanced to zero to provide a firm starting point for each test run with 3.965lbf of preload. Whenever a die set was to be changed or a new cross section of tubing loaded into the machine, this process of zeroing the gage length and load was repeated.

#### Run Times per Segment (load, cease and hold, release, leak down)

Each test run consisted of 3 parts: a load segment, a hold segment, and a leak down segment. Once the test was initiated at a feed rate of .05in/min for the .125” and .1875” diameters and .09in/min for the .250” diameter, the data would stream into LabVIEW where graphs of vacuum versus time, load versus time, and displacement versus time were displayed on the home

screen seen in Figure 20.

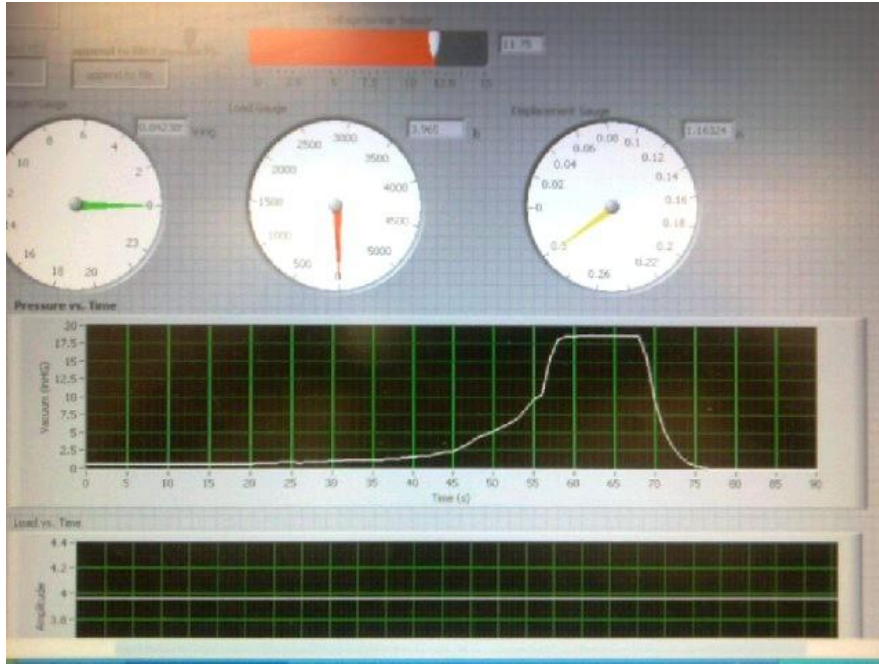


Figure 20: Image of home screen for LabView monitoring program

As the test ran, these graphs would automatically propagate across the screen showing a real-time history. The first segment ended when the head on the Instron machine was stopped. The stopping criteria used to halt the motion of the head came from the vacuum reading. By knowing the maximum vacuum capability of the pump found from calibration runs, the Instron head was halted once this vacuum level was reached. At this value, any opening in the end of the sample had been adequately crimped to stop any atmospheric gases from entering the system. This stopping criterion was the only point that existed within all tests. Between the die sets, the displacement necessary to seal the tube was different for each. To utilize a uniform displacement stopping point for all dies would leave some samples unsealed and others far exceeding the necessary displacement. Allowing the Instron head to proceed beyond the initial point of sealing

the tube walls imparts loads higher than necessary. The same is true for a load stopping criterion. Stopping the Instron head at a consistent load for all the die sets may exceed or stop short of the displacement required for a seal. Each die needs a different amount of load to establish a seal within the tube. With the head now stationary at the maximum vacuum stopping point, the vacuum pump was allowed to run for a time to ensure that the system was essentially at a stable state. The vacuum pump was turned off after allowing this stable state to progress to a time multiple of a 30 second total time interval (i.e.: 60 sec, 90 sec, 120sec, etc.). This time value initiated the next part of the test – the hold section. During this portion of time, the head of the Instron was still engaged in the sample providing a constant deflection and constant load. This segment progressed until another time multiple of 30 seconds had been reached. At this point, the head of the Instron was instantaneously retracted to its gage length. After releasing the load, the system was allowed to rest and any leak collected by still running LabView program. This final leak down segment progressed for at least 30 seconds to provide enough data to calculate the rate of leak from the system. The duration of each of these segments varied depending on the cross section of the sample.

### Repeatability

By following the above listed regimen for setting up each test and operating the Instron, the data collected was statistically consistent. By running 3 tests per die set per cross section, any mean values could be pulled from averaging of the tests. Sample plots of vacuum versus time and load versus time are shown in Appendix A displaying examples of the overlapping test curves between each of the tests and the consistency obtained.

## Sectioning/Polishing

### Cutting with Buehler Saw

After conducting tests and viewing the crimped specimens, a decision was made to section the crimped sample along the longitudinal direction. By cutting the sample on this plane, the sealed portion of the crimp area would be displayed. Available in room EPS248 at Montana State University is the Buehler Isomet 1000 cutting saw. Using a diamond impregnated cutting blade at low rpm and low input force, samples are able to be cleanly cut exposing a bright surface feasible for microstructure analysis. A custom holding fixture to securely clamp the crimped tube and cut along the desired direction was machined and mounted in the apparatus shown in Figure 21.



Figure 21: Image of holding fixture clamped onto tube and Buehler Isomet 1000 saw

After operating at 275 rpm for 45 minutes, the saw cut through the sample as shown in Figure 22. Further cropping of the original 3.5" sample length was needed to separate the tube into 2 pieces at the position of the red lines in Figure 22 This was accomplished by re-mounting the sample

laterally in the saw and proceeding with the additional cuts.



Figure 22: Image of longitudinal slit produced by sectioning blade

#### Polishing within Epoxy Cylinders

Once the Buehler saw method was attempted, an alternate method utilizing a 2 part epoxy encasing crimped samples was employed. In this method, a crimped sample was cut down from its initial length of 3.5” to 1” in order to fit inside a plastic hollow shell. The base of this round cylinder was removable from the shell to enable the resulting solid cylinder to be ground down. The epoxy was mixed from 2 parts of Ted Pella Pelco resin to 1 part of fast curing hardener in amounts of 10grams per cylinder created. Once the crimped samples were laid within the shell in the correct orientation, the mixed epoxy was poured into the shell of the cylinder. The shells were transferred to a glass vacuum chamber where any air bubbles in the epoxy were drawn out. These vacuumed shells were placed in a 158°F oven for 4 hours to expedite curing of the epoxy. After fully cured, the base was separated from the shell and the internal epoxy cylinder was exposed with the crimped samples encased at the lower surface.

The grinding utilizes a Buehler Ecomet IV rotating sandpaper platform with an incorporated Euromet I power head all lubricated by a stream of water. The head holds the coins flush against the sandpaper and exerts a soft force downward while the setup spins illustrated in Figure 23. Operating at a speed of 200RPM and a 6 pound downward force, these coins were spun for 30 minutes atop a sheet of 240 grit sandpaper. A time of 30 minutes was long enough to grind off the epoxy and polish down the copper tubes to expose the interface of the crimped area. A sheet of fine 1000 grit sandpaper was swapped onto the platform and the process continued to finely polish the surface. 3 of the polished disks created are displayed in Figure 24.



Figure 23: Image of Buehler polishing apparatus



Figure 24: Image of crimped samples mounted in epoxy and polished

#### Building New Die Set

Upon completion of the polishing of crimped samples, new information was revealed regarding how the inner walls of the tubes came in contact with each other. Using this new found info as a basis, a fourth, and hopefully improved die set was created. This new die was created from the same carbon steel bar that the others were built from. Its basic shape is seen below in Figure 25 and utilizes the same mounting setup as all prior testing. For comparison purposes, 3 cross sections of copper tubing were chosen from the leftover material in all outside diameters. These samples had wall thicknesses of 0.030". 3 tests runs were performed to obtain a statistical mean all tests followed the same procedure listed above.



Figure 25: Image of attempted optimized die shape hammer and anvil

## ANALYTICAL CALCULATIONS USING DEFORMATION LAWS

Beam Buckling Theory

One method of structural failure is buckling. A structure prone to a buckling failure is an axially loaded column. If a long and slender column is loaded axially in compression, it may deflect laterally as illustrated in Figure 26 and fail by buckling. A load eccentric of the axis of the column may also induce a bending moment into the beam causing a buckling failure. [15]

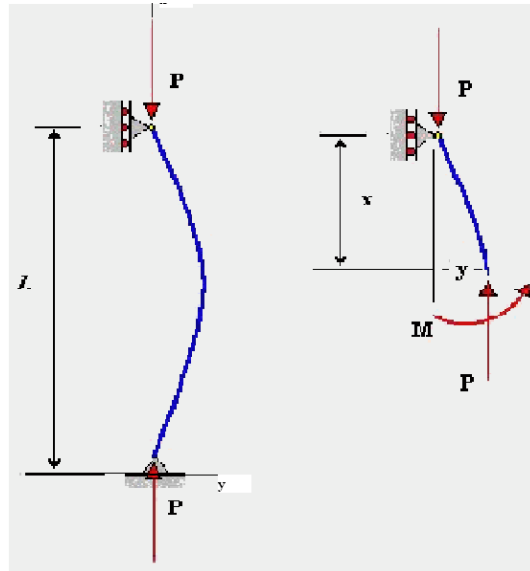


Figure 26: Image of an axially loaded column [16]

The weight or load required to buckle a structure is known as the critical load denoted as  $P_{cr}$ . Material construction and shape determine this critical buckling load, which is often times analyzed using the Euler buckling theory. In this theory, the bending moment equation

$$EIv'' = M \quad (2)$$

with  $E$  being the Young's Modulus,  $I$  being the flexural rigidity of the beam,  $v$  the lateral deflection in the  $y$  direction, and  $M$  the moment at any cross section, is used to obtain the differential equation of the deflection curve. Upon applying boundary conditions from the setup, this curve becomes a homogeneous, linear, 2<sup>nd</sup> order differential with constant coefficients written as

$$EIv'' + Pv = 0 \quad (3)$$

Continuing to solve for the solution of the differential equation, a positive quantity indicated as  $k$  where

$$k = \sqrt{\frac{P}{EI}} \quad (4)$$

is introduced to obtain the general solution

$$v = C_1 \sin(kx) + C_2 \cos(kx) \quad (5)$$

with  $C_1$  and  $C_2$  being the integration constants found from boundary conditions. Utilizing

Figure 26 as a reference and applying the boundary conditions  $v(0)=0$  and  $v(L)=0$ ,  $C_2$  is solved utilizing the first boundary of  $v(0)=0$  condition. Therefore,

$$v = C_1 \sin(kx) \quad (6)$$

The second condition of  $v(L)=0$  gives

$$C_1 \sin(kL) = 0 \quad (7)$$

and from this one can conclude that either  $C_1 = 0$  or  $\sin(kL)=0$ . Considering the first case with  $C_1=0$ , the column will always remain straight and is satisfied for any value of  $kL$ . The second case where  $\sin(kL)=0$  occurs when  $kL$  equals a multiple of  $n\pi$  in increments of 1, 2, 3... . By expanding the initial term  $k$  as,

$$P = \frac{n^2 \pi^2 EI}{L^2} \quad (8)$$

these become the critical buckling values for the load  $P$  with  $n$  defining the mode shape of the buckled column. A quick simplification of the above equation isolates the various possible mode shapes assumable by a buckling column. Introducing an a term called effective length  $L_e$ , the critical buckling equation for a pinned/pinned boundary scenario deforming into the first mode shape is re-written as

$$P_{cr} = \frac{\pi^2 EI}{L_e^2} \tag{9}$$

having an  $n$  value of 1 and the effective length of  $2L$ . Effective length is a way of expressing the distance between points of inflection (zero moment) on a buckled mode shape. The effective length can be expressed as an effective length factor  $K$  being a constant multiple of the original column length  $L$ . [7]

$$L_e = KL \tag{10}$$

A tabulated form of possible  $K$  values stemming from alternate end conditions such as the pinned/pinned boundary conditions from Figure 26, is seen in Figure 27.

Buckled shape of column shown by dashed line							
	Theoretical K value	0.5	0.7	1.0	1.0	2.0	2.0
	Recommended design value K	0.65	0.80	1.2	1.0	2.10	2.0
End condition key		Rotation fixed and translation fixed					
		Rotation free and translation fixed					
		Rotation fixed and translation free					
		Rotation free and translation free					

Figure 27: Chart showing  $K$  values for varying end conditions [17]

The development of this buckling theory is also applicable to beams which are curved in shape. A curved beam with cantilever end conditions loaded at its midpoint is directly relatable to the crimping action experienced by a tube. Taking the example beam in Figure 28, by mirroring the beam across the pinned/pinned end conditions, the hemispherical shape becomes a full circle, or as desired to relate to this research, a *tube* running in and out of the page.

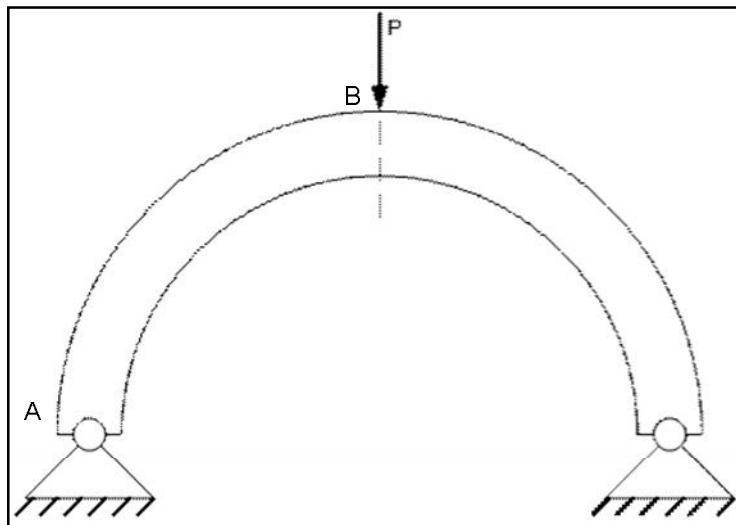


Figure 28: Figure of load placement on a curved beam with pinned end conditions

The pinned end conditions allow the beam to rotate, but do not allow any translation vertically or horizontally at the ends. The buckling theory for curved beams gathers some of its clout from the sectioning method as shown in the inset of Figure 26. This sectioning method is essential for calculating the shear and moment existing within the curved beam loaded as shown. Sectioning along the dotted line aligned with load P in Figure 28, the internal shear and bending moment are revealed as below in Figure 29.

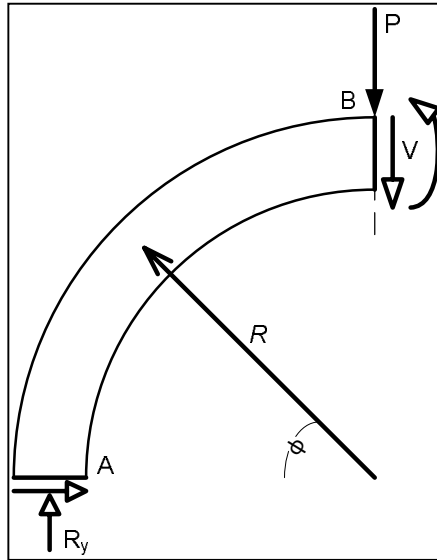


Figure 29: Figure of curved beam section cut for analysis

Table 4 and Table 5 show the theoretical load values required to seal the tube using the beam buckling analysis method.

Table 4: Table of copper buckling law load calculations for varying end conditions

Copper (ASTM B75)								
Area Moment of Inertia $I_x = (\pi r / 64) * (d_o^4 - d_i^4)$								
Critical Buckling Loads ( $P_{cr}$ )		Pinned - Pinned	$\pi^2 EI / L^2$					
		Fixed - Fixed	$4\pi^2 EI / L^2$					
		Fixed - Pinned	$2.046\pi^2 EI / L^2$					
Yield Strength (PSI)		45000						
Ultimate Strength (PSI)		50000				lbf	lbf	lbf
Modulus		1.74E+07	PSI			L= 1/2 Circ	L= 1/2 Circ	L= 1/2 Circ
INCHES			in <sup>2</sup>	in	in <sup>4</sup>	Lbf		
Outside Diameter	Wall Thickness	Inside Diameter	CX Area	Circumference	M.O.Ix	Pinned- Pinned $P_{cr}$	Fixed - Pinned $P_{cr}$	Fixed-Fixed $P_{cr}$
0.12500	0.014	0.09700	0.00	0.39	7.639E-06	34034.03	69633.63	136136.12
0.12500	0.03	0.06500	0.01	0.39	1.111E-05	49492.28	101261.21	197969.13
0.12500	0.032	0.06100	0.01	0.39	1.13E-05	50368.18	103053.29	201472.71
0.1875	0.03	0.12750	0.01	0.59	4.77E-05	94453.95	193252.79	377815.81
0.1875	0.032	0.12350	0.02	0.59	4.925E-05	97528.99	199544.32	390115.98
0.25	0.03	0.19000	0.02	0.79	0.0001278	142328.86	291204.85	569315.45
0.25	0.032	0.18600	0.02	0.79	0.000133	148142.59	303099.74	592570.37
0.25	0.049	0.15200	0.03	0.79	0.0001655	184398.90	377280.15	737595.60
0.25	0.065	0.12000	0.04	0.79	0.0001816	202247.68	413798.76	808990.73

Table 5: Table of stainless steel buckling law load calculations for varying end conditions

Stainless Steel									
(304SS)									
Yield Strength		31200.00000	Yield Strength		30000.00	PSI			
Ultimate Strength		73200.00000	Ultimate Strength		75000.00	PSI			
Area Moment of Inertia $I_x = (\pi/64) * (d_o^4 - d_i^4)$					(Red refers to the 1/8 hard Aircraft Grade)				
Modulus		2.80E+07	PSI				L= 1/2 Circ	L= 1/2 Circ	L= 1/2 Circ
INCHES			in <sup>2</sup>		in <sup>4</sup>		Lbf		
Outside Diameter	Wall Thickness	Inside Diameter	CX Area	Circumference	M.O.Ix	Pinned- Pinned P <sub>cr</sub>	Fixed - Pinned P <sub>cr</sub>	Fixed-Fixed P <sub>cr</sub>	
0.12500	0.02	0.08500	0.01	0.39	9.422E-06	67517.08	138139.96	270068.34	
0.12500	0.028	0.06900	0.01	0.39	1.087E-05	77905.83	159395.33	311623.33	
0.12500	0.035	0.05500	0.01	0.39	1.154E-05	82660.41	169123.21	330641.65	
0.12500	0.049	0.02700	0.01	0.39	1.196E-05	85692.31	175326.47	342769.24	
0.1875	0.02	0.14750	0.01	0.59	3.744E-05	119227.97	243940.42	476911.86	
0.1875	0.028	0.13150	0.01	0.59	4.599E-05	146479.70	299697.48	585918.82	
0.25	0.01	0.23000	0.01	0.79	5.438E-05	97423.84	199329.18	389695.36	
0.25	0.02	0.21000	0.01	0.79	9.628E-05	172489.72	352913.98	689958.90	
0.25	0.02	0.21000	0.01	0.79	9.628E-05	172489.72	352913.98	689958.90	
0.25	0.028	0.19400	0.02	0.79	0.0001222	218952.26	447976.33	875809.05	

As seen in the above tables, the amounts of forces required to buckle these small tubes according to the buckling theory are extremely high requiring a minimum of 34034lbf to induce buckling. This high load value is a result of the buckling theory being based on a vertical column that is long and slender. This situation is vastly different from the small tubing walls becoming buckled. These tube walls have a short circumference corresponding to the buckling length ranging from 0.39in up to 0.79in. A short effective length is less apt to buckle, and will require loads higher than what was seen in the experiment.

For analytical calculations using the power law relationship, the formula is linked to only the plastic strain seen within the deformed material. This value could be taken as the full distance traveled required to seal a tube, with the elastic strain being negligible compared to the plastic strain, but was still only an assumption. By knowing the *K* and *n* values for the copper and stainless steel materials, and by setting the displacement equal to the inside diameter of the tube, the stress at that point was identifiable. However, determining the physical quantity for the amount of strain being experienced by each small element of the tube requires many assumptions and becomes far too involved for the scope of the research. While being crimped, the elements of

tube away from the impacting die set move in the horizontal direction away from the centerline of the tube. Elements directly in contact with the die set move in the vertical direction, and in a different amount than the other elements. Once the value for strain is known, the force at a strain which removes the inside diameter of the tube can be determined. This requires in depth analysis using Finite Element Analysis to obtain mesh deformation under plastic loading. The power law approximation could provide a beneficial mathematical analysis base which is more accurate than the buckling theory.

## ANALYSIS AND TESTING RESULTS

Leak Rates of Tested Specimens

The first result of interest after testing was the resulting leak rate of the tube after crimping. If the vacuum did not hold at the maximum permissible leak rate established during calibration runs, the sample was losing vacuum from the end of the tube and was not completely sealed. By viewing an example of a vacuum versus time plot in Figure 30, one can see that this particular sample did not seal adequately. Further referencing this chart, indication lines have been overlain on the chart illustrating the different segments of the tests runs. The left vertical line corresponds to the point in time when the vacuum pump was turned off. For this particular test on stainless steel material with 0.125" outside diameter, .049" wall thickness and using the flat die set, these points in time fall at 90 seconds and 120 seconds. During the time after stopping the vacuum pump until the release of the load from the Instron head, the samples did lose vacuum at an average rate of 0.01516 inHg/sec. At 120 seconds when the Instron head was retracted from the sample, the leak increased to 0.0305 inHg/sec. This increase in leak rate without a force pressing on the sample displays the effect of spring back on the crimped area.

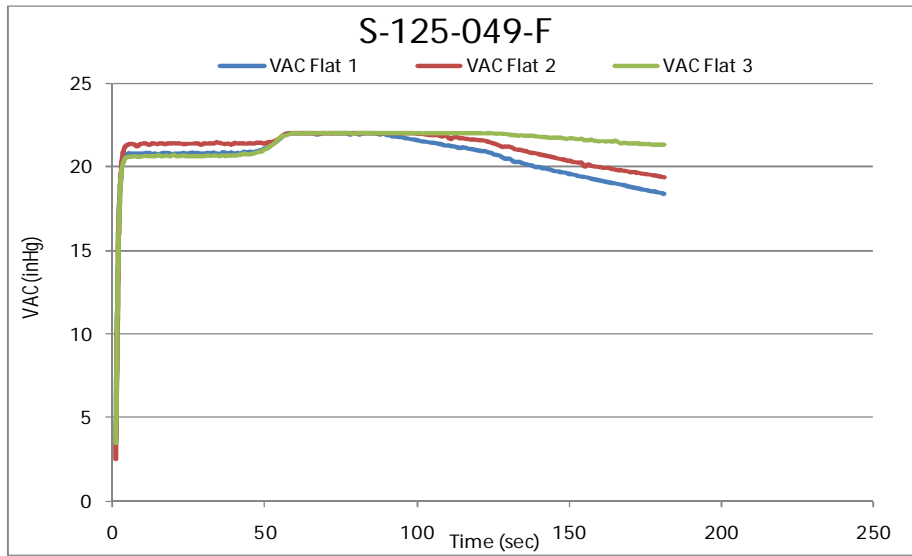


Figure 30: Graph of S-125-049 vacuum vs. time for flat die runs

In this same cross section, the runs using the shear die set produced results shown in Figure 31.

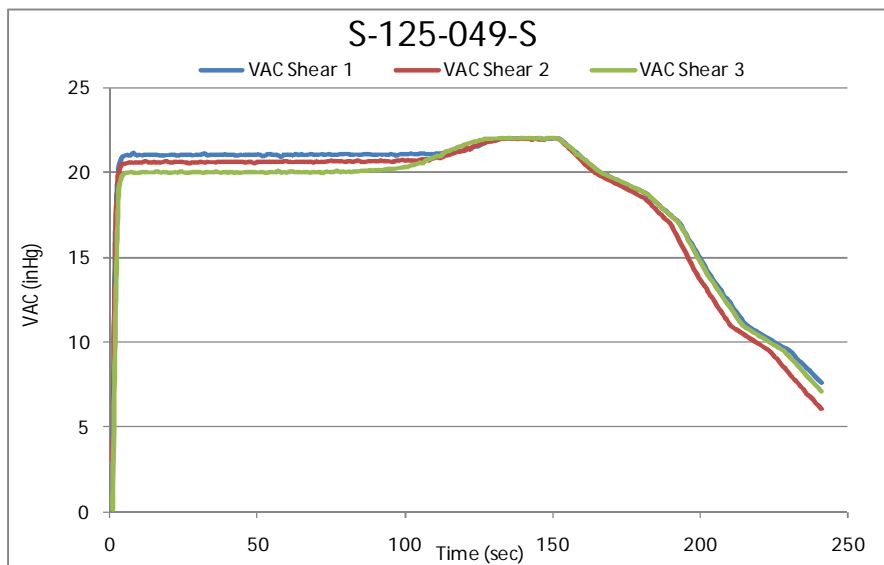


Figure 31: Graph of S-125-049 vacuum vs. time for shear die runs

On these shear runs, the times corresponding to the testing segments occurred at 150 and 180 seconds respectively. Between 150 to 180 seconds, the average leak rate from the samples was .1149 inHg/sec. After releasing the head of the Instron, this leak increased to .2035 inHg/sec, again displaying the effect of spring back on the quality of a seal. Both of these values are larger than the flat die showing that the flat die sealed this cross section more effectively than the shear die. Continuing on to the wedge shaped die runs, Figure 32 displays these curves. A complete record of these vacuum versus time plots can be seen in Appendix A.

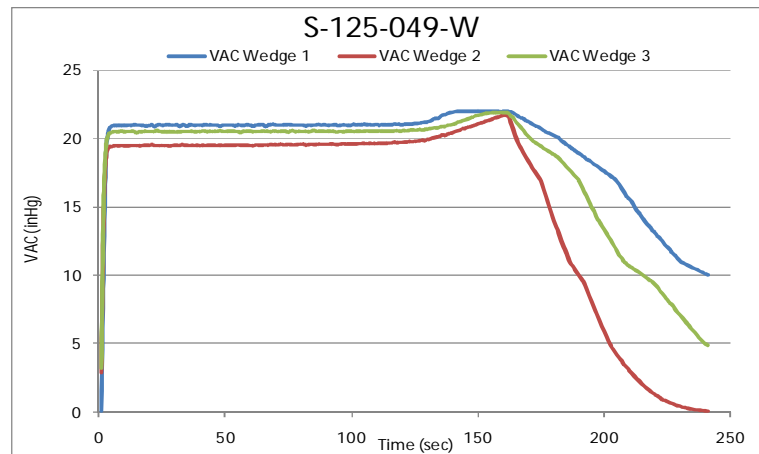


Figure 32: Graph of S-125-049 vacuum vs. time for wedge die runs

During the first leak detection segment corresponding to the time after vacuum pump was turned off and the release of the Instron head, the wedge samples produced an average leak rate of 0.2079 inHg/sec. After releasing the head, the leak rate became 0.2207 inHg/sec. In this case, the flat die again produced the best seal between the three die sets.

This trend of the flat die set producing the best seal among the three die sets maintained consistent throughout the testing of the stainless steel specimens almost 100% of the time in the various cross sections. The copper specimens did not have a consistent die set that produced the

best seal when the head was still engaged in the specimen. However once the load was removed, the flat die again became the clear die set that produced the best seal. A table of the stainless steel material average leak rates is provided in Table 6, and a table of the copper material average leak rates in Table 7. The highlighted cells indicate the test run with the lowest leak rate among the three die sets. Graphical representations of the leak rates for stainless steel are also provided in Figure 33 and Figure 34 while the copper material is displayed in Figure 35 and Figure 36.

Table 6: Table showing leak rates of stainless steel crimped samples with load on and load off for 3 die sets

	Leak Rates of Stainless Steel (inHg/sec)					
	Flat on	Flat off	Shear On	Shear off	Wedge on	Wedge off
S-125-020	0.034	0.100	0.213	0.434	0.287	0.280
S-125-028	0.064	0.266	0.159	0.533	0.165	0.493
S-125-035	0.138	0.267	0.149	0.293	0.114	0.317
S-125-049	0.015	0.031	0.115	0.204	0.208	0.221
S-187-020	0.092	0.354	0.149	1.697	0.163	1.356
S-187-028	0.106	0.440	0.251	1.296	0.047	1.980
S-250-010	0.087	0.248	0.112	0.530	0.139	1.963
S-250-020	0.087	1.235	0.194	2.062	0.250	1.884
X-250-020	0.007	1.543	0.012	2.763	0.167	2.183
S-250-028	0.062	0.415	0.104	2.081	0.157	0.892

Table 7: Table showing leak rates of copper crimped samples with load on and load off for 3 die sets

	Leak Rates of Copper (inHg/sec)					
	Flat on	Flat off	Shear on	Shear off	Wedge on	Wedge off
C-125-014	0.033	0.077	0.010	0.310	0.175	0.495
C-125-030	0.038	0.052	0.221	0.191	0.171	0.144
C-125-032	0.277	0.021	0.131	0.100	0.273	0.144
C-187-030	0.040	0.187	0.010	0.353	0.069	0.259
C-187-032	0.151	0.187	0.289	0.109	0.102	0.215
C-250-030	0.176	0.145	0.000	0.278	0.240	0.237
C-250-032	0.080	0.224	0.067	0.819	0.011	1.170
C-250-049	0.016	0.032	0.035	0.336	0.000	0.291
C-250-065	0.016	0.061	0.029	0.303	0.045	0.264

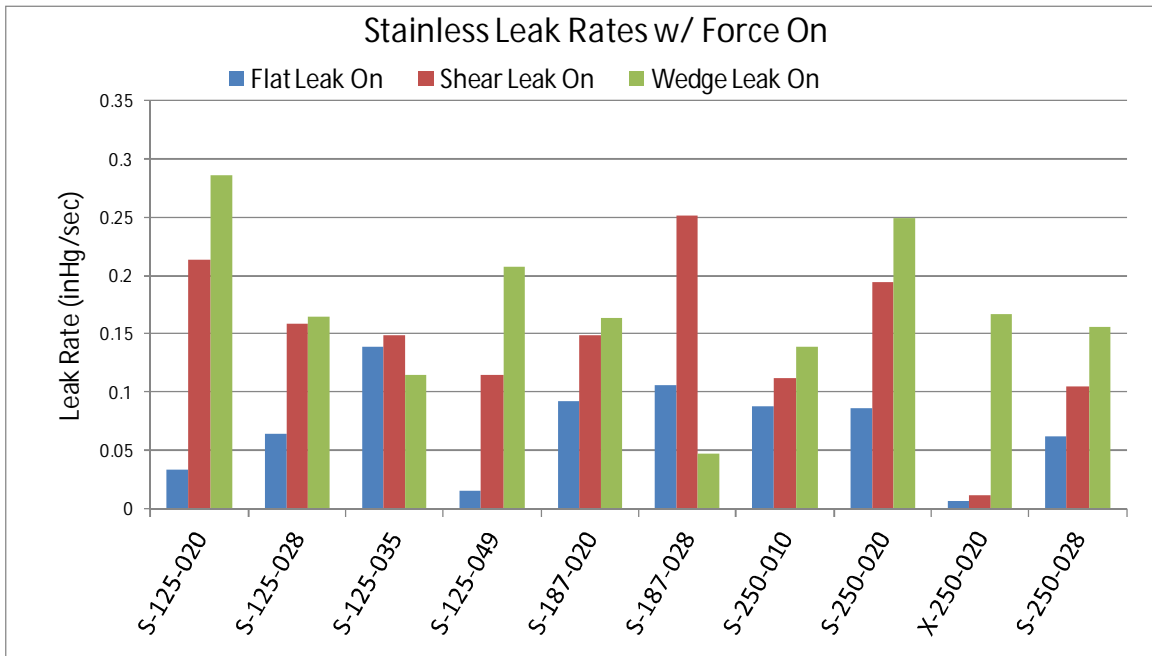


Figure 33: Chart depicting leak rates of stainless steel crimped samples for 3 die sets with force on

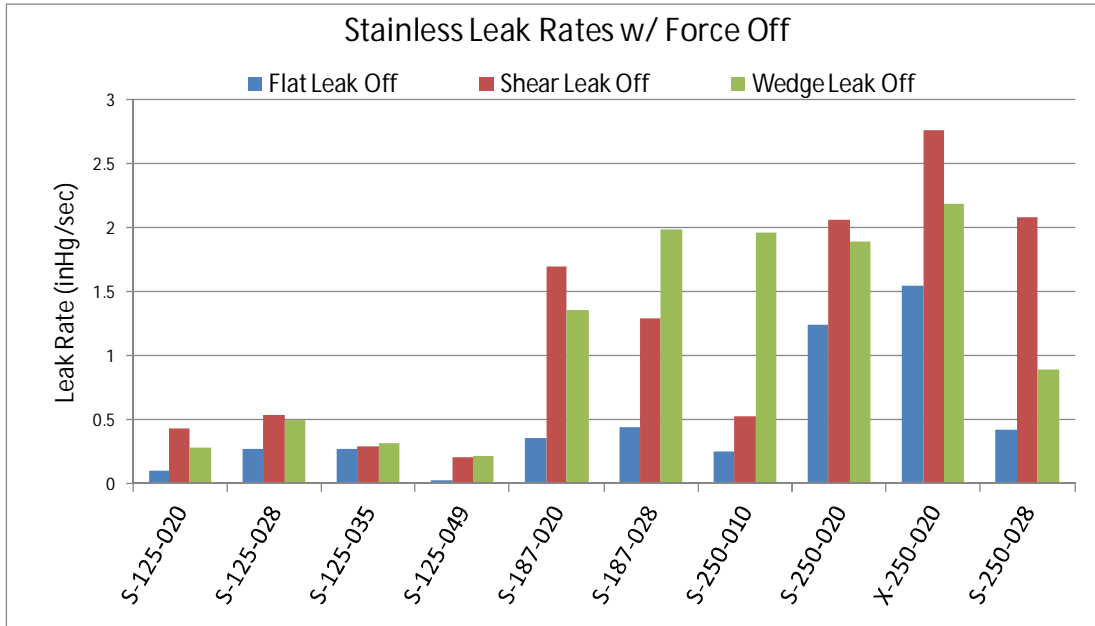


Figure 34: Chart depicting leak rates of stainless steel crimped samples for 3 die sets with force off

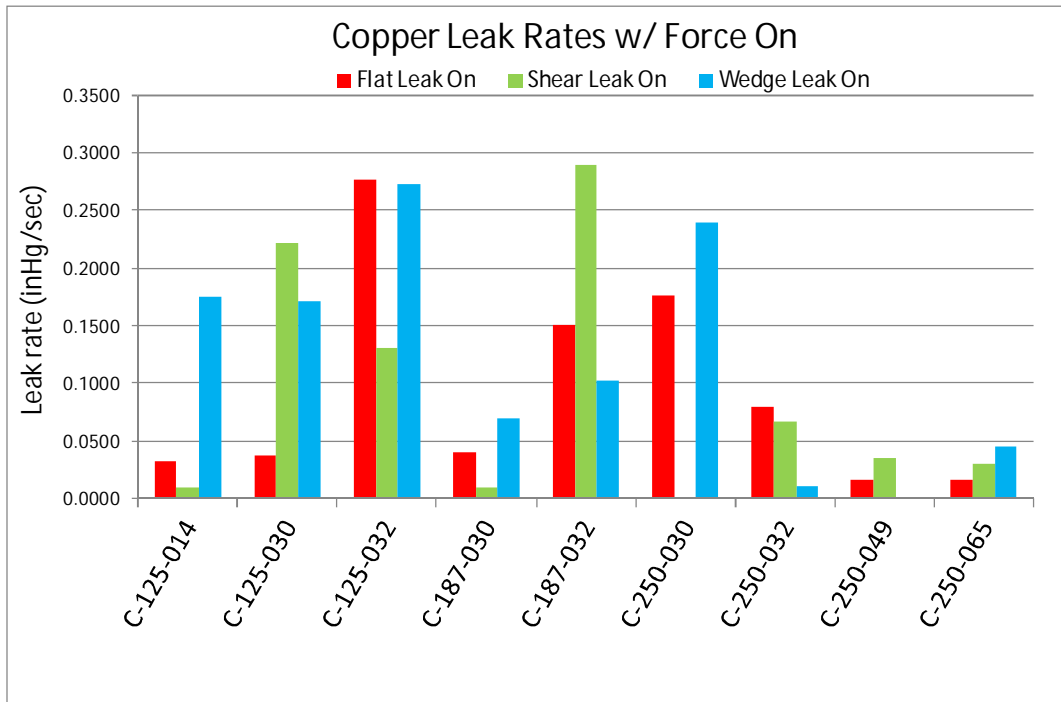


Figure 35: Chart depicting leak rates of copper crimped samples for 3 die sets with force on

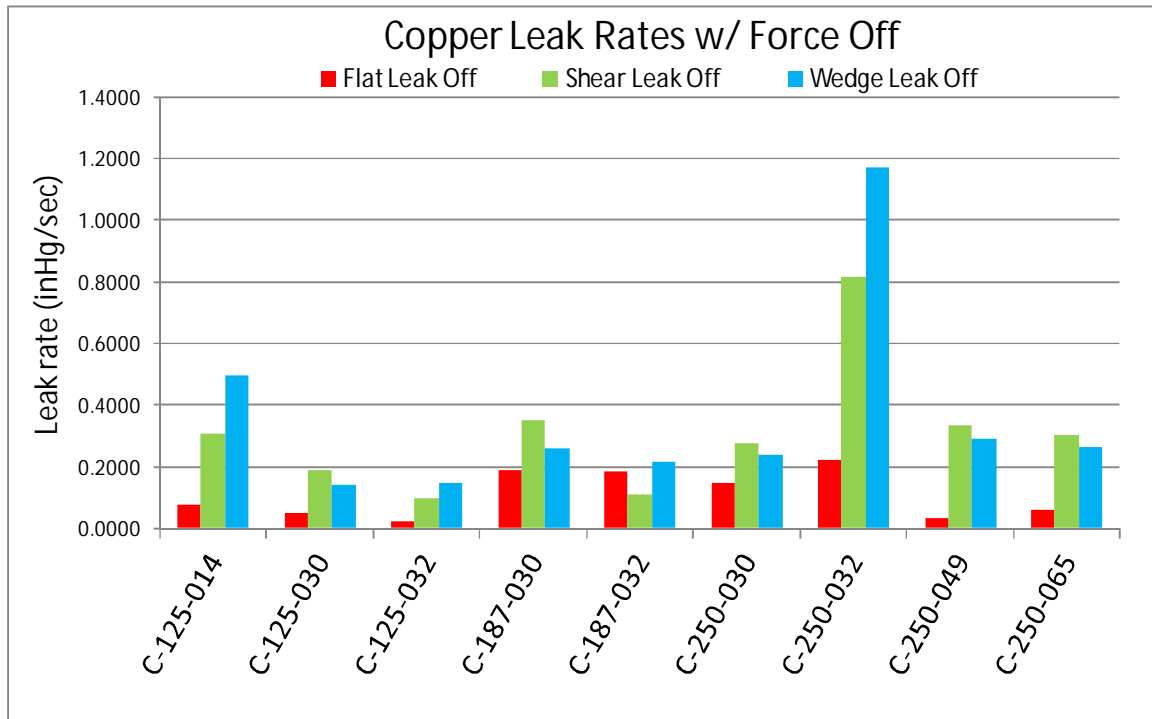


Figure 36: Chart depicting leak rates of copper crimped samples for 3 die sets with force off

#### Maximum Loads and Displacements Seen During Test Runs

The second aspect analyzed after testing was the maximum amount of force required to reach the seal point during each test run. This maximum force was dependent on the area of the die that the sample was in contact with. The material stiffness and the cross sectional area of the tube being crimped also had direct impact on the resultant maximum force. Recalling the dimensions of the die sets, the flat die had a contact dimension of 0.5" in width, the shear die had a contact dimension of 0.125" in width, and the wedge die had little area available due to its pointed construction.

The displacements that occurred during each test also varied throughout the testing. The inside diameter of the sample, which was a directly related to the outside diameter and wall thickness, governed the maximum displacement seen during a test run. Once the inside walls of

the tube had been pushed together thereby sealing the tube from outside air, the system would begin to build vacuum up to the maximum capability of the pump. At this point, the Instron head would be halted. A notable difference among the die sets was the anvil paired with the shear and wedge sets. As stated previously, this anvil had a square channel removed down its centerline. Both the shear and wedge hammer deformed the material downward into this cut channel resulting in larger displacements when compared to that of the flat die which used an anvil that solely protruded upward. Typical results of crimped samples are shown in Figure 37 .

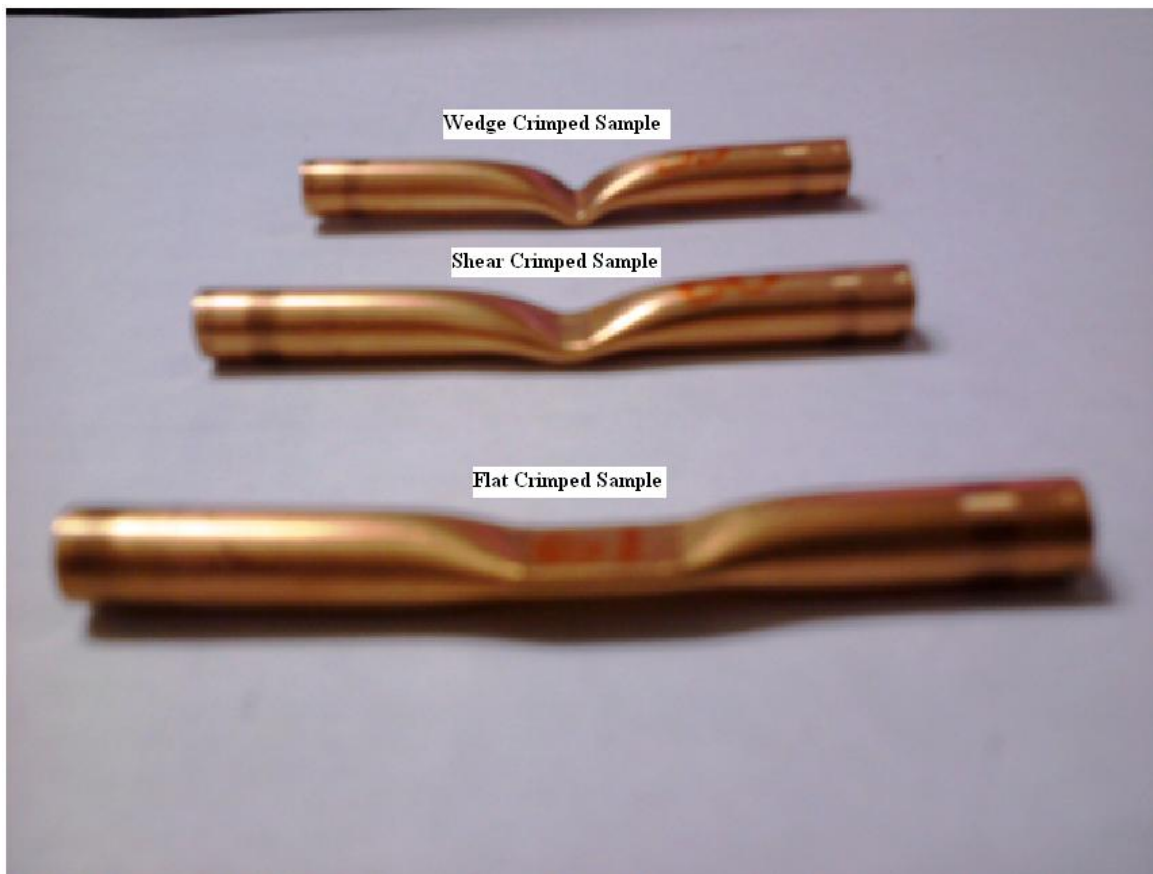


Figure 37: Image of resulting crimped sample shape after testing for 3 die sets

A plot of the maximum loads for the copper material is shown in Figure 38 below. This plot shows that the loads exerted by the flat die set are the largest among the three sets of dies. Also visible on the chart is the rather steady increase in load as the respective diameters and wall thicknesses increase. This occurrence is linked to the increasing cross sectional area of the samples. As the area increases, a larger amount of material must be deformed thus requiring greater load.

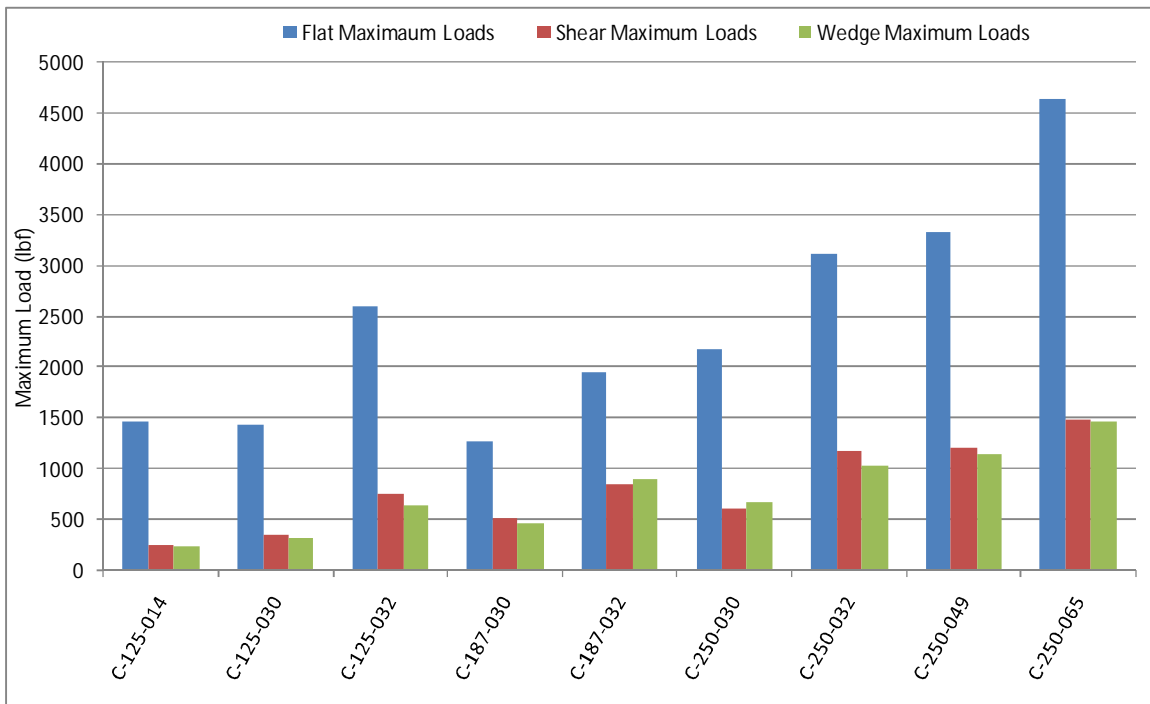


Figure 38: Chart of maximum loads required to reach sealing point for copper material

The next figure displayed is Figure 39 depicting the displacements required for the copper material to reach the sealing point during test runs. As predicted from the construction of the dies, this plot shows that the flat die set needs slightly less displacement to reach the seal point. The channel being cut out of the anvil paired with the shear and wedge shapes result in larger motion required.

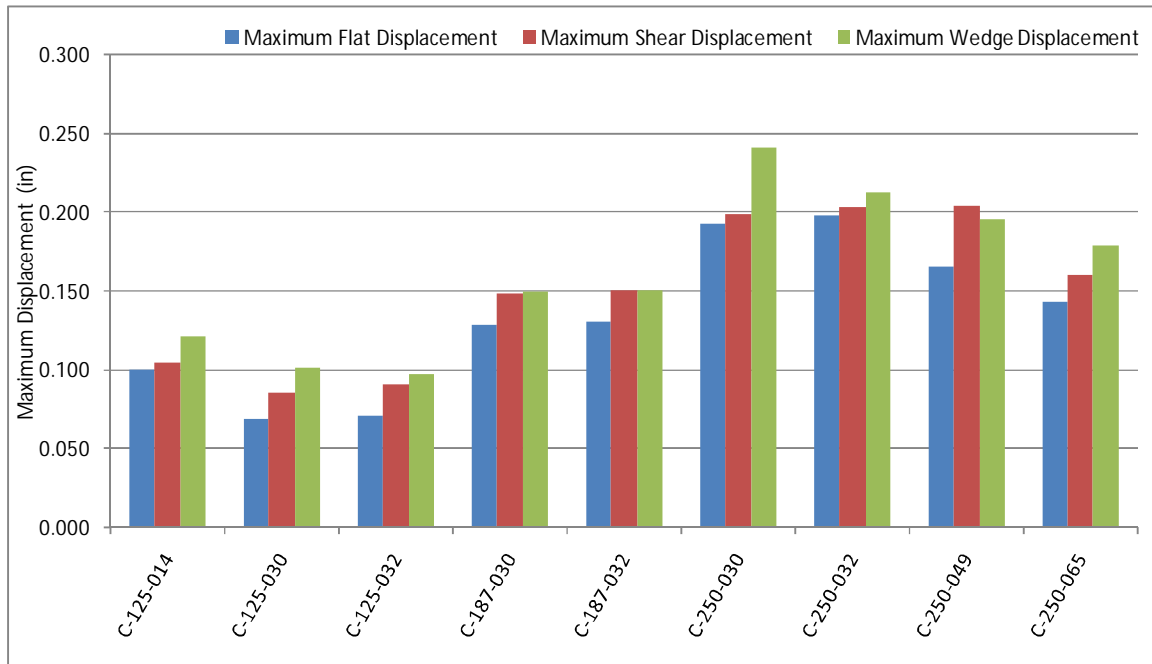


Figure 39: Chart of maximum displacement required to reach sealing point for copper material

The stopping criterion solely being based on the maximum vacuum level allows the displacement and the load to proceed to any value level required to create a seal within the tube walls. Once maximum vacuum was reached, the Instron was stopped by pressing the “stop test” button on the machine. Sampling rate was important during testing to ensure that the LabView program was not lagging behind the Instron loading. By having a sampling rate of 1 Hz, the data was tracked once each second creating a maximum lag time of 1 second. A 1 second lag time is relevant when relating to the feed rate of the Instron. With feed rates of .05”/min or .09”/min used during runs, the Instron head could over-travel by amounts of .00083” or .0015” before the test was stopped. Relative to the total displacement of the Instron, these over-run values are a maximum of 1% of the total displacement seen during any of the test runs, thus contributing little error to any collected data.

Work-Energy Required to Seal a Tube

A direct normalizing link between maximum force and maximum displacement is the resulting work energy that the system experiences. Work is a quantity expressed by multiplying the total force by the total distance traveled in the direction of that force. The parameter of “total force” inserted a requirement for integration of a load versus displacement plot. An example graph of force versus displacement from the start of the test until the Instron head is halted is shown in Figure 40 below. In this test run, the stainless steel tube had dimensions of 0.125” for outside diameter, the wall thickness was 0.020”, and this was the second test of the wedge die set.

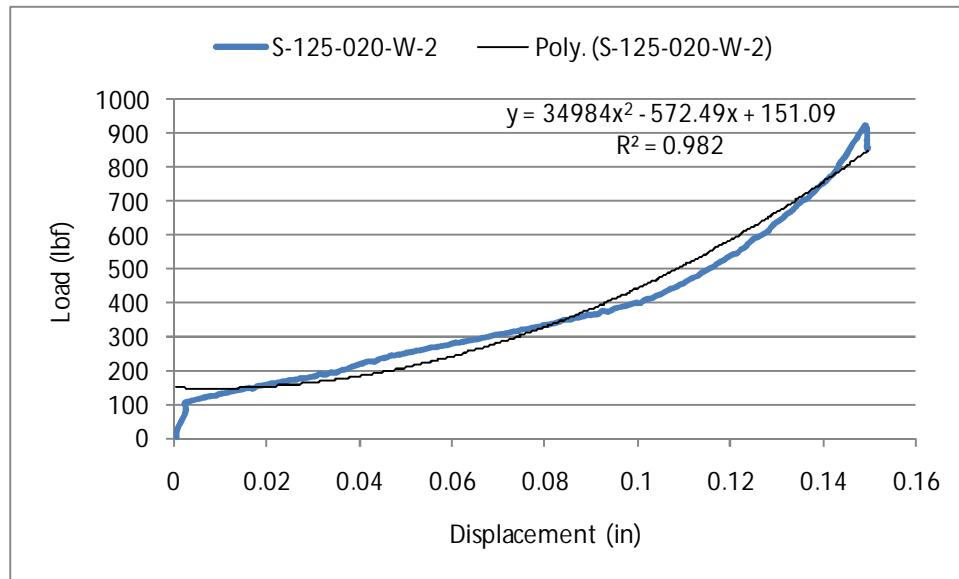


Figure 40: Example plot of load vs. Displacement up to sealing point

On the chart shown, a second degree polynomial trendline has been fitted to the data with a correlation coefficient of .982. Every test run, however similar, had its own unique trend equation and overall shape. A majority of the test runs exhibited a steepening portion just before the sealing point was reached. This complex shape required the use of a polynomial fit line as

opposed to a simple linear regression. All data sets were fit to an  $R^2$  value of at least .930. By collecting the three coefficients of the equation of the trendlines, the area under the curve can be found. This area corresponds to the integral of the equation between 0 and maximum displacement – or when related to this research, the work energy of the test. For this specific case, the form is:

$$W = \int_0^{.1496} 34984x^2 - 572.49x + 151.09 dx \quad (11)$$

Solving this integral, a third degree polynomial is obtained and after substituting the limits, the solution for W is equal to 55.2lbf-in. Every test run was integrated in this same fashion and the resulting work energy values tabulated in Table 8 for copper and Table 9 for stainless steel.

Table 8: Tabulated work energy for all test runs of copper material

	Flat Energy (lbf-in)		AVG Flat	Shear Energy (lbf-in)		AVG Shear	Wedge Energy (lbf-in)		AVG Wedge
C-125-014	C-125-014-F-1	30.7	31.4	C-125-014-S-1	14.3	14.5	C-125-014-W-1	14.1	13.8
	C-125-014-F-2	34.0		C-125-014-S-2	14.4		C-125-014-W-2	13.3	
	C-125-014-F-3	29.7		C-125-014-S-3	14.8		C-125-014-W-3	14.0	
C-125-030	C-125-030-F-1	34.6	34.7	C-125-030-S-1	17.7	17.2	C-125-030-W-1	13.2	16.4
	C-125-030-F-2	34.9		C-125-030-S-2	16.2		C-125-030-W-2	16.0	
	C-125-030-F-3	34.6		C-125-030-S-3	17.6		C-125-030-W-3	19.9	
C-125-032	C-125-032-F-1	76.2	76.6	C-125-032-S-1	43.5	44.8	C-125-032-W-1	42.2	37.5
	C-125-032-F-2	78.4		C-125-032-S-2	40.4		C-125-032-W-2	37.4	
	C-125-032-F-3	75.2		C-125-032-S-3	50.6		C-125-032-W-3	32.9	
C-187-030	C-187-030-F-1	46.7	48.4	C-187-030-S-1	35.1	35.2	C-187-030-W-1	29.5	29.7
	C-187-030-F-2	49.3		C-187-030-S-2	34.5		C-187-030-W-2	30.7	
	C-187-030-F-3	49.1		C-187-030-S-3	35.9		C-187-030-W-3	28.8	
C-187-032	C-187-032-F-1	120.5	121.0	C-187-032-S-1	110.3	101.6	C-187-032-W-1	75.0	81.2
	C-187-032-F-2	120.9		C-187-032-S-2	94.0		C-187-032-W-2	84.0	
	C-187-032-F-3	121.5		C-187-032-S-3	100.4		C-187-032-W-3	84.6	
C-250-030	C-250-030-F-1	86.1	77.5	C-250-030-S-1	37.3	39.1	C-250-030-W-1	58.5	54.2
	C-250-030-F-2	73.0		C-250-030-S-2	39.8		C-250-030-W-2	54.1	
	C-250-030-F-3	73.4		C-250-030-S-3	40.3		C-250-030-W-3	50.1	
C-250-032	C-250-032-F-1	213.0	218.3	C-250-032-S-1	137.5	137.4	C-250-032-W-1	132.2	131.3
	C-250-032-F-2	221.1		C-250-032-S-2	138.0		C-250-032-W-2	128.7	
	C-250-032-F-3	220.8		C-250-032-S-3	136.9		C-250-032-W-3	133.2	
C-250-049	C-250-049-F-1	169.5	172.3	C-250-049-S-1	103.4	103.3	C-250-049-W-1	110.3	107.6
	C-250-049-F-2	182.9		C-250-049-S-2	101.5		C-250-049-W-2	108.6	
	C-250-049-F-3	164.5		C-250-049-S-3	105.0		C-250-049-W-3	103.9	
C-250-065	C-250-065-F-1	184.2	199.6	C-250-065-S-1	129.9	126.2	C-250-065-W-1	131.7	132.0
	C-250-065-F-2	203.0		C-250-065-S-2	123.9		C-250-065-W-2	133.7	
	C-250-065-F-3	211.7		C-250-065-S-3	124.7		C-250-065-W-3	130.6	

Table 9: Tabulated work energy for all test runs of stainless steel material

	Flat Energy (lbf-in)		AVG Flat	Shear Energy (lbf-in)		AVG Shear	Wedge Energy (lbf-in)		AVG Wedge
S-125-020	S-125-020-F-1	82.0	78.0	S-125-020-S-1	36.8	37.2	S-125-020-W-1	60.3	60.5
	S-125-020-F-2	71.4		S-125-020-S-2	37.8		S-125-020-W-2	55.2	
	S-125-020-F-3	80.7		S-125-020-S-3	37.2		S-125-020-W-3	66.0	
S-125-028	S-125-028-F-1	95.4	96.1	S-125-028-S-1	50.1	54.0	S-125-028-W-1	73.3	73.3
	S-125-028-F-2	96.4		S-125-028-S-2	49.7		S-125-028-W-2	75.2	
	S-125-028-F-3	96.6		S-125-028-S-3	62.3		S-125-028-W-3	71.3	
S-125-035	S-125-035-F-1	110.0	109.8	S-125-035-S-1	81.5	72.5	S-125-035-W-1	108.9	105.2
	S-125-035-F-2	107.4		S-125-035-S-2	63.1		S-125-035-W-2	96.9	
	S-125-035-F-3	112.0		S-125-035-S-3	72.9		S-125-035-W-3	109.8	
S-125-049	S-125-049-F-1	92.3	101.4	S-125-049-S-1	108.3	111.2	S-125-049-W-1	104.5	121.6
	S-125-049-F-2	96.7		S-125-049-S-2	118.6		S-125-049-W-2	132.4	
	S-125-049-F-3	115.1		S-125-049-S-3	106.8		S-125-049-W-3	128.0	
S-187-020	S-187-020-F-1	85.8	90.7	S-187-020-S-1	51.8	49.4	S-187-020-W-1	57.2	52.7
	S-187-020-F-2	95.8		S-187-020-S-2	46.9		S-187-020-W-2	51.9	
	S-187-020-F-3	90.4		S-187-020-S-3	49.5		S-187-020-W-3	48.9	
S-187-028	S-187-028-F-1	157.6	164.7	S-187-028-S-1	114.7	119.2	S-187-028-W-1	87.3	88.4
	S-187-028-F-2	165.5		S-187-028-S-2	130.8		S-187-028-W-2	88.7	
	S-187-028-F-3	170.9		S-187-028-S-3	112.2		S-187-028-W-3	89.4	
S-250-010	S-250-010-F-1	59.2	61.0	S-250-010-S-1	40.4	43.2	S-250-010-W-1	25.1	25.3
	S-250-010-F-2	63.4		S-250-010-S-2	44.4		S-250-010-W-2	25.4	
	S-250-010-F-3	60.4		S-250-010-S-3	44.7		S-250-010-W-3	25.3	
S-250-020	S-250-020-F-1	222.4	205.0	S-250-020-S-1	142.1	143.5	S-250-020-W-1	129.0	124.6
	S-250-020-F-2	188.9		S-250-020-S-2	144.8		S-250-020-W-2	127.7	
	S-250-020-F-3	203.6		S-250-020-S-3	143.5		S-250-020-W-3	117.0	
X-250-020	X-250-020-F-1	180.2	210.4	X-250-020-S-1	116.6	115.8	X-250-020-W-1	107.4	109.1
	X-250-020-F-2	242.7		X-250-020-S-2	117.4		X-250-020-W-2	109.7	
	X-250-020-F-3	208.4		X-250-020-S-3	113.4		X-250-020-W-3	110.4	
S-250-028	S-250-028-F-1	245.2	235.2	S-250-028-S-1	200.2	162.2	S-250-028-W-1	172.6	177.1
	S-250-028-F-2	216.2		S-250-028-S-2	149.5		S-250-028-W-2	179.7	
	S-250-028-F-3	244.2		S-250-028-S-3	136.9		S-250-028-W-3	178.9	

In graphical display, Figure 41 shows the copper comparison of the die shapes to the corresponding work required to reach the sealing point while Figure 42 shows the stainless steel.

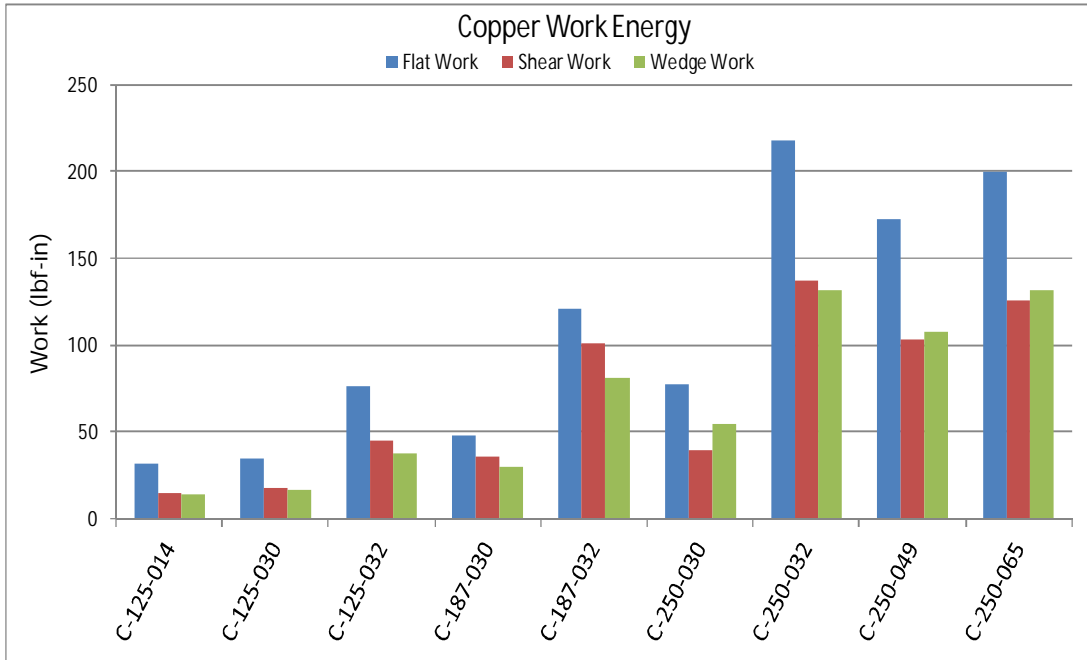


Figure 41: Chart of copper work energy for each cross section and each die set

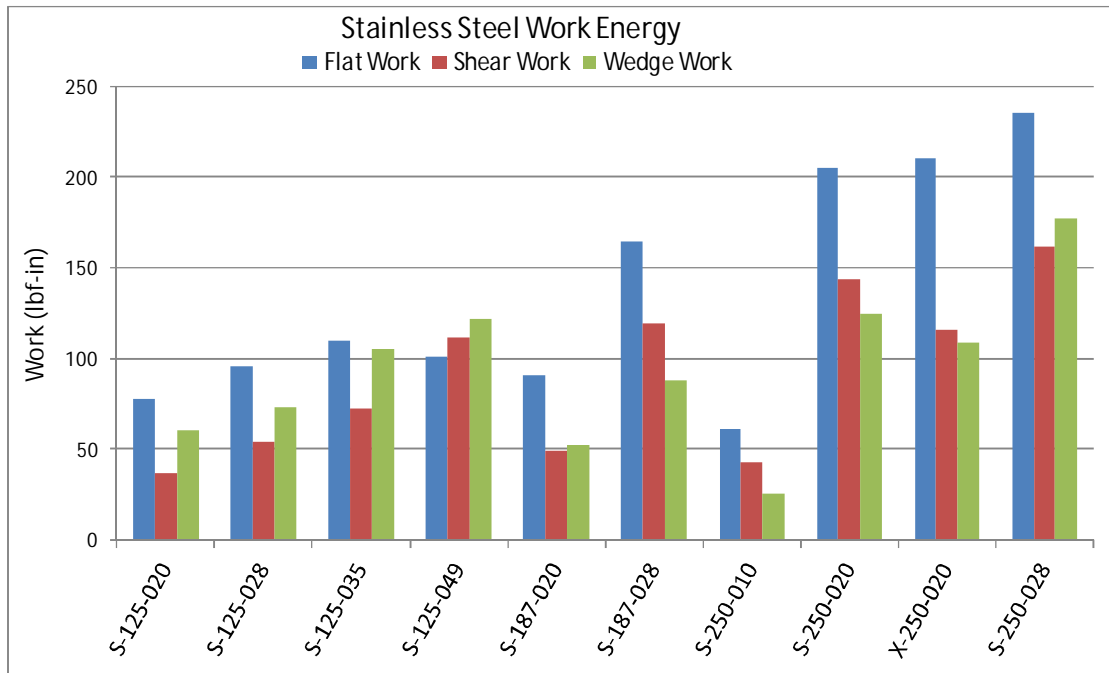


Figure 42: Chart of stainless steel work energy for each cross section and each die set

From the above figures, one can see that the flat die set required more work to reach the sealing point than the wedge and shear sets in every case but one. This occurs due to the dramatically higher forces experienced during the tests utilizing the flat die when compared to the other 2 sets. While the flat die had a slightly lower displacement as shown in Figure 39, this lesser value was not enough to counteract the higher load required the work energy overall for the flat runs.

While Figure 41 and Figure 42 adequately display the values for work energy for the cross section, a normalizing link to show how the data relates to the die sets is needed. In Figure 43, the work energy capturing the load and displacement is compared to the cross-sectional area of the test specimen which captures the diameter and wall thickness.

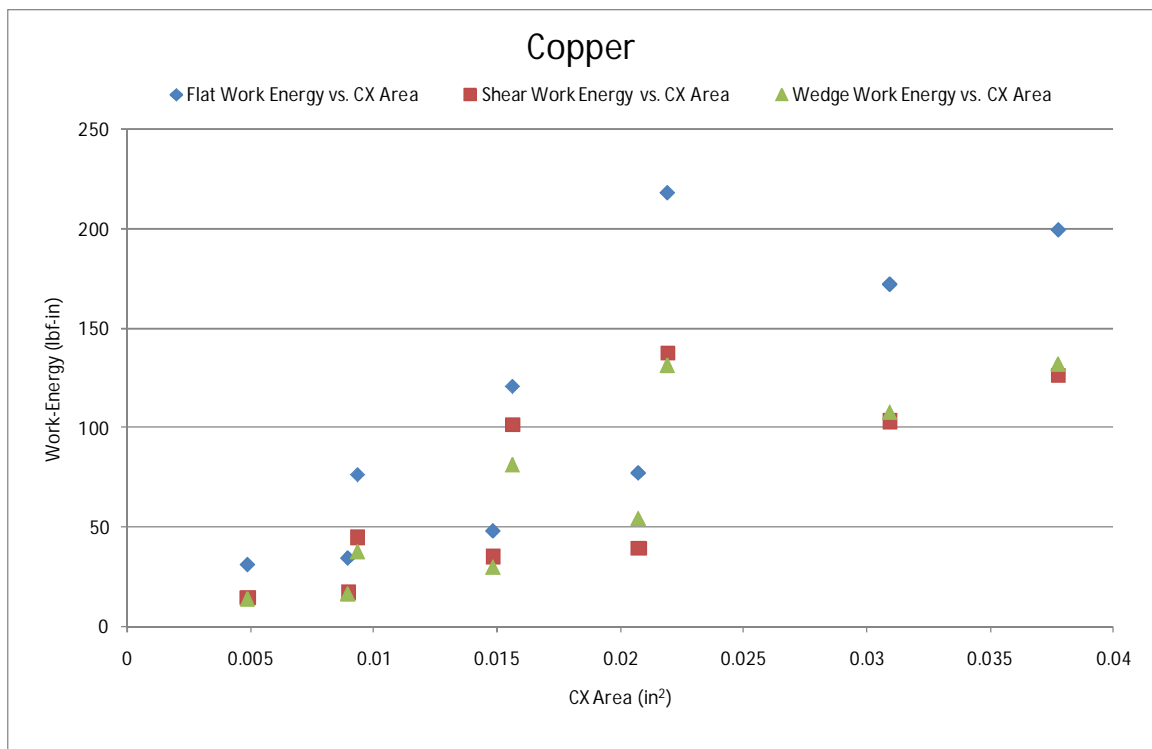


Figure 43: Chart of work energy compared to cross-sectional area for copper

This plot clearly shows that a tube with a larger cross-sectional area requires more work to reach the sealing point. Starting at the left of the plot with an area of  $.0048\text{in}^2$  corresponding to a tube 0.125" in diameter with a wall thickness of 0.014", these specimens required work-energy near 22lbf-in. At the right side of the plot, these points indicate that a cross-sectional area of  $.037\text{in}^2$  corresponding to a tube with a 0.250" diameter and 0.065" wall thickness require an amount of work up to 200lbf-in. Within these values, it is shown that when increasing the cross-sectional area by 7.7x (the smallest cross-section to the largest), the work done by the flat die set increases by 6.4x, the shear die by 9.2x and the wedge die by 10.1x. Correlating these values and establishing a slope for the rate of increase in required work compared to the cross-sectional area on copper material, the flat die slopes to  $5106\text{lbf-in/in}^2$ , the shear die at  $3282\text{lbf-in/in}^2$ , and the wedge die  $3587\text{lbf/in}^2$ . Employing this same technique for the stainless steel material displayed in the chart seen in Figure 44, when the area is increased by  $2.96\text{in}^2$ , the slope of the for the flat die is  $12332\text{lbf-in/in}^2$ , the shear die is  $9660\text{lbf-in/in}^2$ , and the wedge is  $9042\text{lbf-in/in}^2$ .

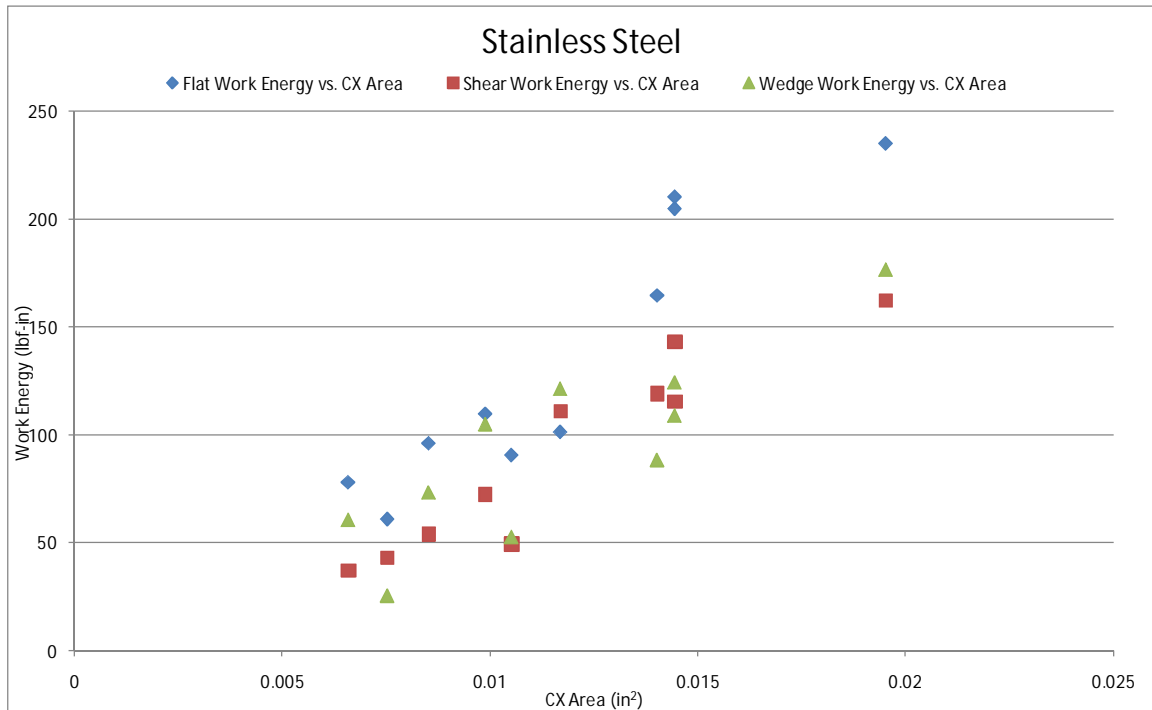


Figure 44: Chart of work energy compared to cross sectional area for stainless steel

### Sectioning/Polishing Results

The sectioning technique using the saw blade to analyze the sealing portion inside the tube walls did not display high quality cuts. The resulting sections became choppy and yielded no insight into how the inner walls of tube sealed together.

3 crimped samples of each die shape of the copper material were selected from the numerous available test runs. These 9 total samples were cut to length and mounted in epoxy as expressed in the sectioning/polishing section of the experimentation chapter. Each of the samples had identical outside diameters of 0.1875" and an equal wall thickness of 0.030". The polishing method revealed how the material was being crimped together between the hammer and anvil during a test run. To obtain a magnified view of the crimped area, these epoxy coins were placed under a Bausch & Lomb variable power microscope set to 12X with model ASZ30L2. 1 crimped

sample of each die set is shown in Figure 45, Figure 46, and Figure 47.

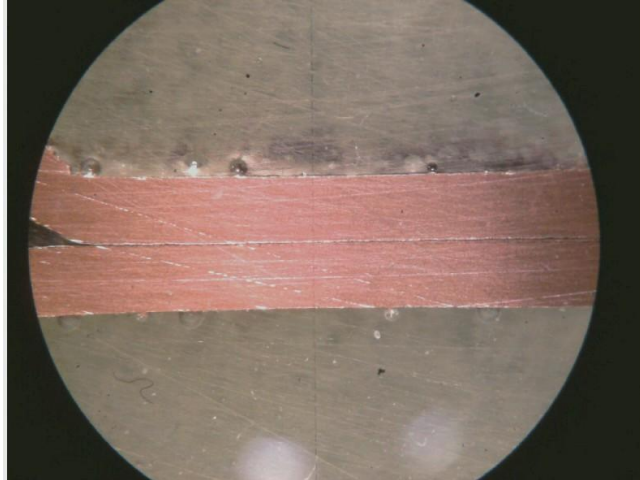


Figure 45: Image of polished flat crimped sample

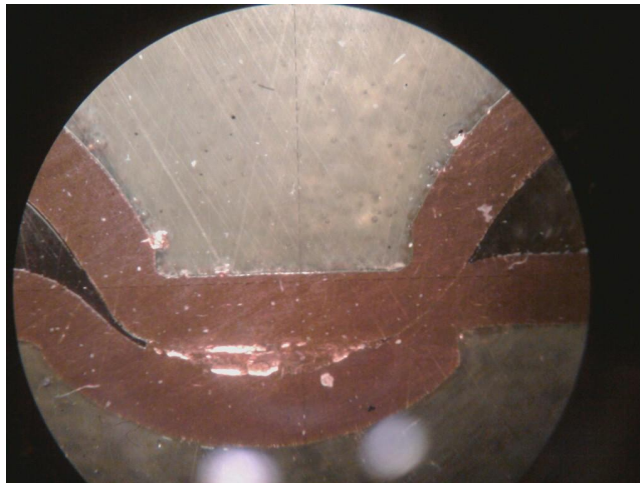


Figure 46: Image of polished shear crimped sample

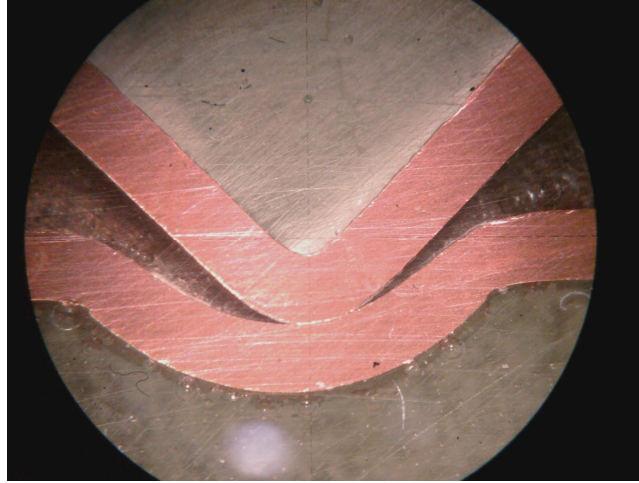


Figure 47: Image of polished wedge crimped sample

The first noticeable feature within the flat die crimped figure is the long, broad area of crimp. The 0.5” contact patch of this die set produced a section which was even too wide for the field of view of the microscope, thus only the left hand portion of the crimp is shown with the right edge being symmetric. The long engagement area unique to the flat die results in the lowest leak rates among the die sets.

Referencing the shear crimped epoxy photo in Figure 46, the image initially reveals that the crimp is not symmetric from the left side to the right side. The clearance between the hammer and anvil on the right edge of crimp is tighter than the left side. Several factors within the testing apparatus or load frame could have produced this anomaly. The threaded mounting holes drilled in the hammer could be off center, or the standoff holes in the bottom surface of the anvil could be shifted slightly to one side. Also the movable head within the load frame itself may be skewed to one side thus not permitting the centerlines of the die sets to line up to one another. It is unknown what effects to maximum load, leak rate, and maximum displacement that a perfectly symmetric crimp with both edges becoming equally smeared together would have on the samples.

To find the cause of this skewed crimp shape during testing, the die sets were marked to keep the front of the die always oriented in the same direction to eliminate any asymmetries within the dies themselves. The hammer and anvil pairs were then indexed from front to back, and also the upper and lower base plates were rotated 180°. No matter the combination of rotating the base plates or swapping die sets end for end, the crimped result was a tighter clearance on the right side of the machine.

Another result of polishing displayed in the figure is the sharp edges of the shear die being directly formed into the tubing. The sealed segment of contact between the inner wall surfaces is rather short in length when compared to that of the flat die. Figure 47 captures the sealed area of the wedge shape die set. Again seen in this figure is the slight offset of the crimp toward the right side.

#### Die Shape Optimization Result

The shape of the optimized die utilized the broad surface contact found in the flat die set as a guideline to its structure. After seeing the wedge sectioning result, it was determined that a sharp point of contact does little in the way of creating a sealing surface within the walls of a crimped tube. Therefore, a die shape with large surface engagement between the hammer and anvil along with rounded curves seemed to best fit the newly gleaned information. In the diagram of Figure 48 below, the new die shape is seen to have rolling contours close to 0.125" in radius. Where the hammer engages the anvil, the mating curve of the outer bend was increased in radius compared to the opposing radius to allow for sufficient clearance for the tube to be compressed but still offer distinct crimping quality. The callout for designation of this new die was set to MY.

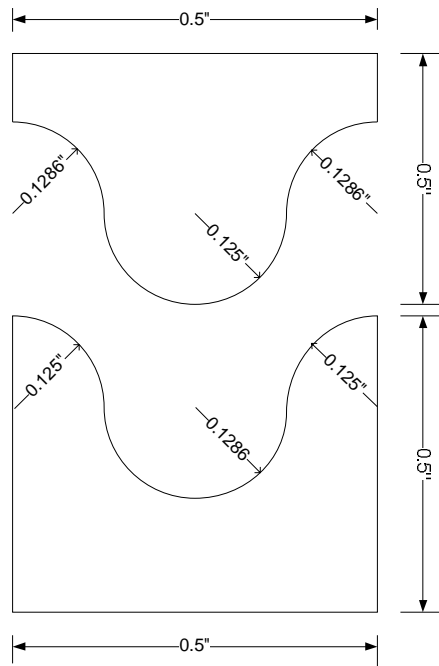


Figure 48: Schematic of the MY attempted optimized die shape

A repeat of the tests conducted on the initial batch of test specimens using 3 runs on all diameters with wall thicknesses of 0.030". These runs performed were a means of establishing a comparative baseline to relate the MY die to the initial batch of tested specimens, not to gain a full set of test data. A numerical comparison used in the above results was the leak rate of the run before and after releasing the load on the tube. Figure 49 and Figure 50 depict the data gathered regarding leak rates among the die sets. According to these charts, the MY die was the best sealer in half of the case where it was tested.

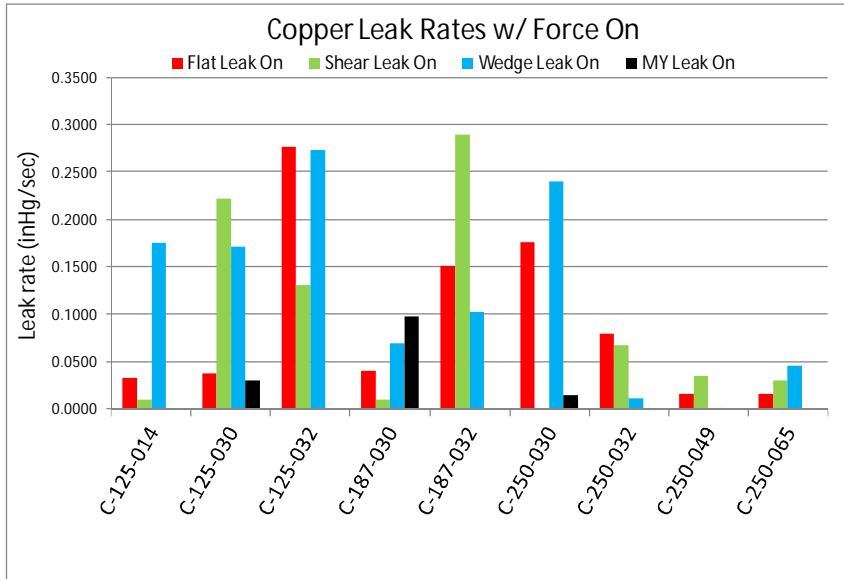


Figure 49: Chart depicting leak rates of copper material with force on with the addition of the MY die

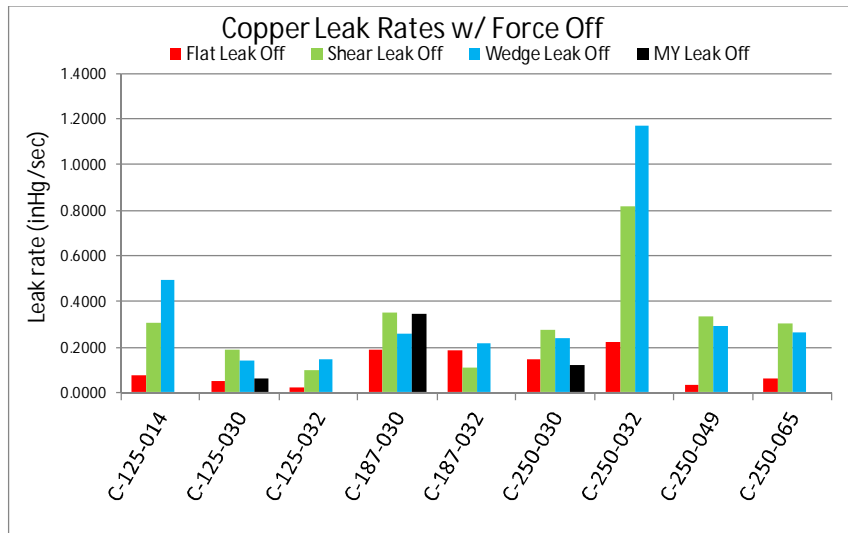


Figure 50: Chart depicting leak rates of copper material with force off with the addition of the MY die

In regards to the load required by the MY die, Figure 51 provides a charted representation of this load, again corresponding to the 0.030” wall thicknesses.

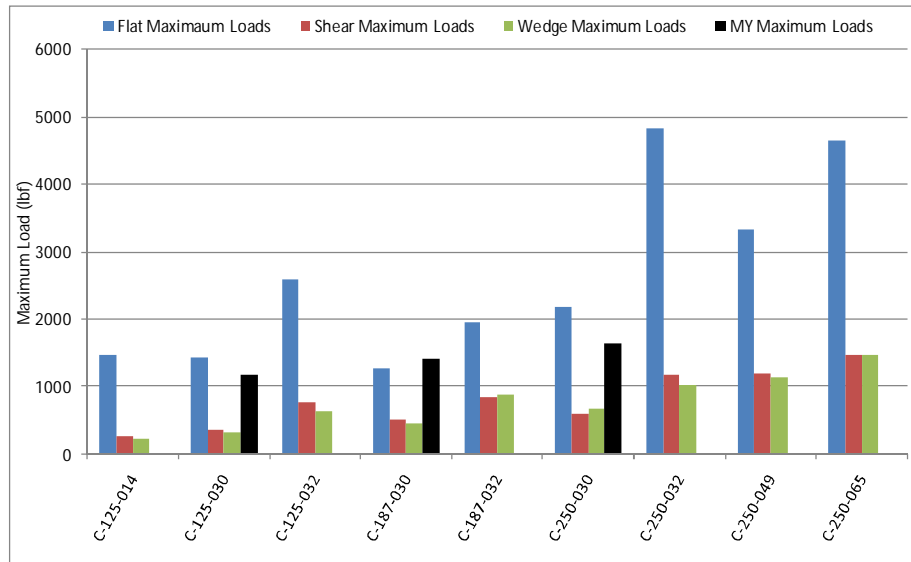


Figure 51: Chart of maximum load required to reach sealing point for copper material with addition of the MY die

This revealed results requiring a large amount deformation required to reach the sealing point as illustrated in Figure 52. Even by only running the 3 cross-sections, empirical results are clearly visible and display comparisons.

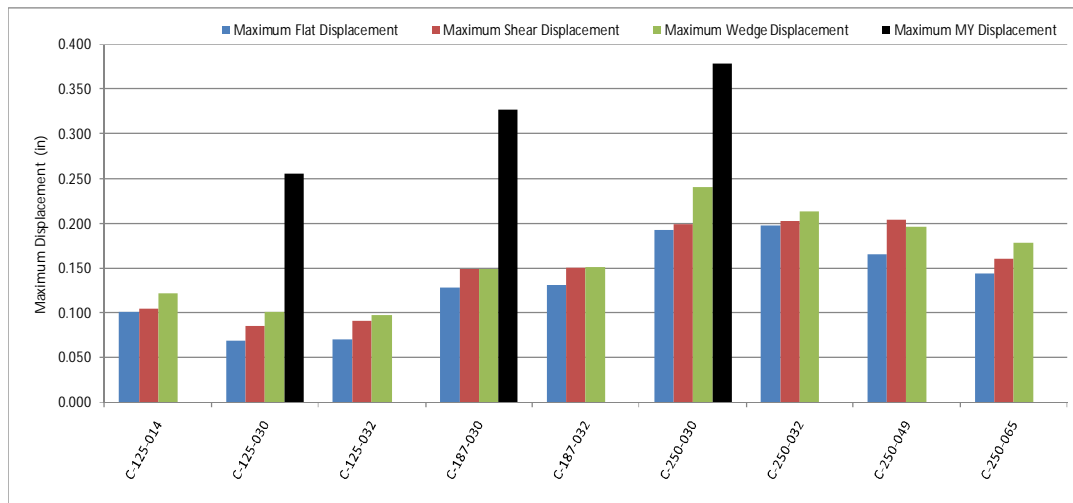


Figure 52: Chart of maximum displacement required to reach sealing point for copper material with addition of my die

Having the deep cut from the center of the anvil required the hammer to progress deeply into the lower section to establish contact to form a sufficient seal. Referring to the 0.125” diameter from the chart, the plot showing the MY die required over 2.5 times the amount of displacement as the other sets.

Table 10 shows all of the loads and displacements for all three die sets and also the attempted optimized die with the highlighted cells indicating the statistical optimum in the category.

Table 10: Table of all average loads and displacements

	LOADS				DISPLACEMENTS			
	AVG Flat LOAD	AVG Shear LOAD	AVG Wedge LOAD	AVG MY LOAD	AVG Flat DISP	AVG Shear DISP	AVG Wedge DISP	AVG MY DISP
C-125-014	1464.54233	256.91433	229.93047		0.10067	0.10467	0.12127	
C-125-030	1436.30487	351.57067	312.50933	1179.253867	0.06830	0.08567	0.10133	0.2562
C-125-032	2592.13600	758.06807	634.72183		0.07040	0.09120	0.09740	
C-187-030	1274.61400	512.63567	459.68167	1417.037	0.12833	0.14833	0.14900	0.326666667
C-187-032	1958.06333	851.43833	893.04400		0.13033	0.15033	0.15067	
C-250-030	2182.67620	598.73417	678.31417	1641.5392	0.19233	0.19873	0.24090	0.3776
C-250-032	4822.98153	1166.57897	1028.52870		0.19820	0.20273	0.21273	
C-250-049	3321.31977	1200.03050	1133.43635		0.16537	0.20423	0.19590	
C-250-065	4644.68173	1472.72800	1470.26963		0.14373	0.15980	0.17883	

The next facet used above in the initial batch of tests to show comparisons between the die sets is work energy which is displayed below in Figure 53. The large amount of displacement required to form a seal during each run pushed this quantity for the MY die to higher values thus not optimizing the energy required to crimp the tube.

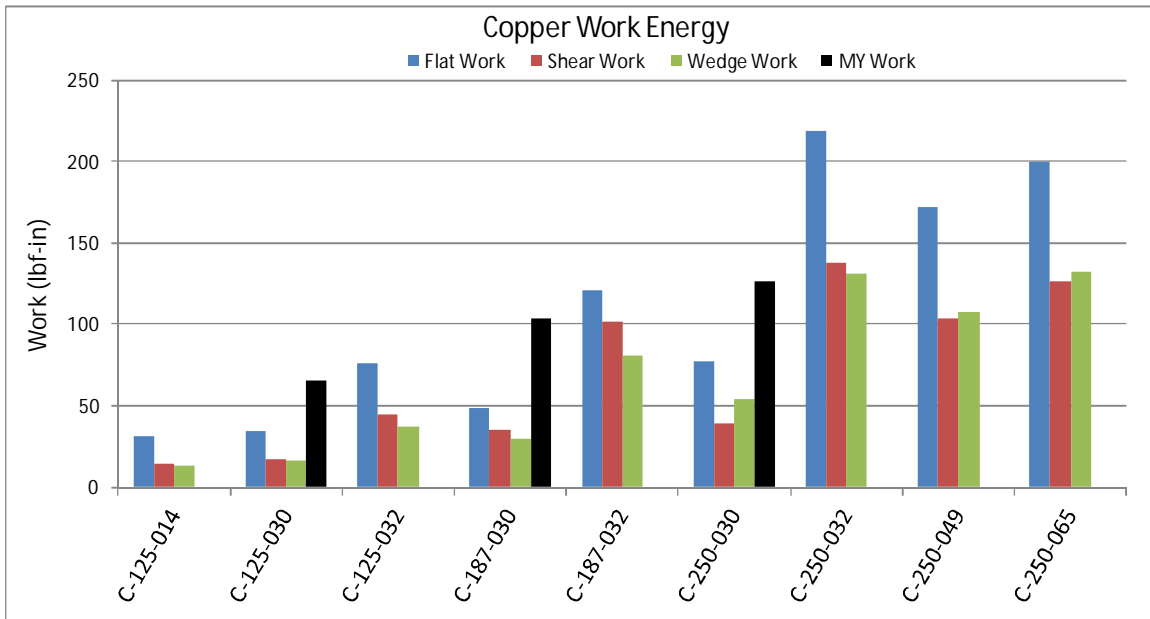


Figure 53: Chart of copper work energy for each cross section with the addition of the MY die

The final qualitative comparison performed on the other die sets was also applied to the MY die set by polishing the tested samples to reveal the internal sealing characteristics of the attempted optimized die. Shown in Figure 54 and Figure 55, the deformed shape suffered the same lateral shift as the other die sets causing only one side of the hammer to fully engage the mating anvil. Even so, this curved method of sealing between surfaces was able to produce the lowest resulting leak rate in half of the cases in which it was tested. Also visible in these figures is the lack of seal in the bottom portion of the tube indicating that the lowest projection of the die had not caused engagement between the inner walls of the tube. Despite the lack of visual linking between the inner walls of the tube, the leak rate of the MY die crimp performed as well or better than the other die sets in the cross sections where it was used.

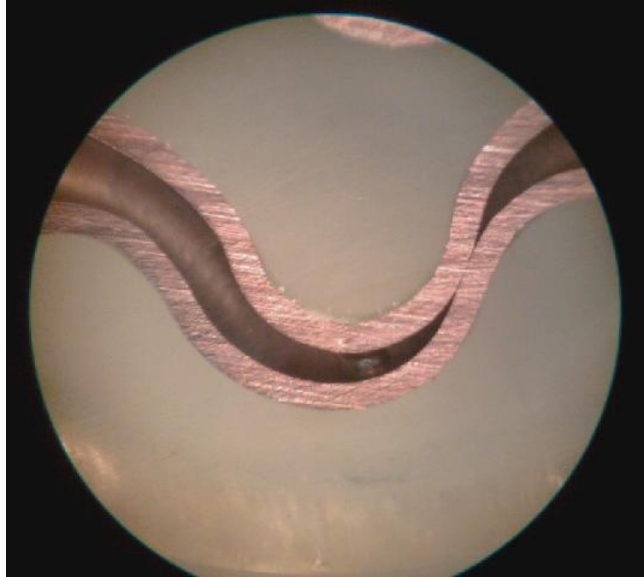


Figure 54: Image of the polished my die set crimped sample (a)

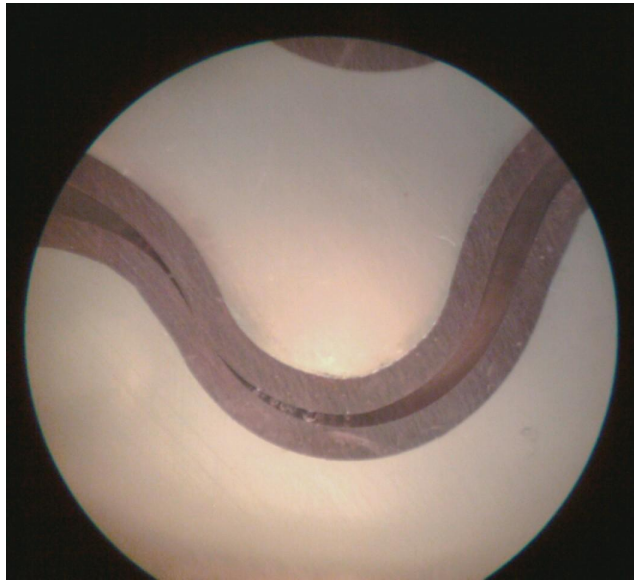


Figure 55: Image of the polished my die set crimped sample (b)

## OPTIMIZATION CONCLUSIONS

### Least Leak Rate Basis

By a drastic margin, the flat die shape worked best to create a seal that held even after the load was released. The large engagement area of this flat die offered more sealing surface between the inside walls of the tube. The main goal of crimping a tube is to stop the flow of a substance within the tube. Therefore, the flat die is best suited should be selected to accomplish this goal.

### Least Load Application Basis

In this category, the wedge was the front runner requiring the least load to establish a vacuum seal. The shape of this die having the smallest engagement area minimized the amount of force required to crimp the tube walls together.

### Least Work Energy Basis and Energy Per Unit Area

In this category, the wedge was the front runner requiring the least work energy to establish a vacuum seal. The combination of the lowest load among the die sets along with a displacement within range of the others gave this wedge shape the win in this category. Expanding on the work energy quantity by comparing it to the cross sectional area of the tube offers beneficial results. Data collected showed the for the flat die set, for every 1 square inch of copper material added to the cross section, an additional 5106lbf-in/in<sup>2</sup> was needed to seal the tube while the stainless steel required 12332lbf-in/in<sup>2</sup>. For the shear die set, the energy per unit area in the copper material equaled 3282lbf-in/in<sup>2</sup> and the stainless steel 9660lbf-in/in<sup>2</sup>. The

wedge die set showed that for copper  $3587\text{ lbf-in/in}^2$  is the necessary amount while the stainless steel requires a value of  $9042\text{ lbf-in/in}^2$ .

### Cross Section of Dies

Attempting to create a shape that minimizes the required energy input while producing the lowest leak rate introduces a variety of issues into the problem. As seen from the initial batch of tests, a broad contact surface between the die and the tube produces the most efficient crimp. When a sharp point or minimal area of contact is used, the leak rate of the resulting crimp is much higher. The factors contributing causing the leak are the opposing springback of the tube attempting to return to the pre-crimped shape, and the opposing residual stresses which lock the walls together, as described in the background above. When optimizing the shape of the die crimping the tube, one must determine which contours result in the highest residual stresses that can resist the springback.

Examining the flat polished samples, the arrows overlaid on Figure 56 depict the directions that the springback forces act. These directions are coherent with internal forces which attempt to return the deformed tube to the pre-crimped shape.

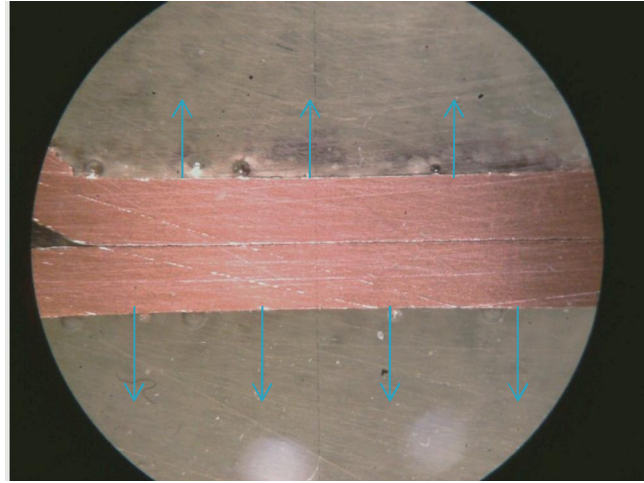


Figure 56: Image displaying the flat die's recovery force direction

Another result of the crimping act is a change in arc length of the walls of a tube. Before crimping, the tube is straight and the shape displayed in the dotted lines of Figure 57.

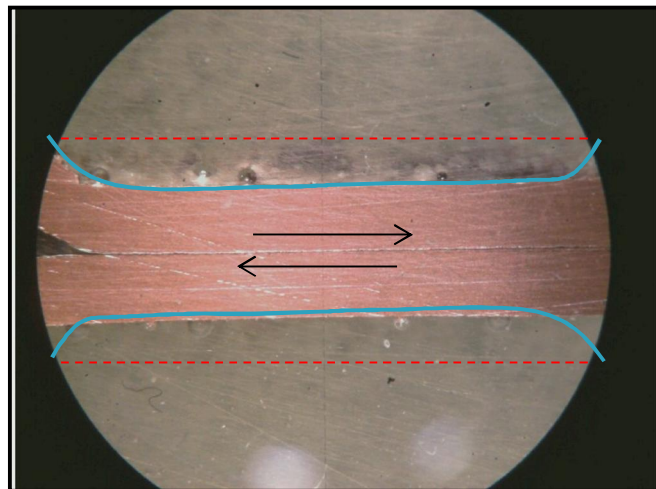


Figure 57: Image showing friction forces resulting from a change in length of the flat crimped tube

After crimping, the new length and contour of the walls is shown as the solid lines in the figure. Since the resulting lines have a longer length due to the end arcing dimension, the recovery force from the length change attempts to straighten the tube in the horizontal direction as well as the

vertical. Through this recovery mechanism and the inside of the tube walls desire to move laterally, a friction force develops at the interface of the crimp displayed as the arrows. A less visible factor assisting with keeping the tube walls locked together is the microstructure of the tubes not being smooth on the inside. Any imperfect grains which protrude from the inside walls act as Velcro when compressed together. It is this lateral friction force developed by the compression that restricts the vertical motion which attempts to separate the tube walls leading to an effective crimp.

In the case of the shear die set, the image in Figure 58 displays the recovery forces existing in those crimped samples. The directions of the springback for this set shown by the arrows are both in the same direction due to the construction of the die set allowing the lower portion of the tube to move downward as the head of the Instron pushes the upper wall into channel that is cut in the die.

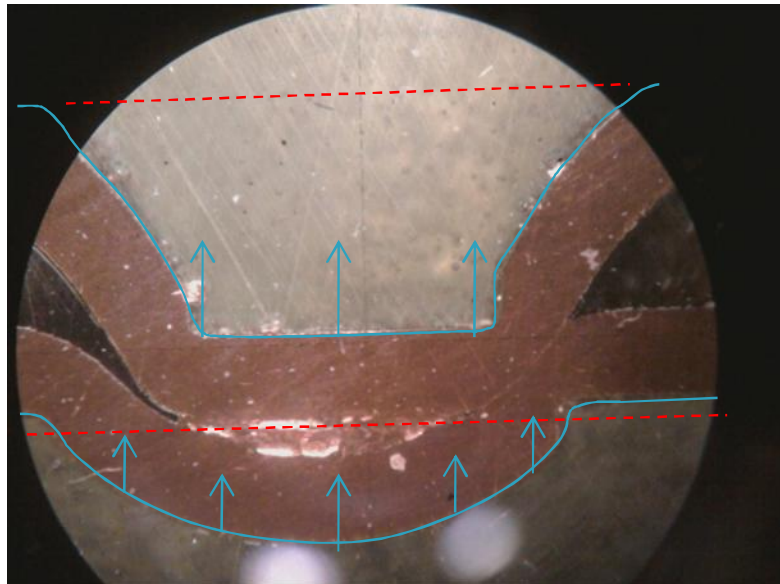


Figure 58: Image displaying the shear die's recovery force direction

Illustrated by the solid lines in Figure 58, the lower wall has been displaced a much smaller amount than the upper wall, again due to the construction of the channel cut in the anvil of the die set. The difference in displacement of the two walls induce a larger recovery force in the top wall as it attempts to elastically spring back to its pre-crimped state. This effectively pulls the two walls apart because the lower wall lags behind the upper wall thus separating the crimp and allowing a leak to occur.

The resistive residual friction force is still present in the shear crimp shape as shown in Figure 59. The arrows on the figure are placed at the only location of contact within the shear die crimp. Compared to the contact area of the flat die, the shear contact is smaller thus offering less force resisting the springback. This quality gives the shear die set a less effective crimp.

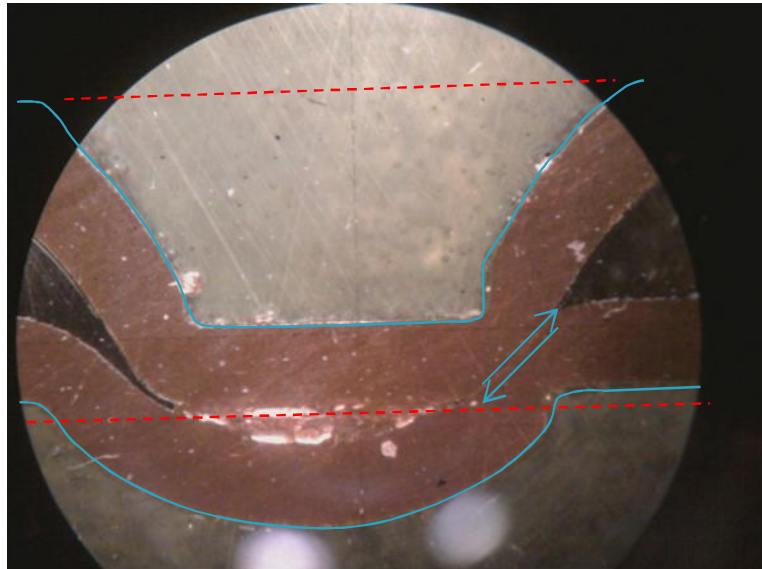


Figure 59: Image showing friction forces resulting from a change in length of the shear crimped tube

The polished section analysis of the wedge die shape show that the resulting recovery forces in Figure 60 exhibit similar characteristics to that of the shear set.

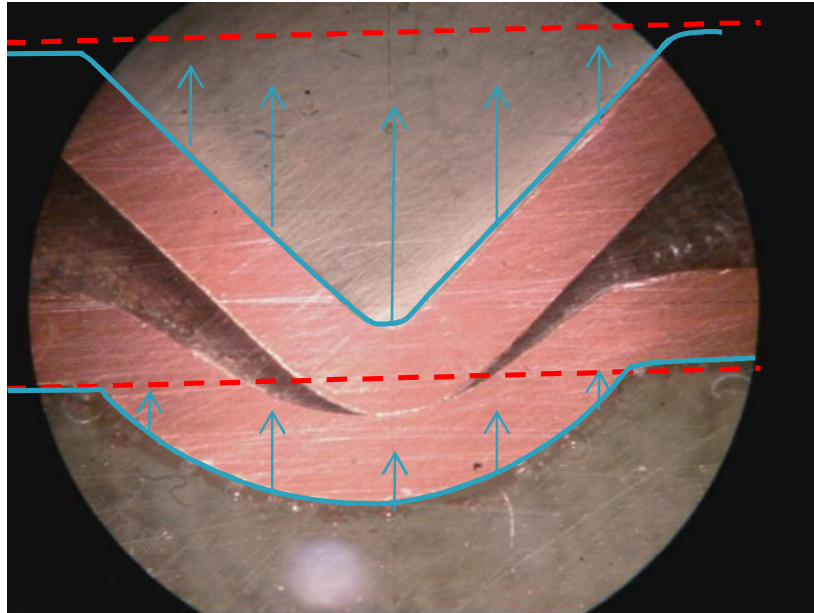


Figure 60: Image displaying the wedge die's recovery force direction

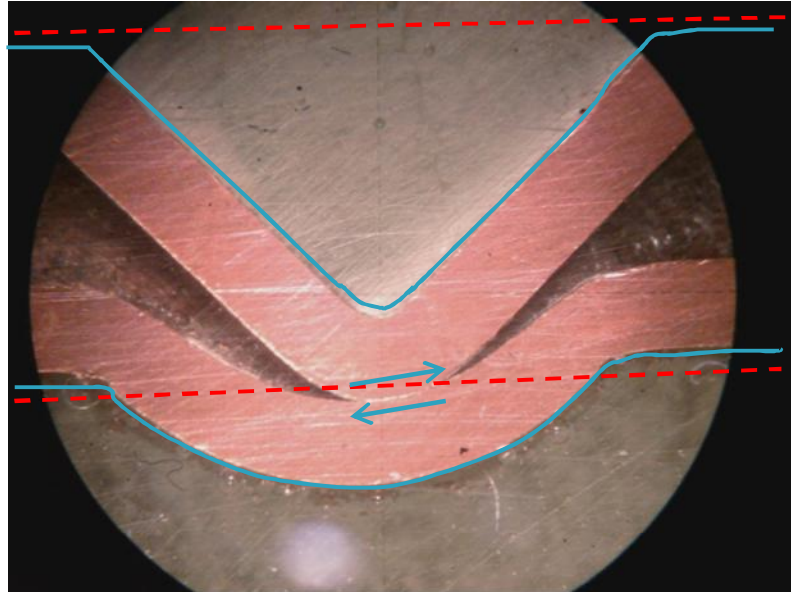


Figure 61 Image showing friction forces resulting from a change in length of the wedge crimped tube

In Table 11, a decision matrix is employed by assigning a numerical value to the shape of the die for the ranking within the category. The categories allow a ranking from 1-3 with the number 1 corresponding to the best statistical shape in the category and 3 the worst. By adding all of the numbers for the individual test runs together, the statistical winner for each category can be selected. The die shape which places consistently high in each of the categories becomes the choice for the best die shape. With this basis, the shear die set becomes the proper selection for an optimal die shape. However, the final place of each die set is slightly misleading by not assigning any weighting factors to the decision matrix. With the main goal being to establish a seal producing the lowest possible leak rate, the final two categories of the decision matrix should have a higher importance factor when choosing the optimal die. With this said, the flat die is by far the most effective choice to seal a tube.

Table 11: Decision matrix to classify optimal die

	LOAD				DISP				WORK ENERGY				FORCE ON				FORCE OFF			
	FLAT	SHEAR	WEDGE	MY	FLAT	SHEAR	WEDGE	MY	FLAT	SHEAR	WEDGE	MY	FLAT	SHEAR	WEDGE	MY	FLAT	SHEAR	WEDGE	MY
C-125-014	3	2	1		1	2	3		3	2	1		2	1	3		1	2	3	
C-125-030	4	2	1	3	1	2	3	4	3	2	1	4	2	3	4	1	1	4	3	2
C-125-032	3	2	1		1	2	3		3	2	1		3	1	2		1	2	3	
C-187-030	3	2	1	4	1	2	3	4	3	2	1	4	2	1	4	3	1	4	3	2
C-187-032	3	1	2		1	2	3		3	2	1		2	3	1		2	1	3	
C-250-030	4	1	2	3	1	2	3	4	3	1	2	4	3	1	4	2	2	4	3	1
C-250-032	3	2	1		1	2	3		3	2	1		3	2	1		1	2	3	
C-250-049	3	2	1		1	3	2		3	1	2		2	3	1		1	3	2	
C-250-049	3	2	1		1	2	3		3	1	2		1	2	3		1	3	2	
	29	16	11	10	9	19	26	12	27	15	12	12	20	17	23	6	11	25	25	5
Ranking in category:	4	2	1	3	1	2	3	4	3	2	1	4	3	1	4	2	1	4	4	2
	FLAT	SHEAR	WEDGE	MY																
	12	11	13	15																
Final Place:	2	1	3	4																

Asymmetry in Test Setup

The cause of skewed offset within the crimped sections revealed in the polishing of the disks was a mystery once discovered. As stated, during testing calibration, attempts to index the die set and base plates front to back did not change the outcome of the crimp. No matter the

combination of rotating the base plates or swapping die sets end for end, the end result was a tighter clearance on the right side of the machine. Within the testing fixture, all dimensions were re-measured for precision and found to be free of error. The concluded cause of the problem was linked to the movable head of the Instron being off center from the bottom stationary portion. A perfectly symmetric testing machine is the base requirement in producing accurate results.

## FUTURE WORK

The most essential item to be studied in the future is the effect of the alignment of the crimping head to create a symmetric seal. A different, properly tuned machine is required for this work. Or the other option would be to recreate the base plates of the holding fixture with this misalignment built into the base. Creating a symmetric crimp will offer information with much more clout than the current works.

To enable mathematical analysis of the crimping scenario, an intense Finite Element Analysis model should be created to insert the total strain quantity into the power law theory. This theory may provide the correct analytical results which properly relate to the experimental data.

This data collected stemmed from a quasi-static loading condition where the head slowly progressed downward into the tube. In real-world situations, crimping pliers, or the powder-actuated crimping tool exert a force very rapidly and impart strain to the material at a very high rate. The effect of strain rate can be studied with a drop tower test or similar setup to determine if the energy required in a quasi-static case is identical or proportional to the dynamic impact load case.

Expansion of the wall thicknesses into thicker samples will also be a future path to proceed with. A material with a higher yield stress and a higher modulus is needed to accomplish this work. Deformation of the die sets when attempting to crimp the thicker-walled stainless steel introduces error into the test runs. Within this study, only the cross sections that did not deform the dies were studied.

A capability of some loading machines like the Instron is the ability to run a portion of the test, reach a stop point, and then proceed with a different loading condition. A secondary test profiler is required to specify this alternate and reversed rate that the machine would travel. By

having this feature, the test runs could be essentially repeated up until the sealing point where the machine stopped, but then add in a slow, upward travel rate for the movable head. In these tests, once sealing had occurred, the head was stopped and left at rest, then retracted instantaneously to the gage length. After the head had fully deformed the tube and while it would be retracting slowly, the reaction load that the tube is exerting on the head could be captured. This reaction load occurring during retraction is a quantitative assessment of the spring back of the material.

## REFERENCES

- [1] Upfront Crimpers., 2009. *Imperial®-Stride Tool Inc.* See also URL [http://www.stridetool.com/tools/electrical\\_datatools/stripper\\_12\\_and\\_13.html](http://www.stridetool.com/tools/electrical_datatools/stripper_12_and_13.html). May.
- [2] K-Tool International., 2011. *ToolTopia*. See also URL <http://www.tooldtopia.com/k-tool-international-71100.aspx>. June.
- [3] Sonobond Ultrasonics., 2010. Tube Terminator™. See also URL <http://www.sonobondultrasonic.com/pdf/Tube-Terminator.pdf>, Oct.
- [4] Powder Actuated Fasteners., 2003. *American Institute of Steel Construction*. pp 40-41. See also URL <http://www.aisc.org/content.aspx?id=17560>. May.
- [5] What is a Hermetic Seal., 2011. *WiseGeek: Clear Answers for Common Questions*. See also URL <http://www.wisegeek.com/what-is-a-hermetic-seal.htm>. June.
- [6] Cape Canaveral, A.P., 2004, “Space Station Air Pressure Dropping; NASA Probing Leak,” *USA Today.*, See also URL [http://www.usatoday.com/news/nation/2004-01-05-space-station\\_x.htm](http://www.usatoday.com/news/nation/2004-01-05-space-station_x.htm). July.
- [7] Nepershin, R. I., 2009. “Pressing of a Thin Wall Tube by a Curvilinear Matrix”. *New Technologies in Machinery Manufacture*. 38(3), pp 263-269.
- [8] Degarmo, P. E., Black, J. T. Ronald A., 2003. *Materials and Processes in Manufacturing*. Wiley, Hoboken, NJ.
- [9] Cozzarelli, F. A., Shames, I. H., 1997. *Elastic and Inelastic Stress Analysis*. Taylor-Francis, Philadelphia, PA.
- [10] Kalpakjian, S. Schmid, S. R., 2003. *Manufacturing Processes for Engineering Materials*. Prentice-Hall, Upper Saddle River, NJ.
- [11] Smith, W. F., Hashemi, J., 2006. *Foundations of Materials Science and Engineering*. McGraw-Hill, New York, NY.
- [12] Technical Support., 2008. *Instron Materials Testing Solutions*. See also URL [http://www.instron.us/wa/home/default\\_en.aspx](http://www.instron.us/wa/home/default_en.aspx). May.
- [13] Welch, Rietschle, Thomas., 2004. Owner’s Manual for DuoSeal Vacuum Pumps. See also URL <http://www.welchvacuum.com/pdfs/manual/67-0777R2.9%20%28DUOSEAL%29.pdf>, May.
- [14] VTMV Series Ultra Miniature Vacuum Sensor., 2009. *Vaccon Vacuum Products*. See also URL <http://www.vaccon.com/Sensor-VTMV-home.aspx>. Feb.
- [15] Gere, J. M., 2004. *Mechanics of Materials*. Thomson-Brooks/Cole, Belmont, CA.

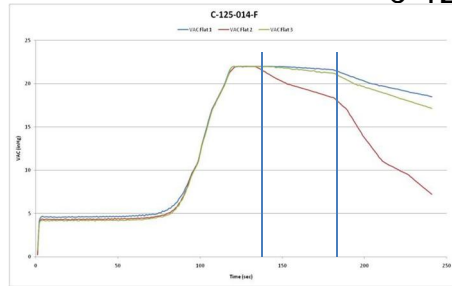
- [16] Columns and buckling I., 2009. *Technical Mechanics 3*. See also URL [http://physicsarchives.com/course/technicalmechanics3\\_bestanden/image407.gif](http://physicsarchives.com/course/technicalmechanics3_bestanden/image407.gif). June.
- [17] Column., 2011. See also URL <http://upload.wikimedia.org/wikipedia/commons/thumb/a/a2/ColumnEffectiveLength.png/360px-ColumnEffectiveLength.png>. June.

APPENDIX A

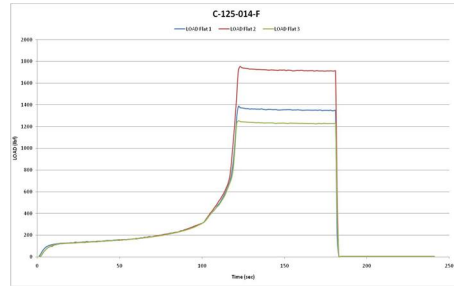
COMPARATIVE VACUUM AND LOAD VERSUS TIME PLOTS OF ALL TEST RUNS

# C-125-014

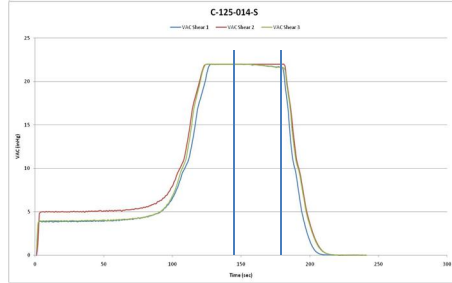
Flat  
VAC



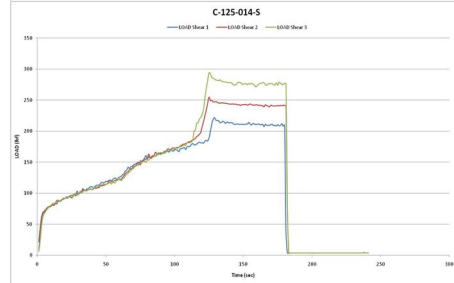
Flat  
LOAD



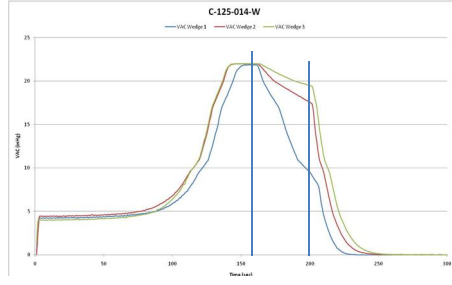
Shear  
VAC



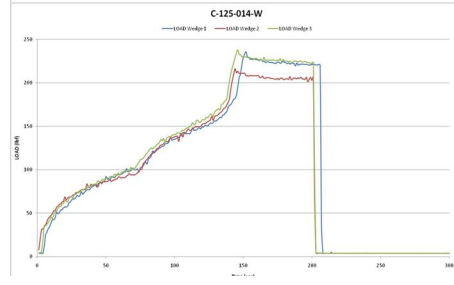
Shear  
LOAD



Wedge  
VAC

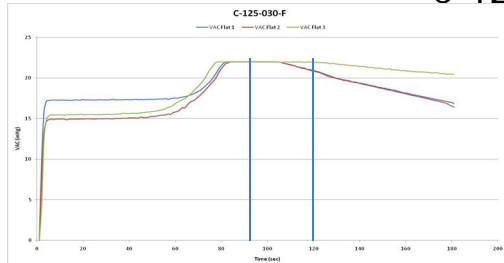


Wedge  
LOAD

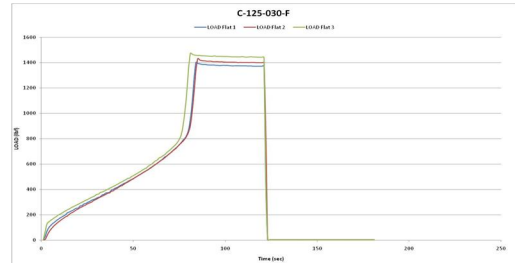


### C-125-030

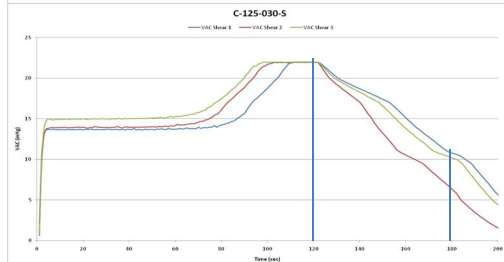
Flat  
VAC



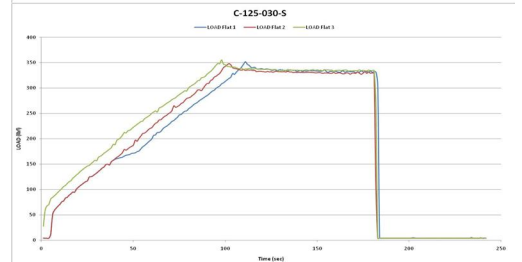
Flat  
LOAD



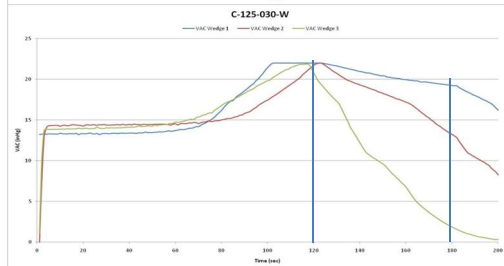
Shear  
VAC



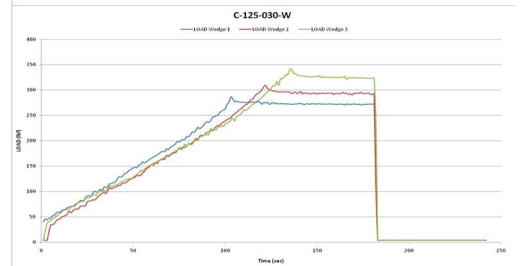
Shear  
LOAD



Wedge  
VAC

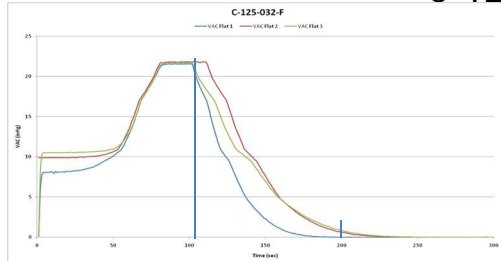


Wedge  
LOAD

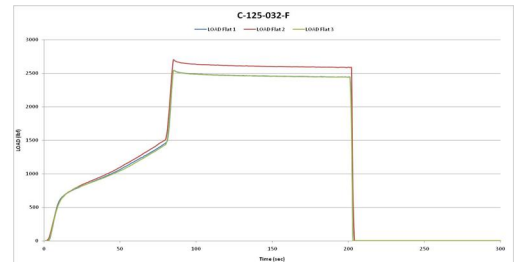


### C-125-032

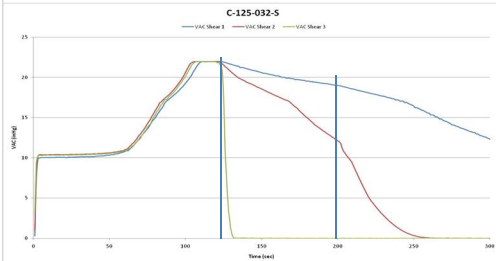
Flat  
VAC



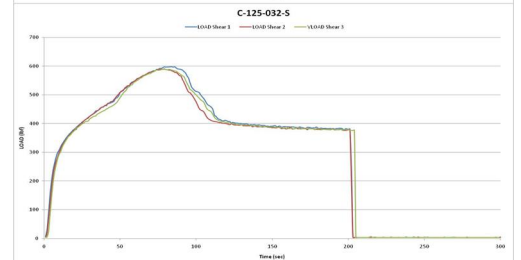
Flat  
LOAD



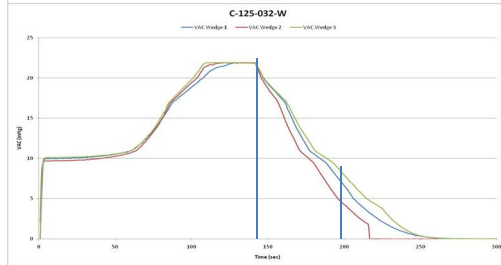
Shear  
VAC



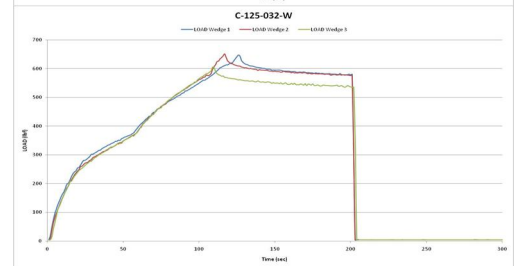
Shear  
LOAD



Wedge  
VAC

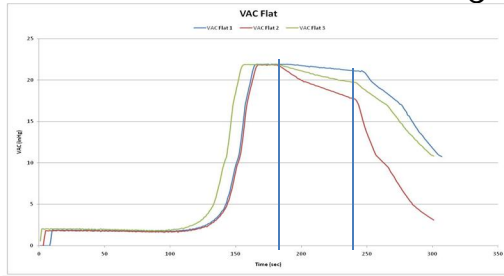


Wedge  
LOAD

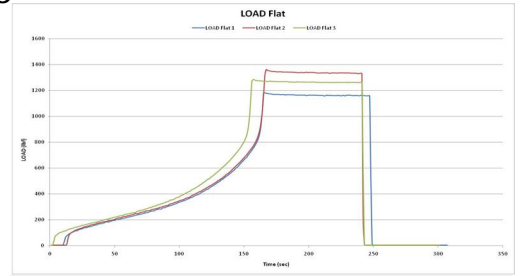


C-187-030

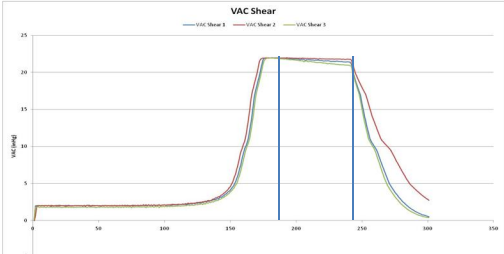
Flat  
VAC



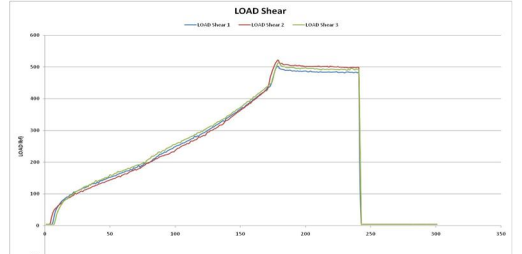
Flat  
LOAD



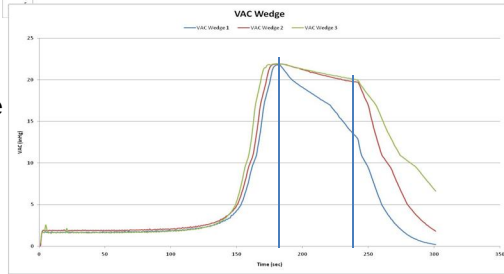
Shear  
VAC



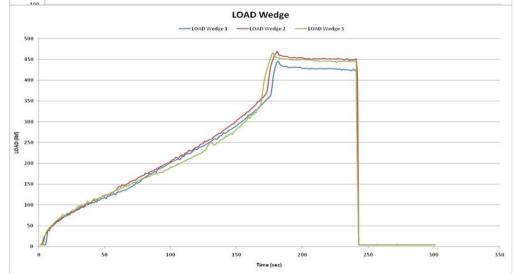
Shear  
LOAD



Wedge  
VAC

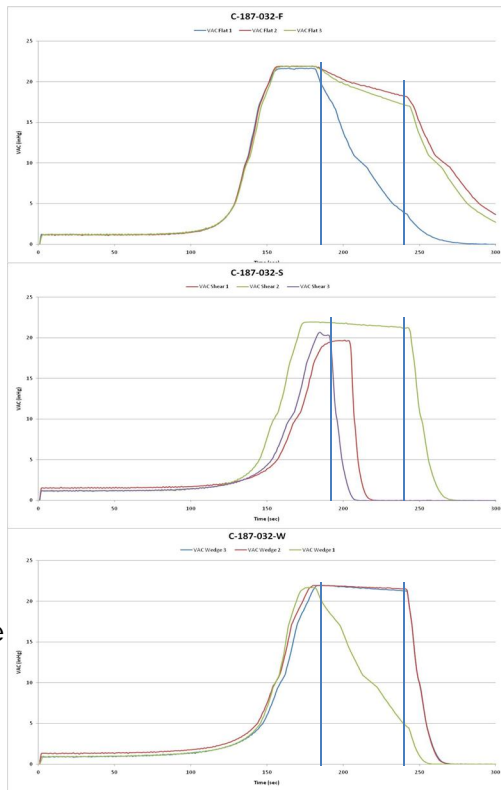


Wedge  
LOAD

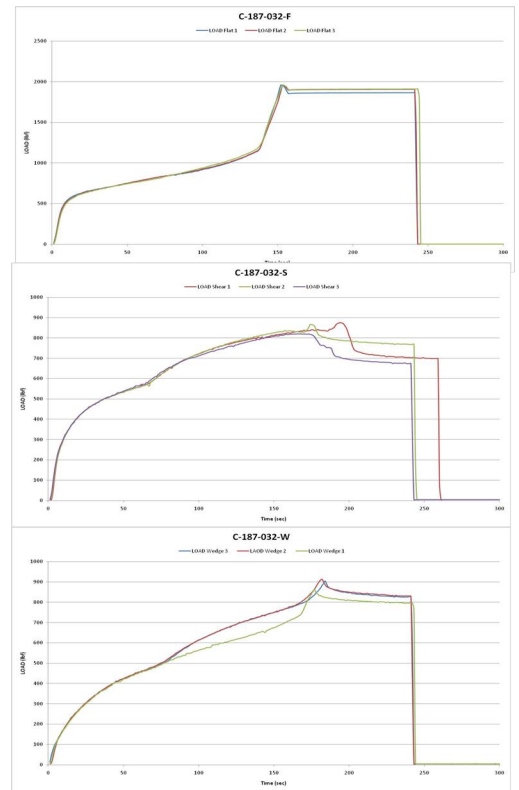


### C-187-032

Flat  
VAC

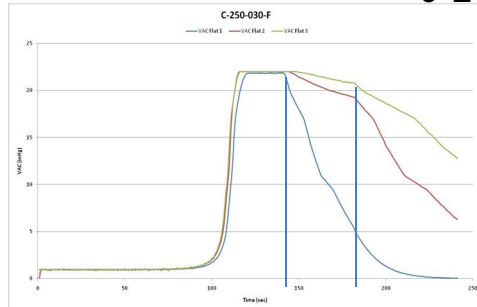


Flat  
LOAD

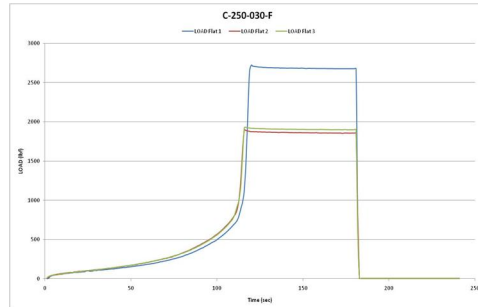


# C-250-030

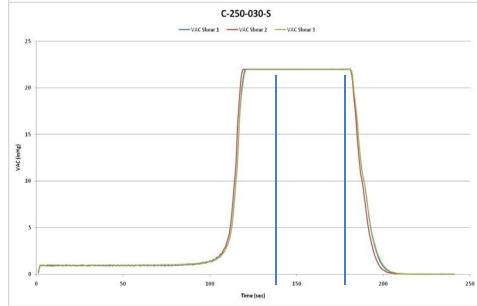
Flat  
VAC



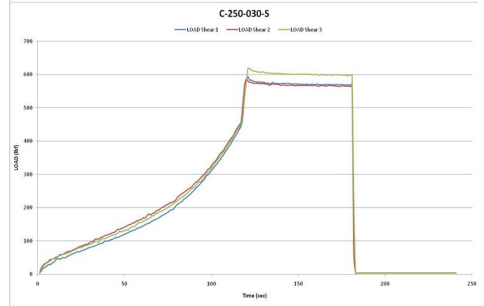
Flat  
LOAD



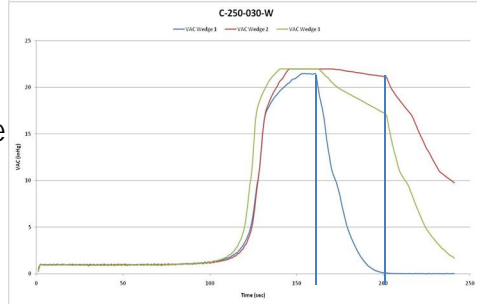
Shear  
VAC



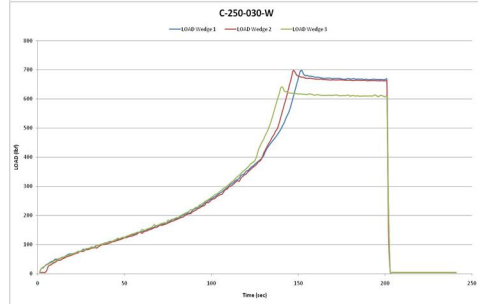
Shear  
LOAD



Wedge  
VAC

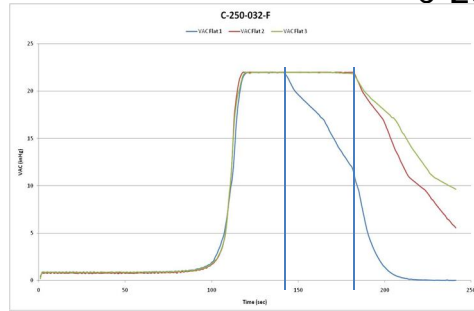


Wedge  
LOAD

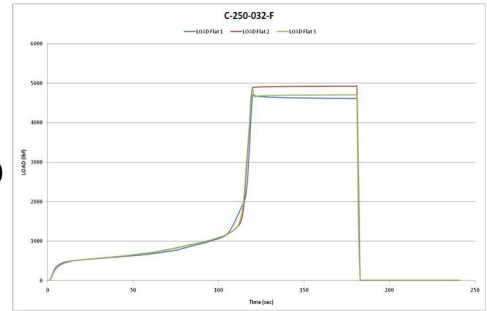


# C-250-032

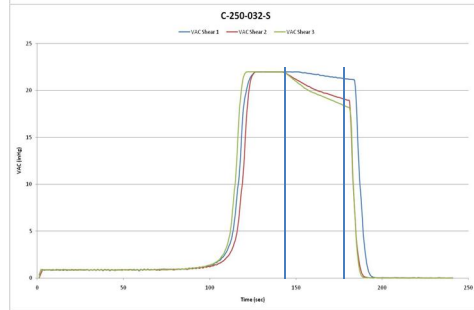
Flat  
VAC



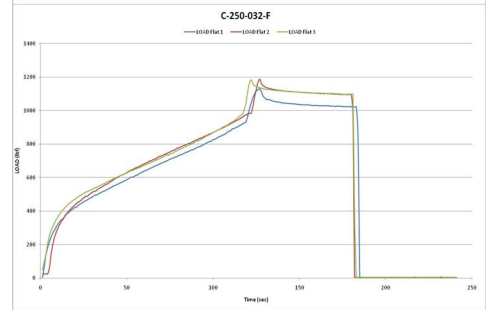
Flat  
LOAD



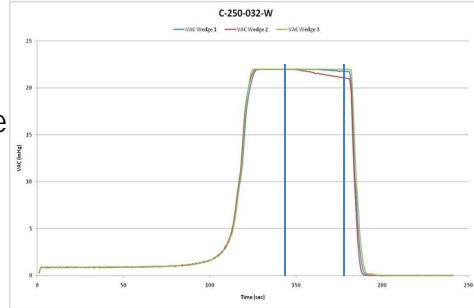
Shear  
VAC



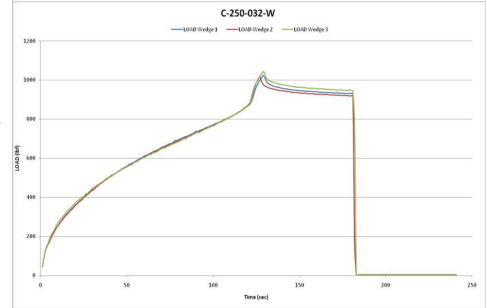
Shear  
LOAD



Wedge  
VAC

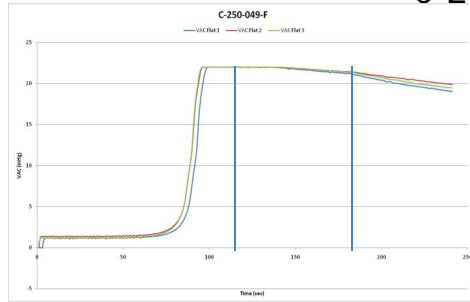


Wedge  
LOAD

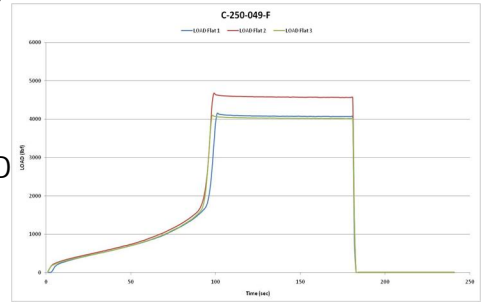


# C-250-049

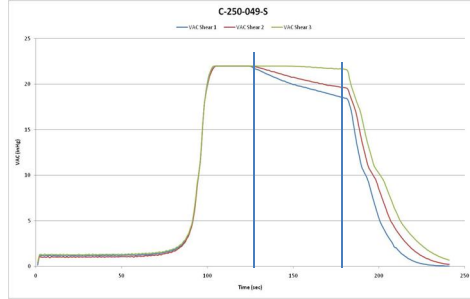
Flat  
VAC



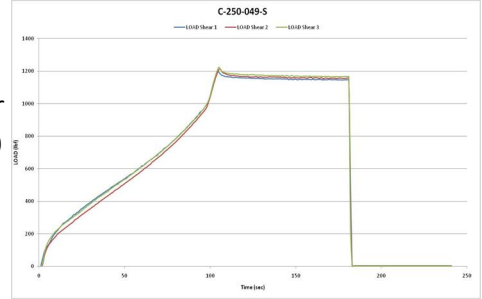
Flat  
LOAD



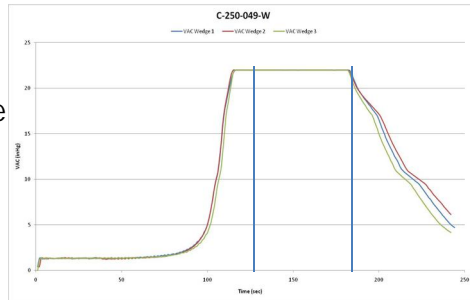
Shear  
VAC



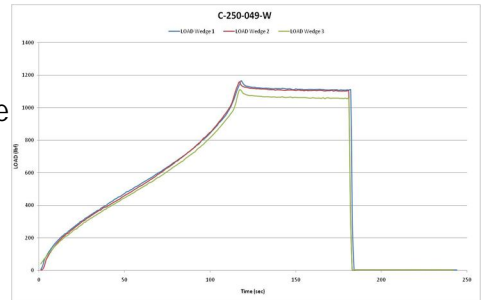
Shear  
LOAD



Wedge  
VAC

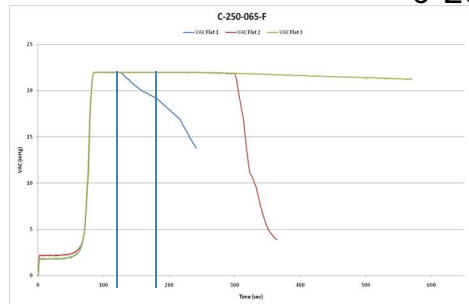


Wedge  
LOAD

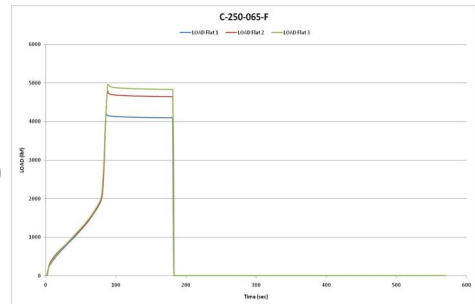


### C-250-065

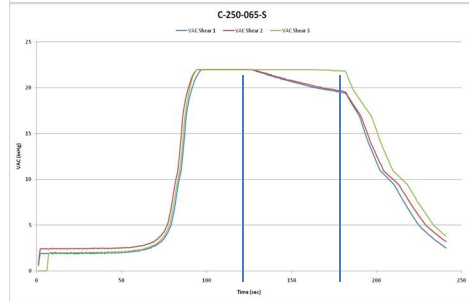
Flat  
VAC



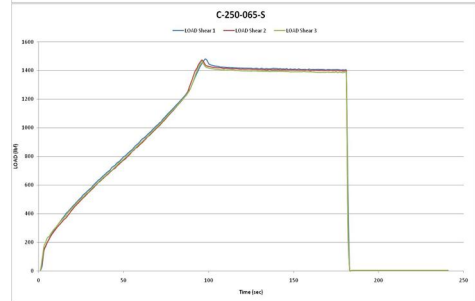
Flat  
LOAD



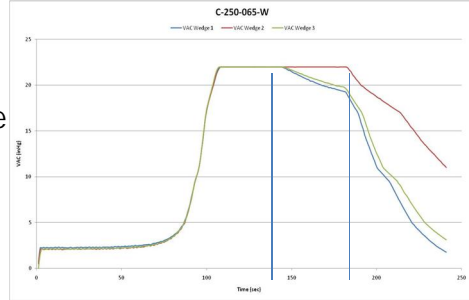
Shear  
VAC



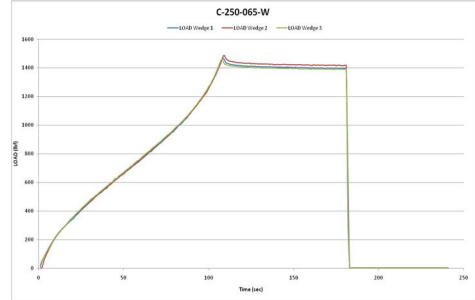
Shear  
LOAD



Wedge  
VAC

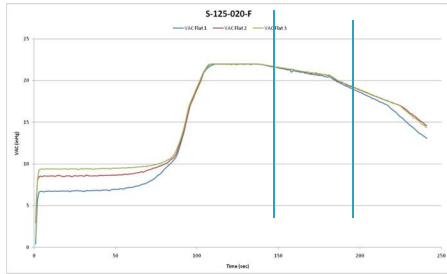


Wedge  
LOAD

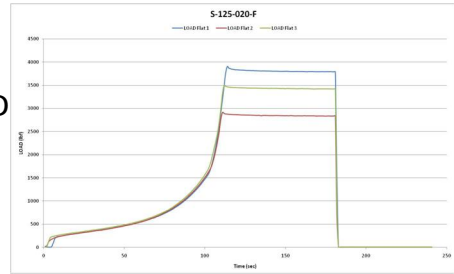


# S-125-020

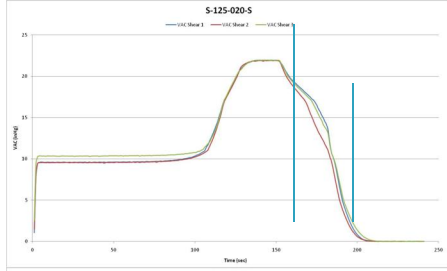
Flat  
VAC



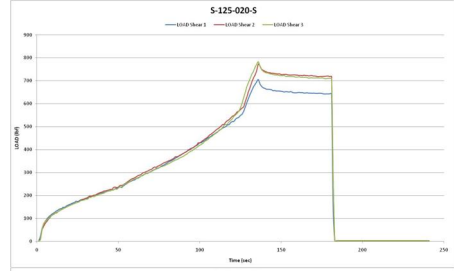
Flat  
LOAD



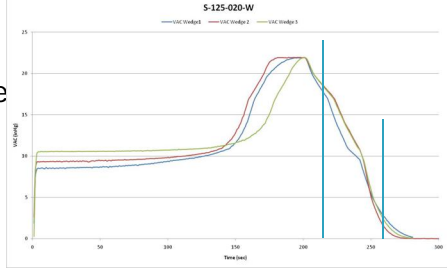
Shear  
VAC



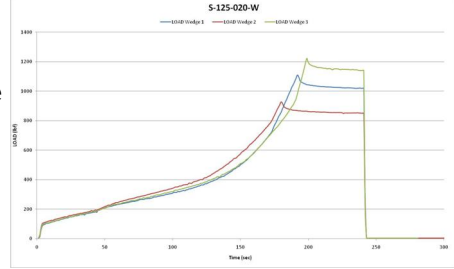
Shear  
LOAD



Wedge  
VAC

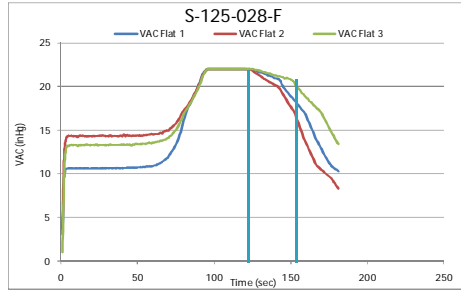


Wedge  
LOAD

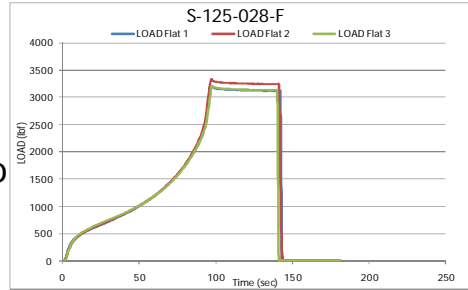


S-125-028

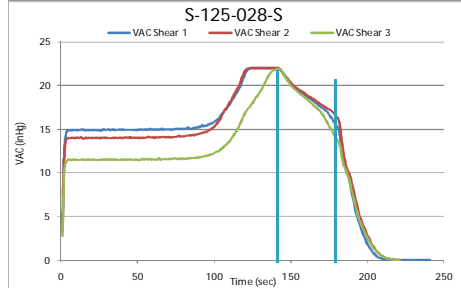
Flat  
VAC



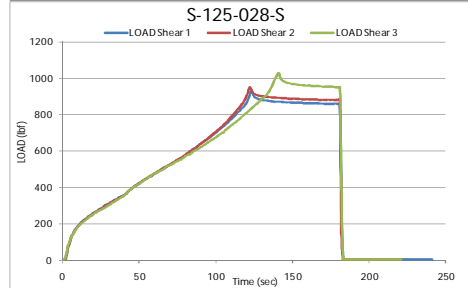
Flat  
LOAD



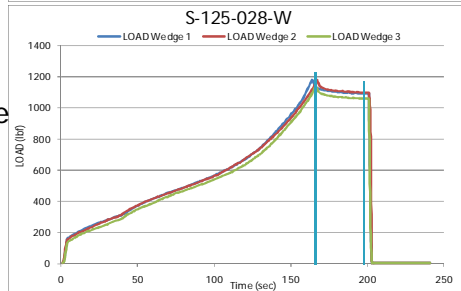
Shear  
VAC



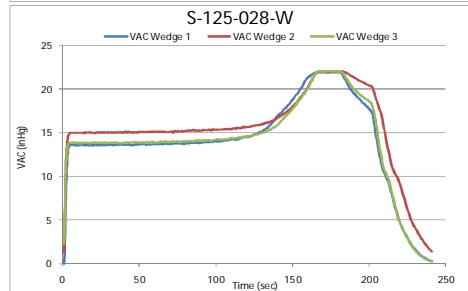
Shear  
LOAD



Wedge  
VAC

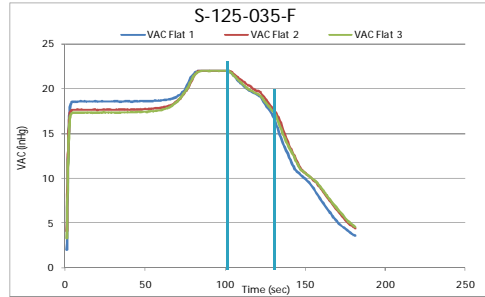


Wedge  
LOAD

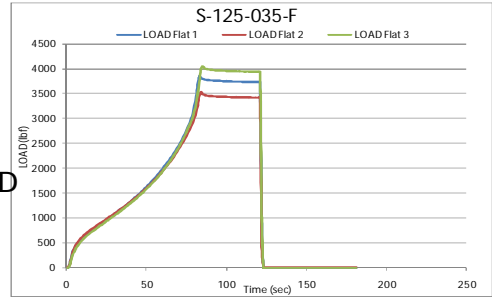


S-125-035

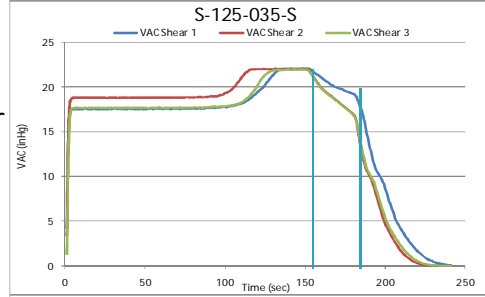
Flat  
VAC



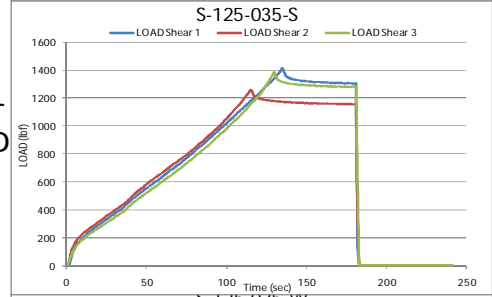
Flat  
LOAD



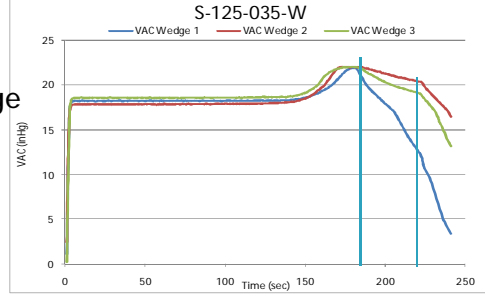
Shear  
VAC



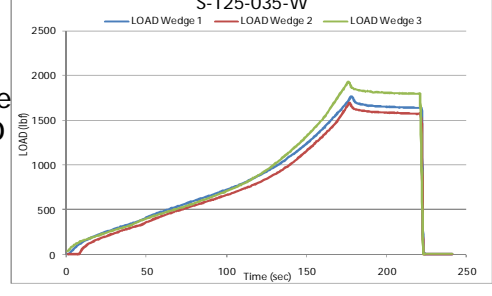
Shear  
LOAD



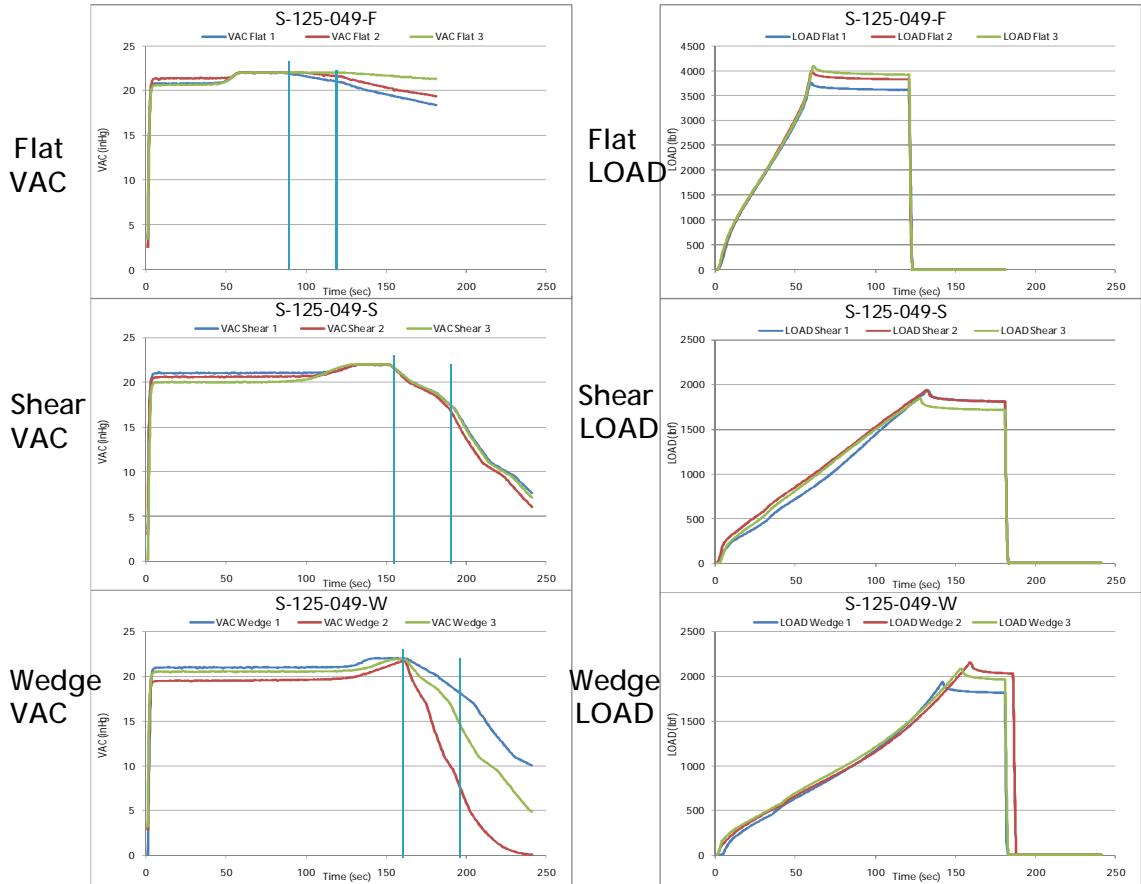
Wedge  
VAC



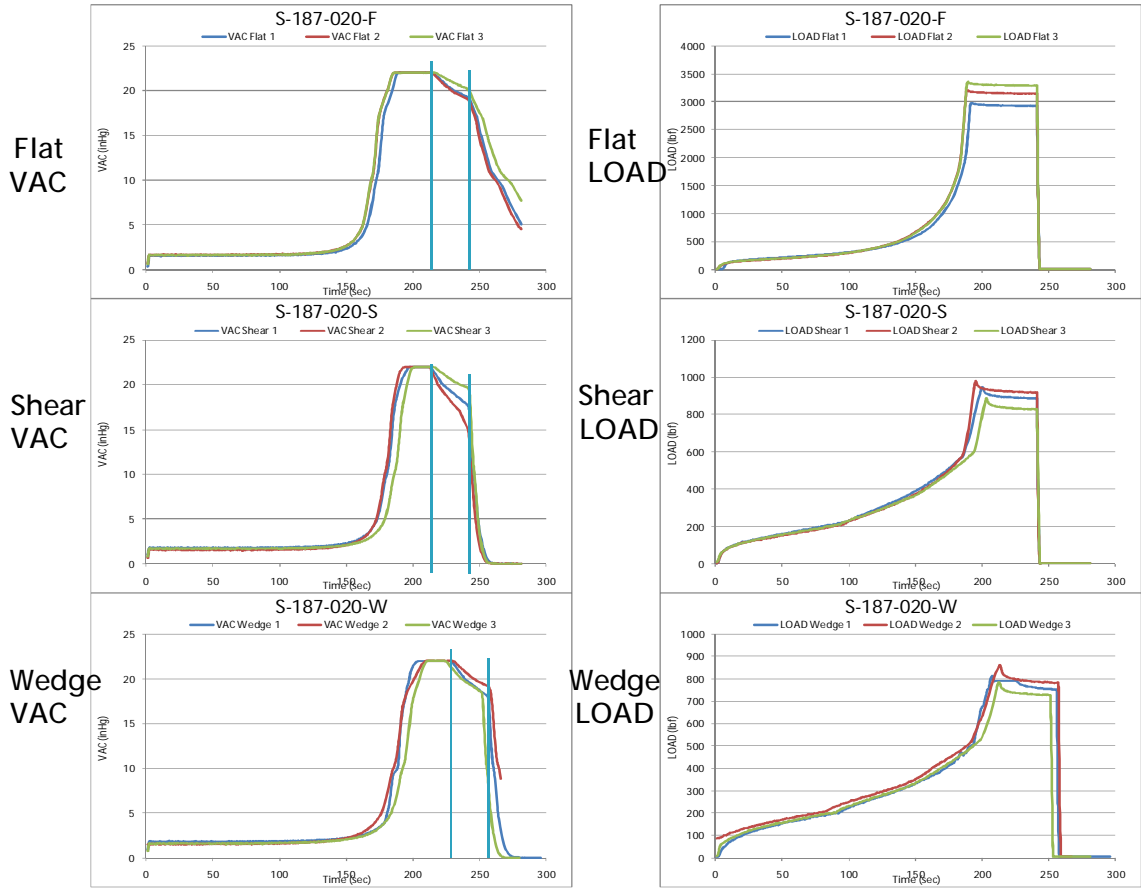
Wedge  
LOAD



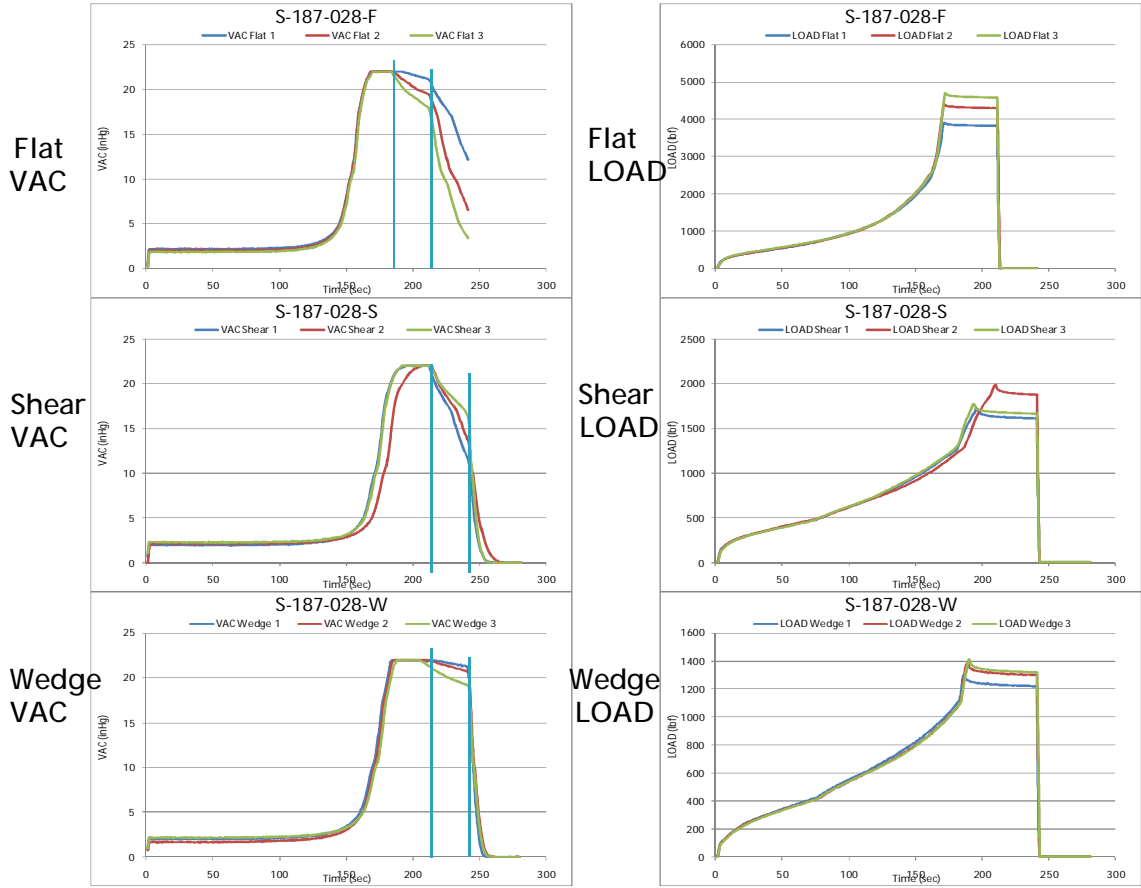
S-125-049



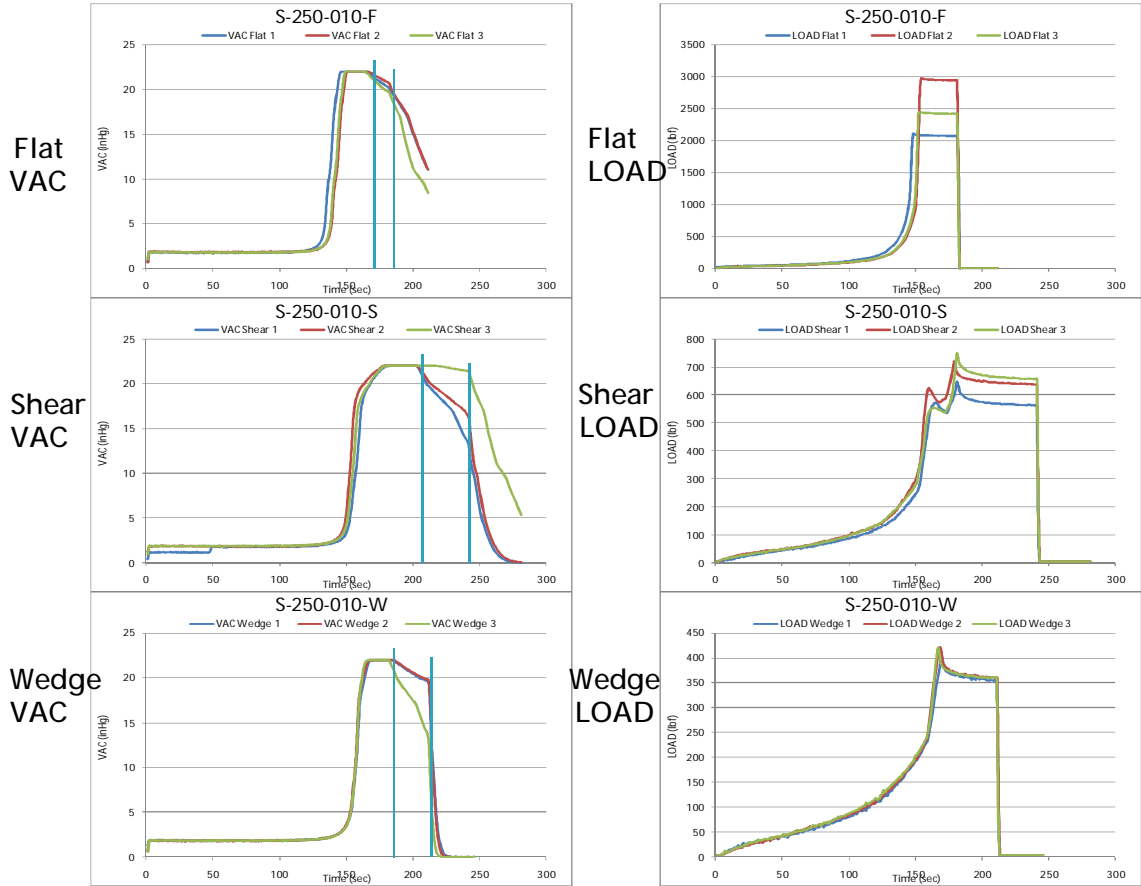
S-187-020



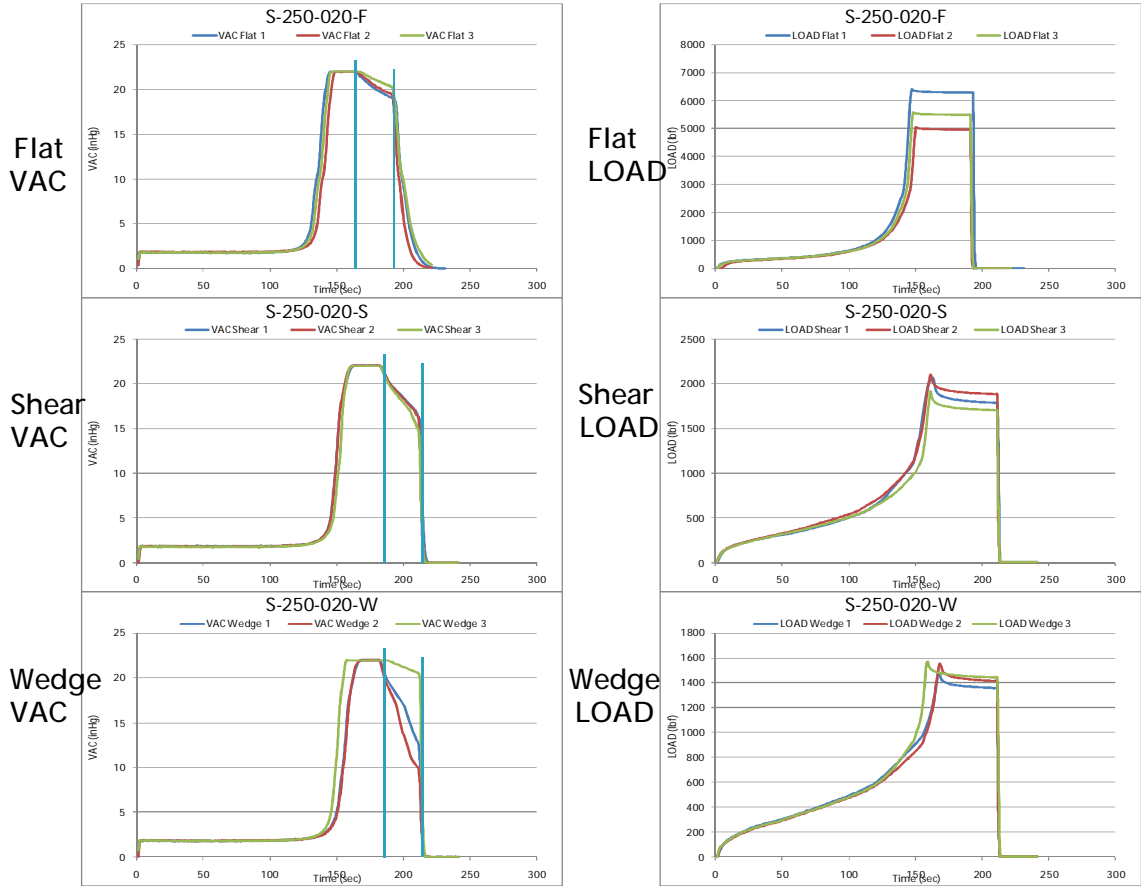
S-187-028



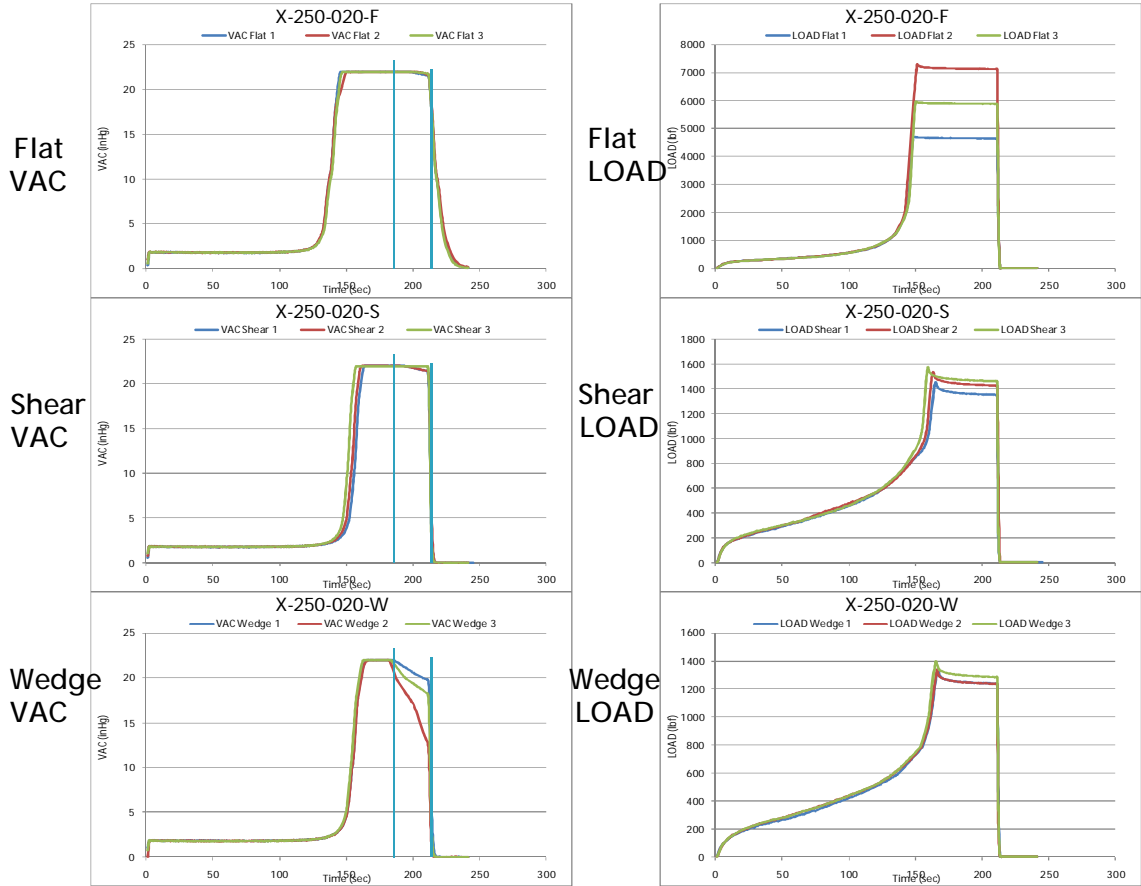
S-250-010



S-250-020



X-250-020



S-250-028

